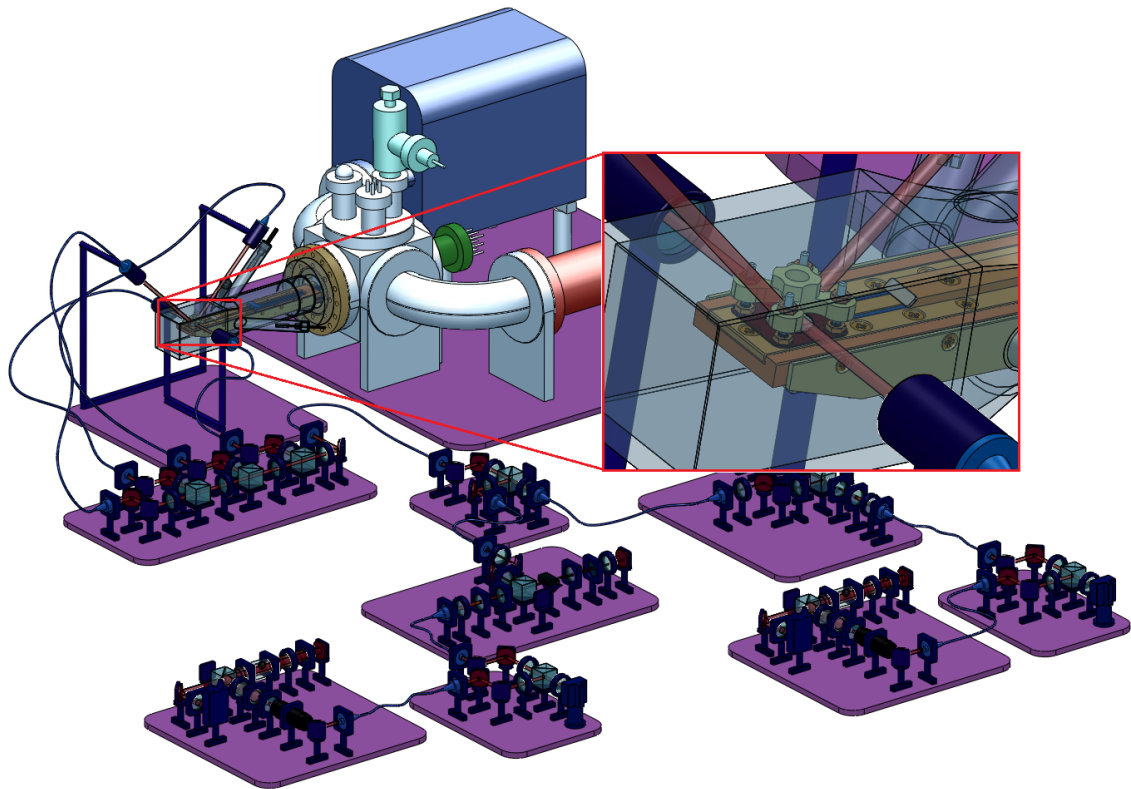# Reflection Magneto-Optical Trap for Single Atom Experiments

Oliver Gugenberger

October 23, 2013

Diploma Thesis

Institute of Atomic and Subatomic Physics, Vienna

Advisor: Thorsten Schumm

Contents

1 Introduction

The aim of this thesis is to design and construct a chip mounting structure for a magneto-optical trap (MOT). This includes creating a layout that meets all demands for the planned experiments, calculations for the wire structures and supervision of the manufacturing. The development of the vacuum chamber, the laser system components, and other relevant elements are also part of the responsibilities.

Magneto-Optical Trapping

The possibility of trapping and cooling atoms using magnetic fields and laser beams was honored 1997 with a Nobel Price. Since then many experiments based on trapped atoms have been performed. One of the first magneto-optical trap on a surface (chip MOT) with a wire construction was realized in 1998 [1]. The scope of this thesis is to find a special modification of the well known structures which enables specific experiments which are planed later on above the chip surface.

Bias Field

Chip MOT's are usually based on the magnetic field from external Helmholtz coils. The second scope of this thesis is to find a current configuration in the mounting of the chip which realizes the required magnetic field without the help of external coils.

Single Atom Trapping

The chip MOT should provide a cloud of Rubidium atoms very near the chip surface. The planned experiments rely on the possibility to catch atoms out of this cloud and capture them in a small potential traps caused by an additional laser beam. The single atom trap is explained in section 2.6. The motivation behind trapping single atoms on a chip is to experiment with their internal states and find ways how they can interact with each other and build quantum gates.

Thesis Tasks

An additional responsibility within this thesis is to supervise the procedure of the realization of the setup. This means to take care of the experiment and order missing components from companies in consultation with the professor so that everything can be constructed in the most efficient way. It is also to realize the construction of the self designed parts and to guide project students which are involved in this experiment.

Structure of this Thesis

In **section 2** a short overview on the theoretical background for magnetical-optical trapping is given. Basic principles and methods are explained which are relevant to run the MOT. The single atom trap experiment and the motivation is described as well. **Section 3** is the scientific part of this thesis. The requirements for the design are discussed and the program which was written to calculate the chip structure is explained. Two different possibilities of the chip structure are examined in-depth and compared to each other. The chosen structure and the related mounting is described afterwards. In **section 4** the technical components necessary to run the MOT are explained and the current status is shown. The imaging systems for the planned experiments are also part of this section. In **section 7** the appendix can be found. This includes technical drawings of all manufactured parts and a list of all involved companies. In the **last section** a conclusion of this thesis is given and the current status of the project is discussed.

2 Theory and General Background

In this chapter the basic knowledge necessary to understand the principle of a magneto-optical trap (MOT) is given. The focus lies on the elements and methods which are specific to our case. Furthermore, the planned experiments on the chip surface are discussed.

2.1 MOT Basics

MOT's are able to capture and cool down neutral atoms [2] [3] [4]. The concept is based on the fact that a laser with a specific frequency can transfer a momentum to an atom [5]. With pairs of laser beams and a magnetic field, it is possible to create a **position-dependent force on atoms**. The basic requirement to run the MOT is an ultra-high vacuum (UHV) with a pressure lower than 10^{-7} to 10^{-8} mbar.
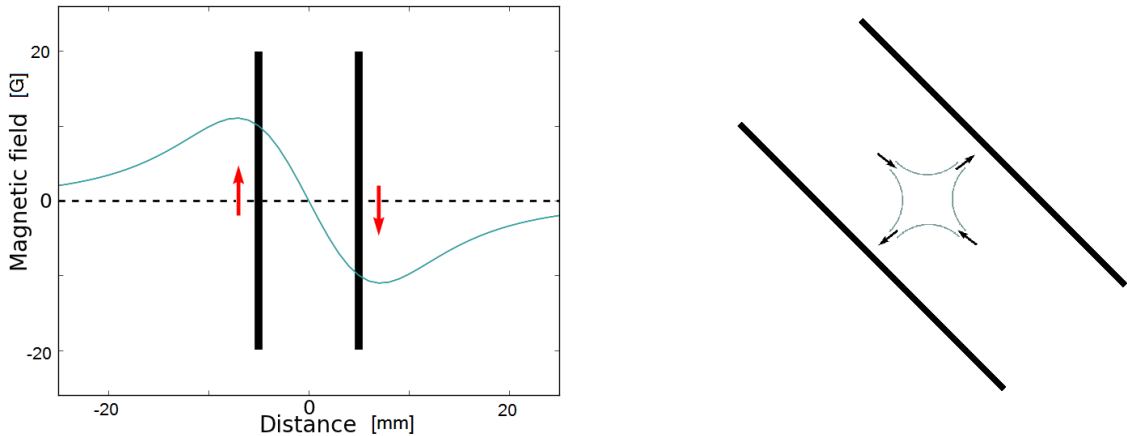

Figure 1: Magnetic field value of anti-Helmholtz coils on the axis (left) and the occurring magnetic quadrupole field (right).

The magnetic field needs to have a zero crossing at the center and increase in strength with distance to the center. An anti-Helmholtz coil is able to create a quadrupole field in the center, shown in figure 1. The field causes a shift of the energy levels of the atoms (Zeeman shift). This changes the resonant frequency of the laser beam. In one dimension, two laser beams with σ^+ and σ^- polarization from opposite directions can force the atoms back to the center of the field. To realize a MOT in free space, laser beams from all spatial dimensions are required.
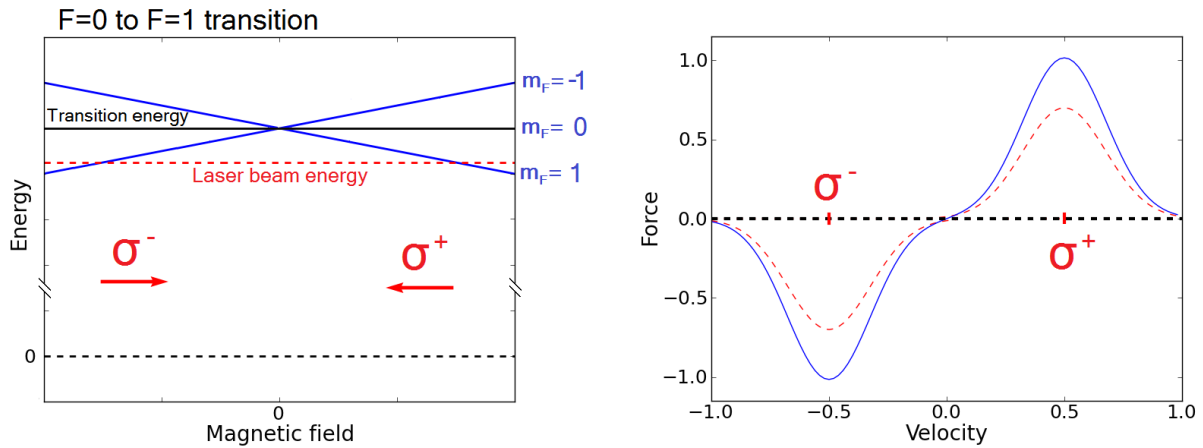
Figure 2: Zeeman energy shift caused by a magnetic field (left). The red dashed line is the laser beam frequencies. The right side shows the velocity dependent force on the atoms caused by the laser beam.

In figure 2 an illustration of the force on the atoms is given. On the left side the Zeeman shift is shown. The energy shift of sublevels m_F are linearly proportional to the magnetic field. The circular polarized laser beam can pump ether the $m_F=1$ or $m_F=-1$ state depending on its polarization and therewith push the atoms back to the center. In reality the used transition is F=2 to F=3 what is a little bit more complicated, but the principle is the same. On the right side in figure 2 an additional effect is shown, which influences the atoms. The doppler shift also depends on the frequency detuning of the laser beam. Both effects (magnetic trapping and doppler cooling) are used together and make it possible to capture atoms.
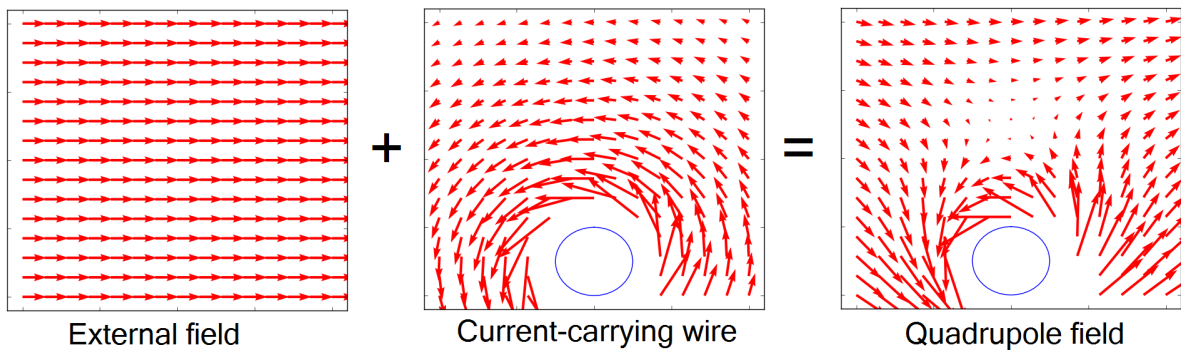
Quadrupole field

Figure 3: Generation of a quadrupole field by a current-carrying wire in an external field.

7

The vectors of the magnetic quadrupole field need to be aligned along the laser beam axes. In free space this can be archived in a limited area by a anti-Helmholtz coil. For MOT's on a surface it can be realized by an external magnetic field and a wire as shown in figure 3. The combination of an external field and the field of a current carrying wire leads to a quadrupole field with 45° rotated symmetry axes near the center on a 2d plane [6]. For the third dimension, the wire shape needs to be modified. This is mostly realized either with a U-shaped wire or with H-shaped wires [7]. A U-shaped wire is shown in figure 4.
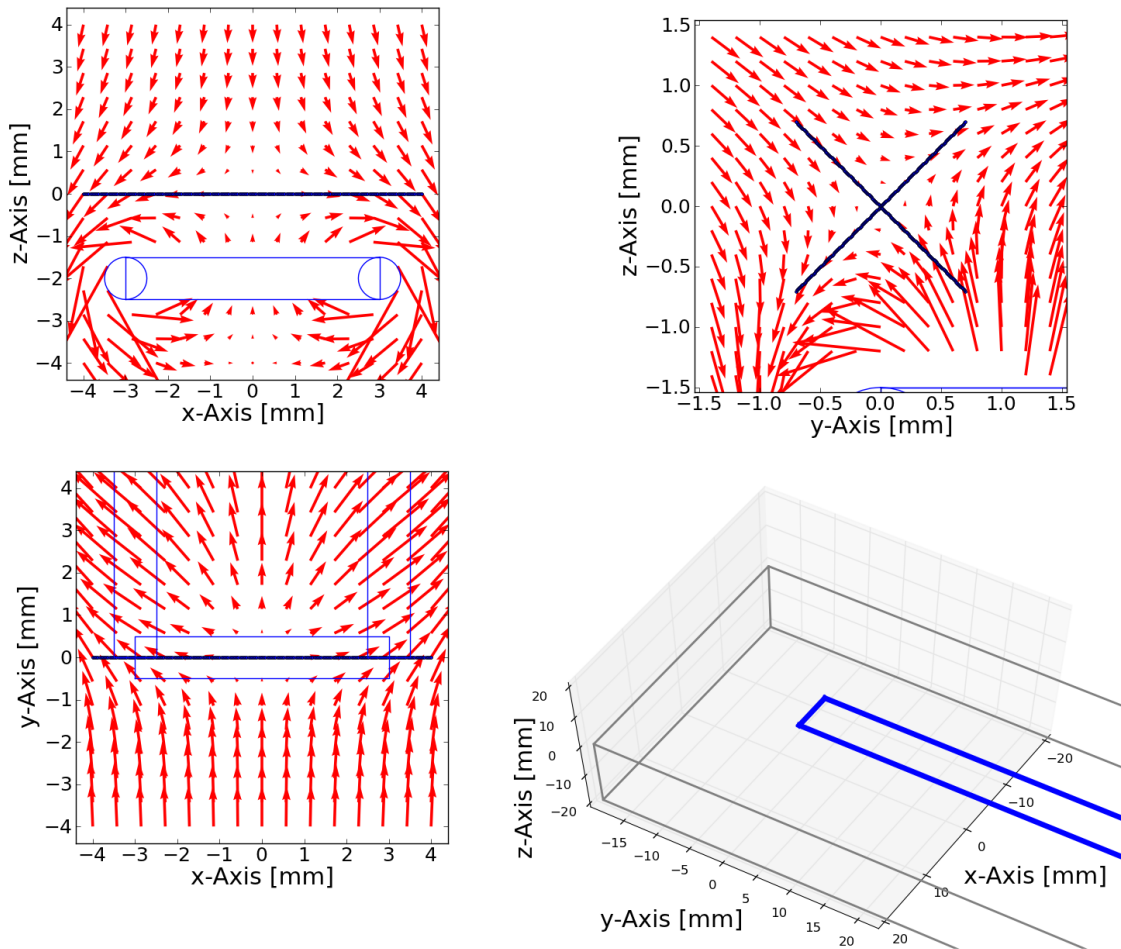

Figure 4: Magnetic field of a U-MOT wire.
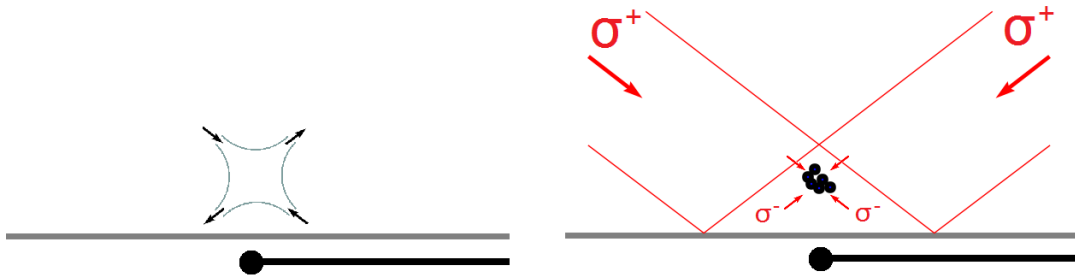
8

2.2 Chip MOT's

Figure 5: Chip MOT. Magnetic quadrupole field position (left) and laser beams (right).

Surface MOT's realize a trapping with only four laser beams and one mirror. A pair of laser beams on one axis needs to have different polarizations. One laser beam should be σ^+ and the other on should be σ^- polarized (depending of the direction of the magnetic field vectors). Reflecting the laser beam on the mirror changes its polarization by π, which makes it possible to use it from the opposite direction. The laser beams force the atoms back into the center of the field, as shown in figure 5. The arrangement of the laser beams in 3 dimensions is shown in figure 6.
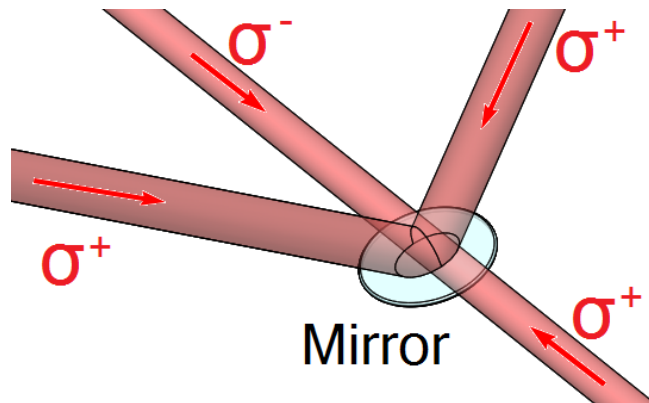

Figure 6: Laser beams in 3 dimensions.

Angular Momentum of Light

The polarization of the laser beam (σ^+ and σ^-) is defined by the angular momentum of the laser beam relative to the field axis which turns the algebraic sign in the center of the magnetic field. This means the angular momentum of two counter-propagating laser beams is the same but their polarizations are inverted.

2.3 Vacuum Components

The planned experiments on the chip surface require the capture of single atoms in an UHV of at least 10^{-11} mbar. This minimizes the danger of atoms colliding with the background gas. To create a vacuum of this magnitude, a system of different components has to be constructed and a special procedure has to be applied.

Chamber   The first step is to build a stable vacuum chamber. All components are securely connected with copper gaskets. All areas on the inside exposed to the vacuum are cleaned with an ultrasonic cleaner to remove a large range of impurities.

Pre-vacuum   The first stage of the vacuum is generated by an ordinary pre-vacuum pump and a turbomolecular pump. They are able to generate a vacuum of around 10^{-7} mbar. Depending on the volume of the chamber, this needs around one day. During the pumping the heating process can be started.

Bake out   Inside of the vacuum system, particles are left on the vacuum chamber walls (mainly water molecules). To remove them it is necessary to heat the chamber up to at least $100°$ to $200°$ C. This can be done by heating tapes, which are placed outside the chamber and thermally isolated with a few layers of Aluminium tape. A crucial constraint is that the chamber needs to be heated evenly, in order to prevent large temperature gradients from causing stress inside the chamber parts. Glass elements are particularly sensitive. The heating process can take up to a week and more. To control the heating a couple of temperature probes are placed on the system.

Ion pump   The Ion pump is started at a vacuum of at least 10^{-7} mbar and when the chamber has cooled down to room temperature. Before starting the ion pump the gauge to the pre-vacuum pumps is locked so the chamber is closed. The Ion pump works by ionizing atoms and catching them on its anode. This operating principle works in already existing vacua. The life time of an ion pump is limited, and it is destroyed if turned on at room pressure.

Titanium-Sublimations pump   Sublimation pumps are only used in already existing vacua as well. By heating tungsten bars inside the pump, titanium atoms vaporize and deposit onto the chamber walls. There they capture remaining molecules on the chamber wall. The deposition process needs to be repeated every few hours when creating the vacuum. After UHV is achieved, it is enough to run it once a month or even less.

2.4 Optics Theory

To provide the laser beams of a MOT, a few methods are necessary. The laser frequency is at first stabilized to an atomic transition and afterwards shifted to the required frequency. The beam has to be split in four equal parts and directed to the chip surface as shown in figure 6. An additional repump-beam is also required as explained later.

Basics

Spectroscopy Simple laser spectroscopy can be done by directing a laser beam through a cell of atoms (usually the same type which are used in the experiment, in our case Rubidium atoms). If the laser is on resonance with the atoms, they absorb photons and send out fluorescence light. This energy loss of the laser beam can be measured. A diode laser's wavelength can be controlled by regulating its temperature and current. By changing the current constantly, for example in form of a ramp, the frequency changes as well. A photodiode after the Rubidium cell can measure the intensity change. The output signal is shown in figure 7.
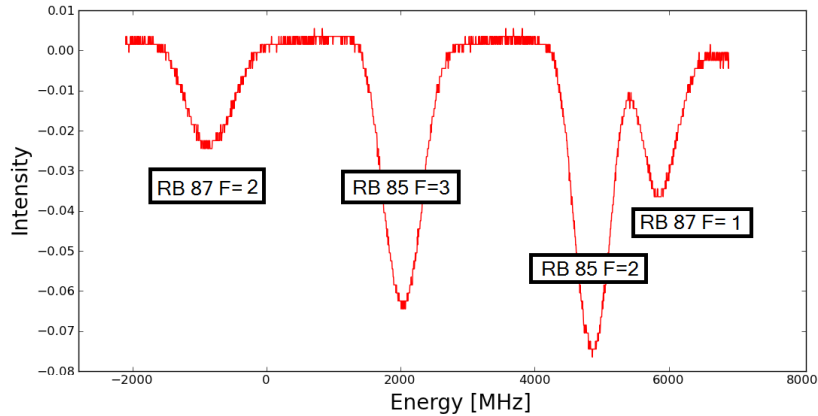

Figure 7: Rubidium spectroscopy.

Doppler-free spectroscopy Since the atoms in the spectroscopy cell are moving, the spectral linewidth of the atomic transitions are Doppler broadened. This limits the maximum resolution at the photodetector. To display the hyperfine structure of the atomic transitions, the Doppler broadening can be avoided. In the Doppler-free spectroscopy, the laser beam is directed twice through the same spectroscopy cell. For certain frequencies, the atoms are already excited when the beam passes the second time and the absorption rate for these atoms is reduced. This leads to a spectroscopy shown in figure 8 on the right side.
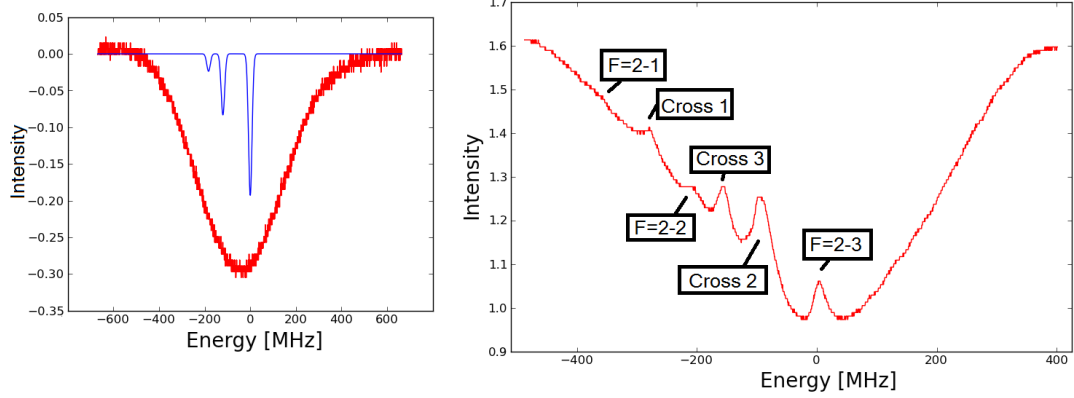
11

Figure 8: Hyperfine structure of ^{87}Rb transition $5^2S_{1/2}$ F=2 to $5^2P_{3/2}$ F=1,2,3. Single spectroscopy with fit function (left) and Doppler-free spectroscopy measurement (right).

Crossover peaks Between two real transition peaks an additional peak appears in the absorption spectrum. The reason for this peaks are slow moving atom which get (because of the Doppler shift) excited from the incoming laser beam a little bit earlier. The reflected laser beam now sees this atom moving in the other direction (relative to the beam direction) and can't excite the other state any more. This means exactly between two states is one additional crossover peak as large as the two real peaks together. On a transition with three real peaks are between state 1-2, 2-3 and 1-3 crossover peak. These peaks are named Cross 1 to 3 in figure 8.

Laser System

The laser system has to provide two laser beams which are stabilized to a specific frequency. Following is a brief introduction to the requirements, more detailed sketches and descriptions of the realization are given in section 4.

Cooling-beam The frequency of the laser beams needs to be almost the same frequency as a specific transition from the atoms which is used to enable a momentum transfer. In our case the transition $S^2P_{1/2}$ F=2 to $5^2P_{3/2}$ F=3 from RB87 is used as it can be seen in figure 9. The diode laser is stabilized to the crossover peak between F=1 and F=3. The frequency shift is archived by a double pass acusto-optical modulator as explained later.

Repump-beam Because of the natural linewidth, atoms can get excited to the state $5^2P_{3/2}$ F=2. In this state the atoms can decay into $S^2P_{1/2}$ F=1 and thereby get lost for further cooling. This is why a second laser is involved. This laser must have the frequency to bring atoms in this so-called dark state back to the excited state $5^2P_{3/2}$ F=2, where they have the possibility to decay into $S^2P_{1/2}$ F=2 and can be used again.

Stabilization   For the laser beam preparation, a few setups are required. At first a small amount of the beam is diverted. This low intensity beam is used to stabilize the frequency to a crossover peak.

Manipulation   This stabilization frequency is usually not the frequency needed to excite atoms, so it is necessary to add or reduce the energy of the beam. This can be done with an acusto-optical modulation setup (AOM). An AOM is able to increase or reduce the frequency of a laser beam by a specific value. There are a few different types of realizations which are explained in section 4.1.

Preparation   After a stable laser beam with the required frequency is prepared, the beam needs to be divided into four beams for the MOT. This is done by $\lambda/2$ plates in combination with polarizing beam splitter cubes.

Intensity   The efficiency of the setup is very important to enable a high intensity at the end. On every step of the beam preparation, intensity loses cannot be avoided. The required saturation intensity of the beams on the MOT for Rubidium 87 is I_sat=3.58 mW/cm^2 [9, P. 11].
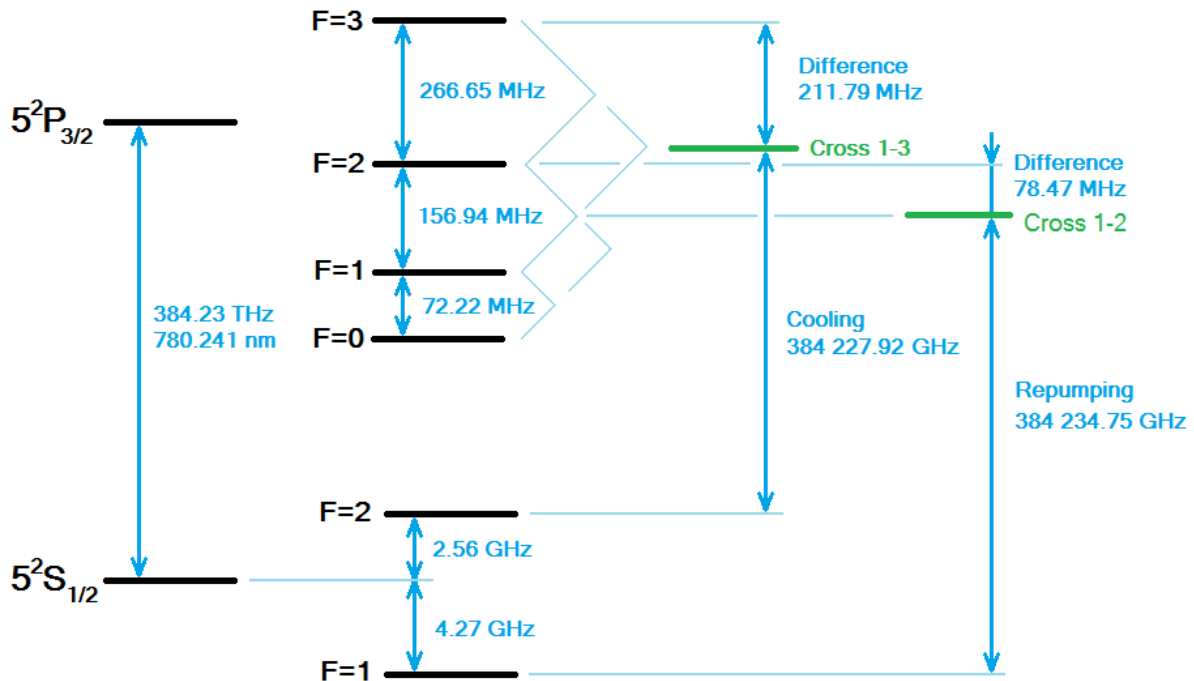
2.5 Rubidium 87

Figure 9: ^{87}Rb D_2 transition hyperfine structure with crossover peaks and required laser frequencies [9].

The Rubidium sources deliver almost the same amount of ^{8}5Rb and ^{87}Rb (around 70/30). The MOT in our case only makes use of the ^{87}Rb atoms and the D_2 line ($5^2S_{1/2}$ to $5^2P_{3/2}$). The transition states for the cooling laser and the repump laser can be seen in figure 9. In figure 9 the hyperfine structure of ^{87}Rb is shown. The laser stabilization frequencies for the cooling laser beam and the repumping laser beam are indicated, as is the energy difference to the driven atomic state. Note that for the cooling laser beam the frequency difference needs to be around 40 MHz lower, as shown in figure 2 on the left side.

2.6 Aperture trap

The MOT prepares a cloud of atoms near the chip surface. Further experiments are more complex and will be done by a PHD student and a Postdoc. The aim of these experiments are to capture single atoms out of this cloud by using the potential of a laser beam behind an aperture. The underlying principle is that a laser beam passing through an aperture with a diameter of a few microns forms a potential in the near field, where atoms can be trapped. On the chip surface there will be a matrix of small apertures, where atoms can be captured and manipulated, as shown in figure 10.
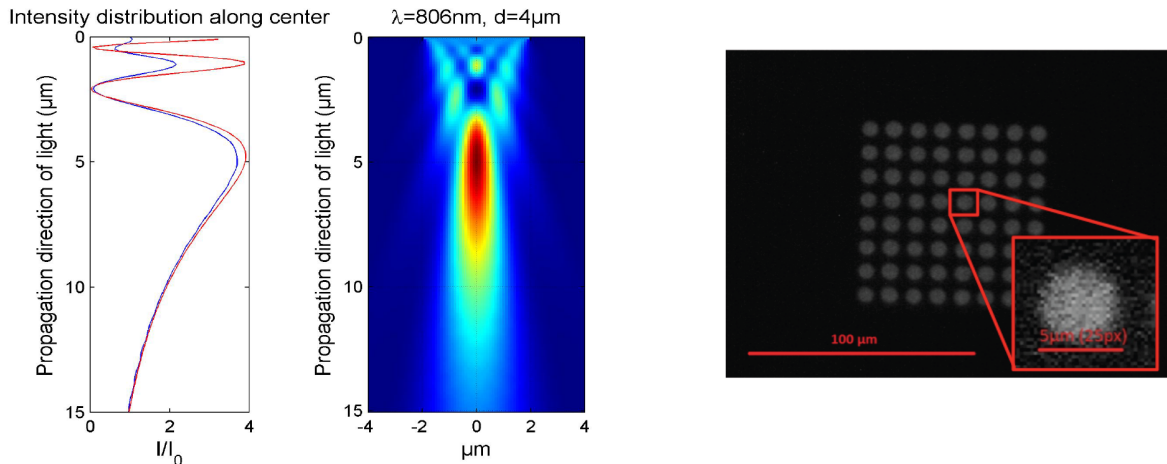

Figure 10: Potential of an aperture for λ=806 nm and d=4 μm (left) (Picture from the proposal for the experiments) and image of the aperture matrix (right).

The procedure will take place in experimental cycles. It consists of turning on the MOT, bringing the cloud of atoms near the surface and turn on the aperture trap laser beam. After a short time, atoms should be captured in the aperture trap and the MOT can be turned of. The presence of atoms can be verified with two imaging systems explained in section 4.4. The further aim of the experiments is to manipulate and entangle the trapped atoms. With an additional laser beam and small electric fields, Rydberg atoms [10] should be realized. The lifetime and the addressability of the atoms should be demonstrated and investigated. In the end, a system of N entangled particles should be generated and characterized.

2.7 Quantum Computation

A conventional computer is based on electricity and the combination of bits to perform calculations. The main logical elements are transistors to process the data. Since the computing power of chips is limited by physical expansion of the atomic structure and the speed of light, the current architecture rate of development cannot continue to increase infinitely. In reality, the edge of evolution cannot be far from now. A single atom transistor has already been realized [11]. However in the last years a new research area has received increased focus. Quantum systems offer a new and not yet totally understood field to solve highly complex calculations. Quantum gates serve as logical elements, which no longer operate in space, but in time. Bits are replaced by Qubits, which cannot just be 1 or 0 but every superposition between. Therefore, the challenge to scientists at this time is to explore atomic states with the possibility to be manipulated and entangled and therewith make quantum circuits possible. Furthermore, gates and methods that benefit from the quantum world have to be found in order to be able to solve complex problems that cannot be calculated by deterministic processes as employed by ordinary computers [12].

3 Chip Design and Mounting

The magnetic field calculation and the resulting layout of the chip structure is the main scientific part of this diploma thesis. This includes also to design the mounting and its components. The magnetic fields and the geometrical construction needs to fulfill specific requirements to enable the planned experiments. In this section the key points are discussed and the simulation of the MOT fields is explained. For the chip design there are two different versions described and compared.

3.1 Requirements

Geometric Requirements

The entire chip mounting is placed in a UHV compatible glass cell, shown in figure 11 on the left side. This means that the dimensions of the mounting are limited by the glass cell and all parts should be highly integrated and as efficient as possible. All current connections pass through a flange into the chamber.
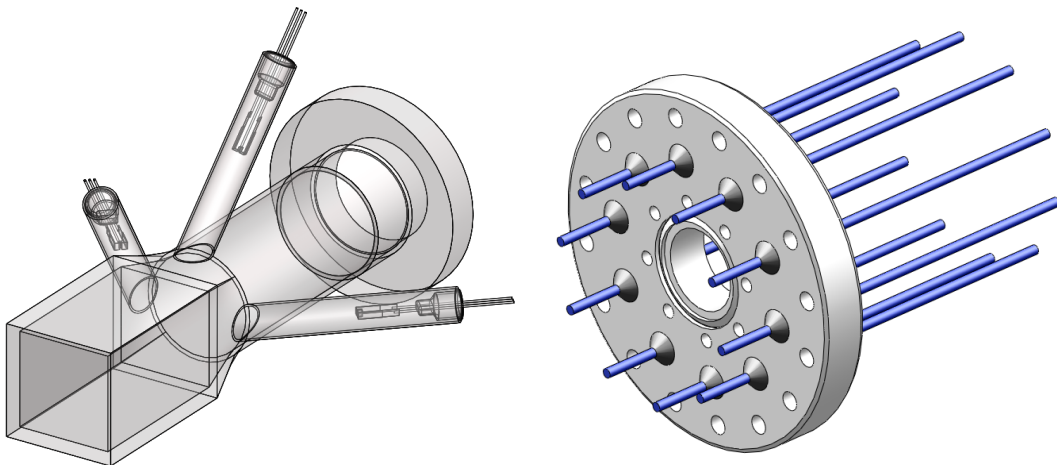
Figure 11: Solidworks drawing of the glass cell (left) and the feedthrough adapter flange (right).

Glass Cell   The custom glass cell is constructed by Precision Glassblowing in the United States. The inner cross section diameter is 55 mm. So everything needs to fit through this hole with a few mm margin. The length of the transition from metal flange to glass is 200 mm and the cell it self is another 100 mm. This length of the glass cell is needed to make a good transition from metal to glass and also to implement the rubidium dispenser and two small sublimation pumps as it can be seen in the figure. The back part is constructed to connect to a CF63 flange. The glass cell can be connected with an adapter flange CF100 which is able to be fixed to the vacuum chamber cube as explained later.

Feedthrough Adapter Flange   We have to consider that all the current connections need to fit in the glass cell as well and need to be able to connect with the outside of the vacuum chamber. The MOT wires need at least one or two pairs of connections, and another two pairs for a bias field (as explaind in section 3.4.4). All current carrying wires need to be controlled from outside of the vacuum chamber. For this, a special feedthrough adapter flange was designed and ordered from Vacuum Praha, in the size of CF100 and with 10 feedthrough conductions as shown in figure 11. The hole in the middle is a CF35 mount for a 32 pin feedthrough as are needed for the later experiments on the chip surface.

Heat Dissipation   In UHV the thermal contact of wires to a surface or heatsink is very important. To avoid the current wires from over heating, also the diameters have to be chosen wisely. The wires need to be isolated with Kapton, most other isolating materials are not UHV compatible, not many diameters can be found with an Kapton isolation (maximum that could be found is d=1.7 mm[1]). Large wire diameters decrease the resistance and therewith reduce the heat production. To increase thermal contact it is possible to glue the wires into the mounting using thermally conducting epoxy.

U-MOT with optical access   What makes the U-MOT unique is the special demand of a hole of 1 mm diameter in the field generating structure, to provide optical access for dipole trapping. Above this hole the chip plate will be placed to trap single atoms out of the atom cloud of the MOT. The plate can be produced with a thickness of 0.5 mm and the hole is necessary to send an additional laser beam from below.

Chip Possibilities

The MOT wire structure can either be realized with a wire configuration or milled out of a copper block. Two versions are examined closer in section 3.4.

Wire   A wire configuration is a very simple and cheap possibility where a Kapton-isolated wire around 1 mm diameter is put direct into a milled furrow in the mount. The isolation needs to be very robust to not create an electrical short with the chip mounting. The disadvantage is that the wire is not very precisely positioned and a rectangle cross section delivers a better quadrupole field [15] and has a lower current density (less heating).

Copper Block   A very common way is to mill a structure out of a copper block and implement it in a ceramic block. This ceramic block isolates the structure to the copper mount. It has a good precision and a efficient current density. The block can be designed perfectly, to the demands, but this process is more complicated and more expensive.

---

[1]www.allectra.com

3.2 Magnetic Field Simulation in Python

To simulate the generated quadrupole field above the wire configuration a program has been written to calculate the optimum currents and geometric structure. The name of the program is Finitewiresolve 1.0, the used language was Python (v 2.7.3.). Python was used because it is simple to handle and has a big range of opportunities.

The Program Finitewiresolve 1.0

The task of the program is to solve arbitrary wire configurations with defined diameter, length, position and current values and plot the occurring vector field and also optimize the values for a maximal atom capturing rate. The procedure is based on the analytic solution for the magnetic field of an infinitely thin, straight conductor with a defined length [13, S. 88]:

$$B = \frac{\mu_0 I}{4\pi\rho}(\sin\alpha_1 - \sin\alpha_2)\vec{e}_a \tag{1}$$

where μ_0 is the permeability constant, I is the current in the wire, ρ is the distance from the wire, α_1 and α_2 are the angles to the two end points of the wire and $\vec{e}_a$ is the unit vector. Figure 12 displays the variables.
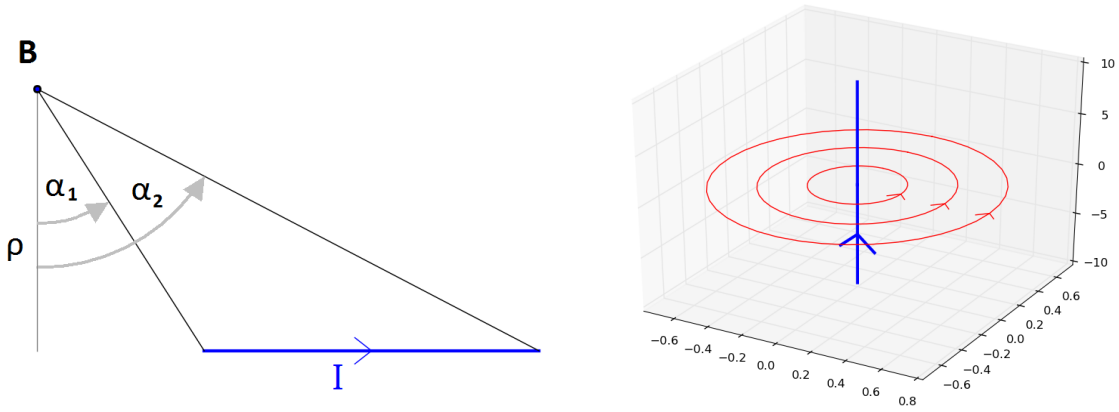
Figure 12: Magnetic field of a thin conductor

The magnetic field is a cross product from the vectors to the start and the end point of the wire line and it decreases with $\frac{1}{\rho}$.

Extended Wire Body
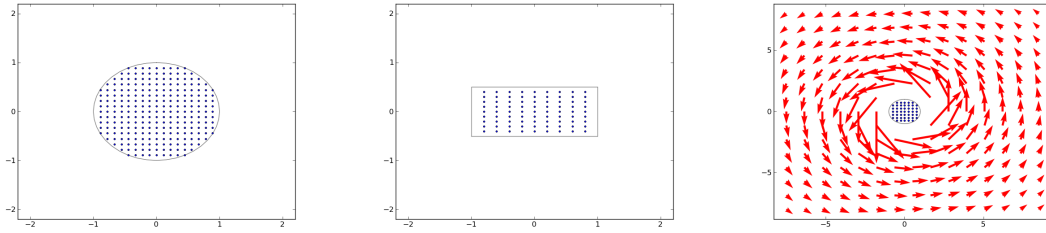
Figure 13: Calculation lines in a circular (left), rectangular wire (middle), and with calculated magnetic field vectors (right)

To calculate a finite sized wire with a given diameter the program fills out the circle or the rectangle by a raster of infinite lines. To do so it rasters the wire diameter as shown in figure 13. The raster number can be controlled by a variable and for example the value 8 leads to 45 calculation lines in the circular and to 64 lines in the rectangular wire.
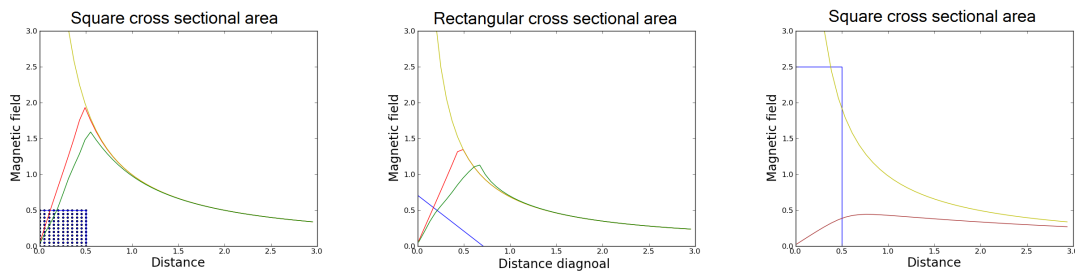
Figure 14: Comparison of the magnetic field of an infinite thin wire (yellow), wire with diameter d=1 mm (red) and square 1x1 mm (green, left and middle figure) and a rectangle with 1x5 mm (brown, right figure)

In figure 14 the magnetic field strength is shown for different wire cross sections. As it can be seen, the finite size is just effecting a very small area close to the surface of a circular or squared cross section. For a rectangular cross section where the height is much larger than the width, the effected area is larger. This plots are showing that the infinite approximation for a circular wire or a squared cross section is good enough to use it for calculations and thereby reduce the calculation time significantly.

Current Density Approximation

In a U-shaped copper block, the current density is not equally distributed in the profile of the body. If there is additionally a hole in the U, as shown in figure 15, the current is not separated in two equal parts.
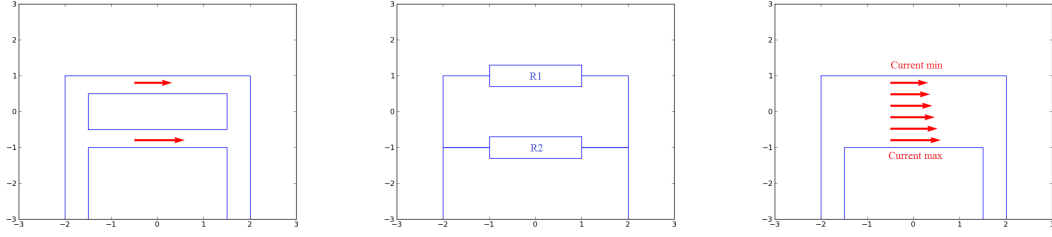
Figure 15: Comparison of the current density in a U wire with a hole (left) and a solid U wire (right).

To approximate the current flow around the hole, the resistance in the two possible paths needs to be known. The proportion can be found with following relation:

$$\frac{R_1}{R_2} \propto \frac{L_1}{L_2} \propto \frac{I_2}{I_1} \tag{2}$$

where R is the resistance, L is the length the current line and I_1 and I_2 are the two current parts.

To get an idea of the impact of the current density effect, an example of a U wire with different widths is given in table 1. The U wire has a diameter of 1 mm and the position of the Current min and Current max are shown in figure 15 on the right side.

Width of the U	Current min	Current max	Difference
2 mm	33.3 %	66.7 %	100.3 %
4 mm	40.0 %	60.0 %	50.0 %
6 mm	42.9 %	57.1 %	33.1 %
8 mm	44.4 %	55.6 %	25.2 %
10 mm	45.5 %	54.5 %	19.8 %
12 mm	46.2 %	53.8 %	16.5 %
14 mm	46.9 %	53.1 %	13.2 %

Table 1: Table of current density in an U shaped wire.

Verifying the Program with Real Measurement

The easiest way to check if a program gives accurate results is to compare to data to existing projects and real measurements. Therefore, the geometry from a chip from the atom chip group at the Atominstitute was used. The current values and the magnetic field values where entered in the program, the geometry is shown in figure 16.

20
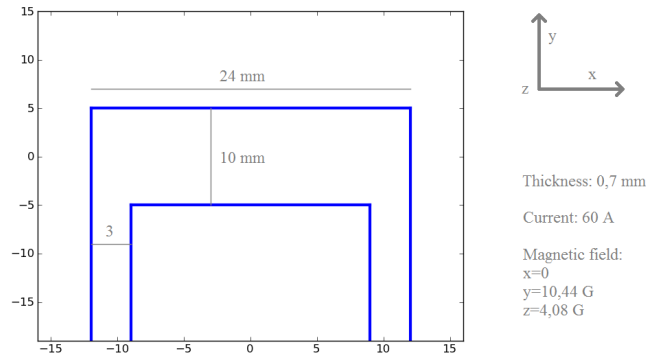
Figure 16: Geometry data from a existing MOT U-shaped wire (atom chip group).

The magnetic fields of this structure were optimized for the best capturing rate in the MOT and the center is approximately 7 to 8 mm above the center of the wire. The result of the program Finitewiresolve 1.0 reproduced this value.

Working principle

The procedure of the program is very straightforward. The wire parameters (position, current value, shape and orientation) are defined at the beginning in an array. For optimal handling, a certain configuration can be chosen by a value in the code. A basic function calculates the field in one point x, y, z. Different plot functions calculate points on a raster and plot them as vector arrows. To get nice contour plots an interpolation function is used to generate a grid that can be coloured to visualize magnetic field areas as it can be seen later.

In the top section of the program is a description how to use the control values. There are a lot of possibilities like making 3d plots with arrow lines in the current direction to proof the validity of the wire design.

Optimisation

A very important part of the program are the optimisation possibilities to find optimal geometric and current values. A few basic functions are needed. These functions need to have as few calculation steps as possible to reduce the compiling time. All basic functions are explained below:

Center function Finding the center of a quadrupole field is very important for further optimisations in the program. To find the minimum of the field fast and with a high precision, a specific function is used. At first the program scans 5x5 points in a large area around the expected center. Then the program generates a 2-dimensional multiquadric interpolation function and receives rough minimum coordinates. The parameters of this function can be controlled, so the function can be run again in a smaller area around the found rough coordinates. So every time the functions is applied, the computer needs

21

25 calculations steps and a fit function to get around a 10 times better accuracy on the center of the MOT. After 75 calculation steps the minimum has a precision of around 0.1 mm in an area of 10 mm. This result can be found faster by a 2-dimensional Newton algorithm, but it turned out, that a Newton algorithm does not always find the global minimum and also has troubles when the parameters are changed[2]. So the raster method was chosen because it is a stable and fast enough calculation method.
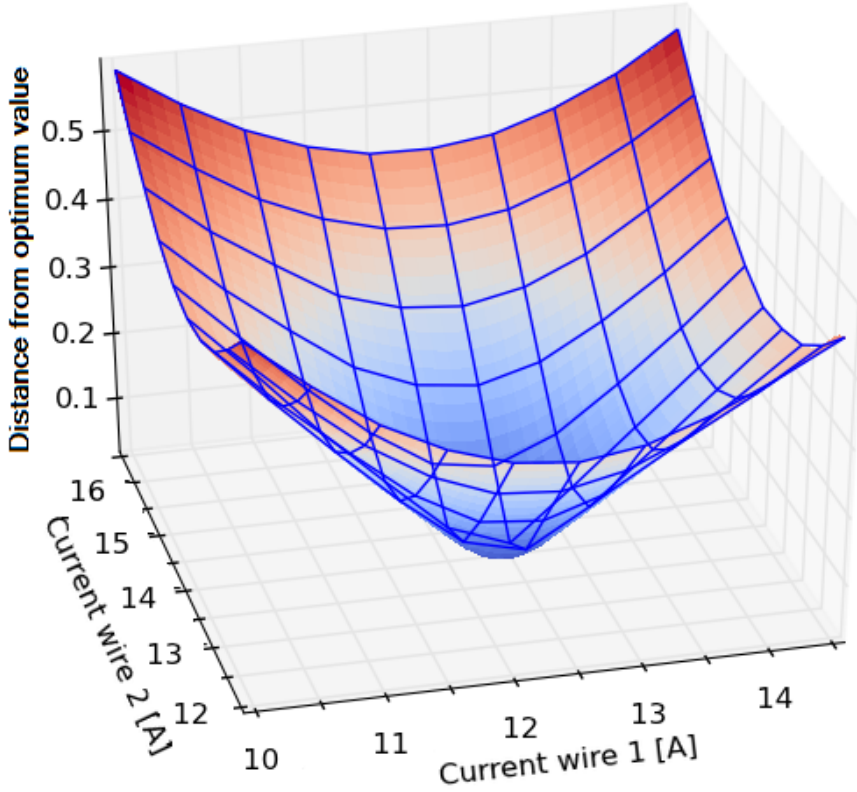

Figure 17: Plot example of a minimization for two degrees of freedom

Current find function   For the optimisation it is important, to compare different configurations which realize the center of the quadrupole field in the same position. In the program the center is mostly chosen to be in (0,0,0). This is why a function was written to calculates the current values required to position the field center in this point or to another defined position. This is done in a similar way as the center function. This time the current values are the free parameters and are scanned and interpolated to find the minimum deviation. For every current configuration in the raster the distance of the quadrupole field from the center can be calculated. An example result can be seen in figure 17, where two currents are changed and the distance from the produced center to the desired center is shown in z direction. This means that for every point the minimum

---

[2]For the optimisation codes it is necessary to change the geometry over a wide area.

function needs to find the position of the quadrupole field. To make the function much faster, instead of the distance from the center it can also minimize the difference of the field value in a specific point. After implementing this, the current find function needs the same amount of calculation steps as the center find function for the quadrupole field to get the same accuracy.

Find magnetic field   Finding the external magnetic field value for a given configuration is much easier. In this case the program can use the field in the desired point produced by the wire configuration and compensate it. This is possible because we know that the system produces a quadrupole field around the zero point of the magnetic field.

Quality values   To verify the quality of a quadrupole field, the magnetic field vectors need to be aligned on the axes of the laser beams as good as possible. In figure 18 the quadrupol field is shown in the (y,z) plane. On the right plot the lines are shown where two of the laser beams cross the center of the quadrupole field. The program calculates the deviation of the field vectors on 100 points on this axes.
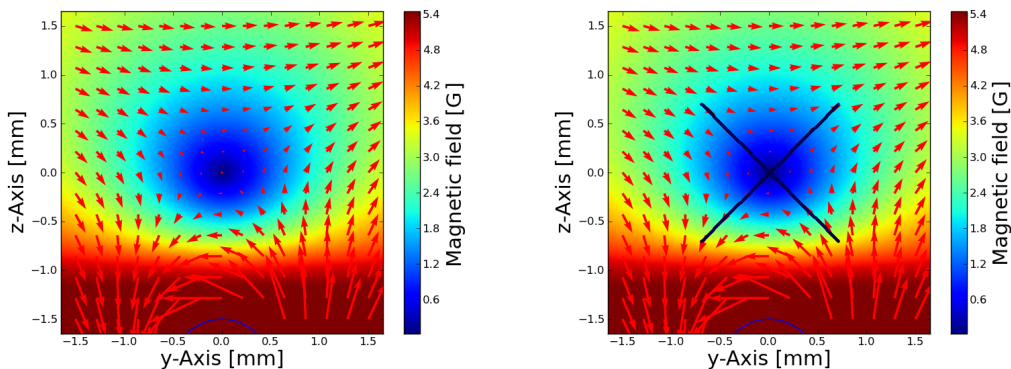
Figure 18: Two plots of the quadrupole field (y,z) plane. One without (left) and one with the laser beam lines (right) where the quality values were calculated.

To compare the quality of different fields the program can produce quality values of the field vectors. To do so, the program scans three lines through the center of the field, one in each laser direction as shown in figure 19. Along these lines the program scans for a couple of quality indicators: the biggest angular deviation, the average angular deviations, the size of the field vector and an effective angular quality calculation. So the result values of the function give information of how well the quadrupole field will perform. To make plots more vivid, the invert value of the average deviation was often used.
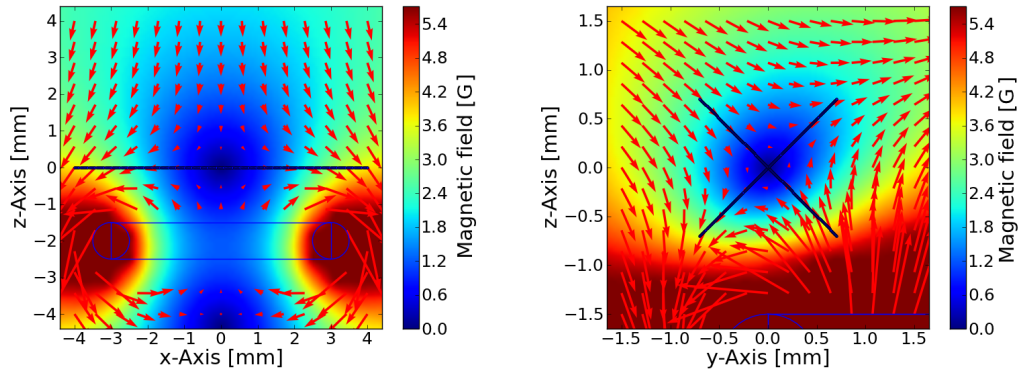
Figure 19: Two plots of the laser beam calculation lines in (y,z) plane (left) and (x,z) layer (right).

Optimisation   Using the previously defined functions, it is possible to find the position of the center of the field, the necessary external field for a given configuration or the required currents to have the field in a defined position. This means that the program knows the position of the field and knows how to move the field to some other position or to keep the field at some point when the construction parameters are changed. It is also possible to get a single quality value for the excellence of the field. This makes further processing easy and enables a lot of possibilities for optimisation codes. Optimisation means that a function changes some parameters in the construction (like currents or distances), then the program "pulls" the field center to the point (0,0,0) and calculates the quality values for the quadrupole field. In the end, the program can compare the results and returns the best configuration. This can also be done by making a raster of the calculated values and interpolate it to make the calculation faster like illustrated in figure 17.

Check field   There is also a function which returns all relevant values of the quadrupole field for a given construction and generates a file from them. Relevant values are position, quality and also the average magnitude of the field vectors on the beam axes, which is important to determine the required currents. This means optimisation codes can use magnitude values as well.

Using the Program

The program is well documented with comments in the code. In the top section, the global variables are declared to control the program. Most important is the variable *plot_this* to control what the program should do. The matrix *wire_con* controls the configuration, it is defined in the subprogram *define_wire()*. With *B_ext* an external magnetic field can be added. With the other variables in the top section a couple of other things like range or scale of the plot and some calculation parameter can be controlled. In the middle section of the program are all the subprograms and also some not relevant

24

subprograms which where used to print the pictures in this theses. In the end section is the actual program start.

The subprogram *vector_plot()* is the standard plot for 2-dimensional vector-fields of the wire configuration. The position defines the perspective (1=yz,2=xz,3=xy). The subprogram *find_min_plot()* finds the magnetic field minimum in a large area around the point (0,0,0) and creates images of the potentials along the laser beam axes x, y' and z' and derivative curves and exports it in the files: *MOT_field_x/y/z.png* and *MOT_field_dif_x/y/z.png*.
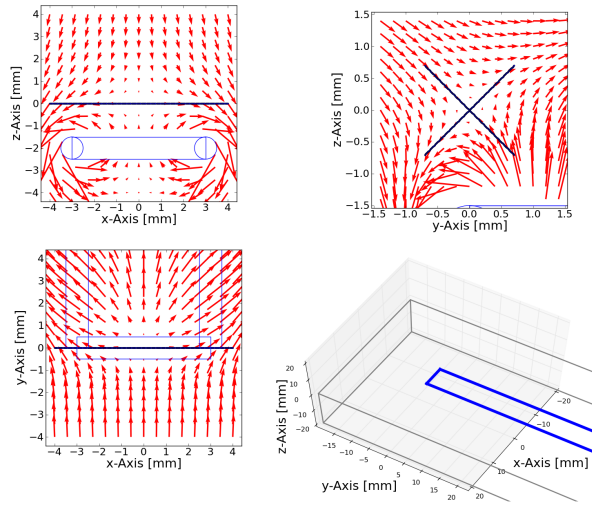
Figure 20: 3D export pictures of a simple U configuration.

To check if the wire layout and the current direction is correct, the function *plot_wire_3d()* can be used to plot the geometry and the current directions in 3 projections and the function *plot_profile()* can be used to plot x, y and z views of the arrangement as shown in figure 20. There is also a contour plot possibility as shown in figure 21 which is added to the vector plots to have a better illustration of the field.
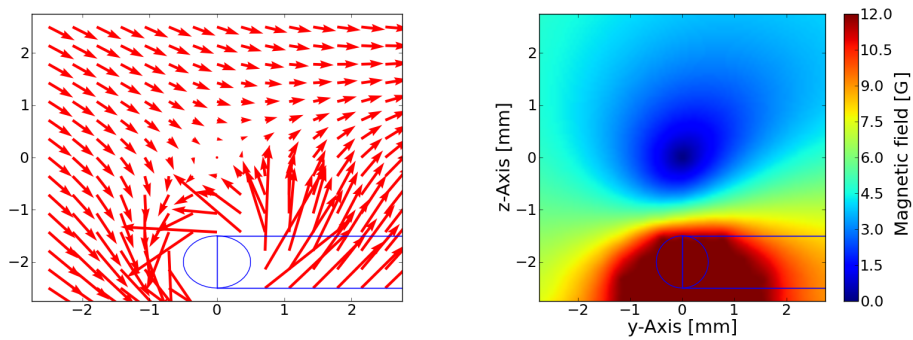
Figure 21: Export plots of a simple U configuration, vector plot (middle) and contour plot (right)

3.3 Magnetic Field Simulation in Comsol

To simulate the chip design in a finite element program and compare the results the software COMSOL Multiphysics v 4.3 has been used. Comsol (former Femlab) is a powerful analysis software with a lot of possibilities. To understand the program it is helpful to start with rebuilding a pre-designed example. There are many examples given in the manual, but none of them shows how to get a magnetic field above a wire configuration, therefore a documentation how to simulate a magnetic field in Comsol is given below.

Example of a wire geometry

The following report can be rebuilt in Comsol v4.3 step-by-step. It describes how to create and export a magnetic field of a current-carrying U wire geometry.
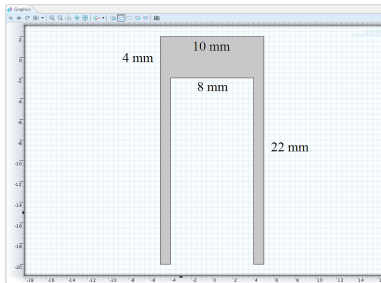
Layout
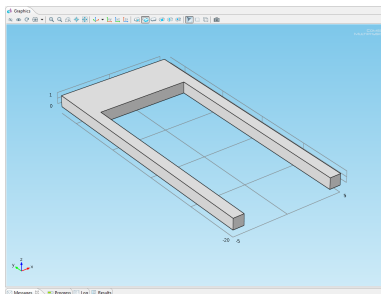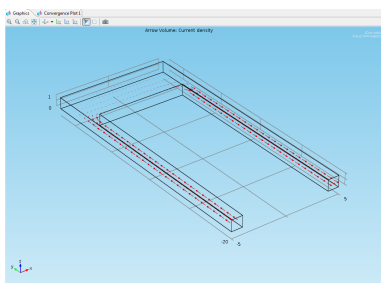
Start electric density: New $\Rightarrow$ 3D $\Rightarrow$ Next
AC/DC $\Rightarrow$ Electric Currents $\Rightarrow$ Next
Stationary $\Rightarrow$ finish
Global Definitions $\Rightarrow$ right click $\Rightarrow$ Parameter
Add: cuurent, expression=60 $[A/cm^2]$
Geometry: Geometry 1 $\Rightarrow$ Length unit: mm
Geometry 1 $\Rightarrow$ right click $\Rightarrow$ Work Plane
Plane Geometry $\Rightarrow$ draw a U
Work Plane 1 $\Rightarrow$ right click $\Rightarrow$ Extrude $\Rightarrow$ Build All

Layout in 3D

Material: Materials $\Rightarrow$ right $\Rightarrow$ Open Material Browser
AC/DC $\Rightarrow$ Copper $\Rightarrow$ right $\Rightarrow$ Add Material to Model
Copper $\Rightarrow$ Selection $\Rightarrow$ 1
Electric Currents $\Rightarrow$ right $\Rightarrow$ Normal Current Density
Selection 2 $\Rightarrow$ Normal current density: "current"
Electric Currents $\Rightarrow$ right $\Rightarrow$ Normal Current Density
Selection 9 $\Rightarrow$ Normal current density: "-current"

Current density

Evaluation: Study 1 $\Rightarrow$ right $\Rightarrow$ Compute
Results $\Rightarrow$ right $\Rightarrow$ 3D Plot Group
3D Plot Group 1 $\Rightarrow$ right $\Rightarrow$ Arrow Volume
Arrow Volume 1 $\Rightarrow$ points x/y/z: 30/30/1 $\Rightarrow$ Plot
Geometry magnetic field: Geometry 1 $\Rightarrow$ Sphere
Sphere 1 $\Rightarrow$ Radius: 30 $\Rightarrow$ Build All
Materials $\Rightarrow$ right $\Rightarrow$ Open Material Browser
Ac/DC $\Rightarrow$ Air $\Rightarrow$ right $\Rightarrow$ Add Material to Model
Air $\Rightarrow$ Selection $\Rightarrow$ 1
Copper $\Rightarrow$ Delete selection: 1
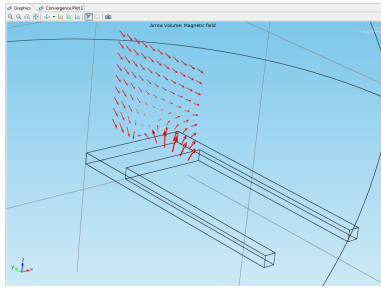
Magnetic field

External field: Model 1 ⇒ right ⇒ Add Physics
AC/DC ⇒ Magnetic Fields ⇒ Next
Stationary ⇒ Finish
Magnetic Fields ⇒ right ⇒ External Current Density
External Current Density ⇒ Selection 2 (Work Plane)
Add J x/y/z: ec.Jx/ec.Jy/ec.Jz
Magnetic Fields ⇒ right ⇒ Magnetic Field
Magnetic Field 1 ⇒ Selection 1 (Sphere)
Add J x/y/z: 0/-17/-7
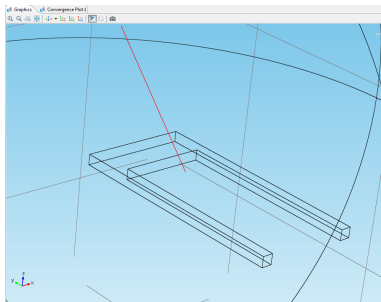
Cut line

Show magnitc field: Study 1 ⇒ right click ⇒ Compute
Results ⇒ right click ⇒ 3D Plot Group
3D Plot Group 2 ⇒ right ⇒ Arrow Volume
Expression: mf.Bx/mf.By/mf.Bz
x/y/z: 0/range(-5,1,5)/range(1,1,10)
Export line: Data Sets ⇒ right ⇒ Cut Line 3D
Cut Line 3D 1 ⇒ Add: 2 Points of your choice
Export ⇒ right ⇒ Data
Data 1 ⇒ Data set: Cut Line 3D 1
Advanced ⇒ Resolution: Costum ⇒ 1
Add Expression: mf.By/mf.Bx ⇒ Export

Comparison with Finitewiresolve 1.0

Finitewiresolve 1.0 is an approximation using the Biot-Savart solution of an infinitesimal thin wire configuration. Comsol is a finite element analysis tool which enables a calculation of a wide range of physical situation. With this quantity of functions Comsol can include a lot of environmental based boundary conditions (like the influence of the copper mount). It also can solve the current density of a hole in a conductor with a very heigh precision. However, with this range of functions, Comsol is also complicated and not easy to use. The rendering time for a simple magnetic field can go up to minutes. This fact makes it hard to test small changes or even geometry optimizations. It is also hard to comprehend the procedures of the program and understand errors while compiling. In Finitewiresolve 1.0, it is much easier to handle the data and create output files. This is why it is efficient to use Finitewiresolve 1.0 to find a first rough approximation and optimize the values, and use Comsol to verify the configuration and analyse the impact of complex boundary conditions.

3.4 Chip Wire Design

In this section, two versions of the MOT wire layout are evaluated and compared, to find the best possible solution for the requirements described in section 3.1. This two versions are calculated and optimized in Finitewiresolve 1.0 to find the best possible quadrupole field. Both versions require an external magnetic field which can be generated by 3 dimensional Helmholtz coils. In section 3.4.4 a specific wire configuration is examined. This so called bias wires are able to replace the external field to a certain amount and should make it possible to run the MOT without the Helmholtz coils. In this section the viability of this arrangement are analysed together with the impact of the environmental influences. In the last section the final values and results are discussed.

3.4.1 Version 1: Two U-shaped wires

The first version is probably the most simple one. It consists of two U wires which are formed out of two copper wires and mounted on the chip plate. The wires need to be covered by a Kapton layer for electrical isolation.
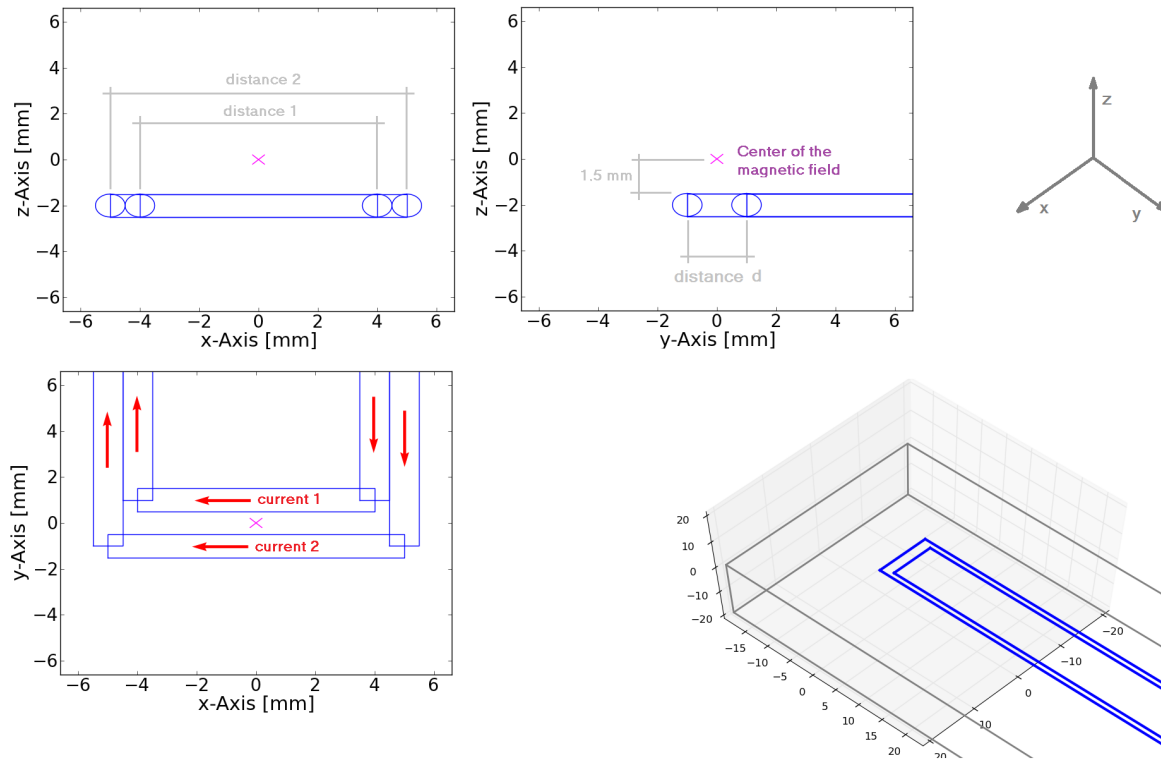
Figure 22: Python plots of the double U wire geometry.

The idea of this layout is to have at least 1 mm space between the two wires which is needed for the 1 mm hole. The advantage is that the individual currents and therefore the coordinates of the center of the magnetic field can be controlled by two different conductors. So there is the possibility to change the height of the field center for an constant external field. Figure 23 shows the movement of the field center when only changing one current value.
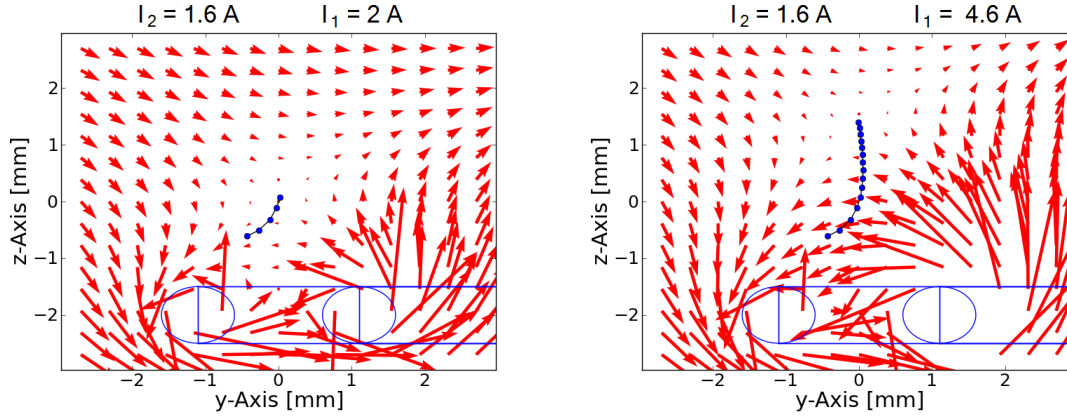
Figure 23: Movement of the field center when changing the current in the right wire (I_1), the current in the left wire (I_2) is fixed and the magnetic field is (0,2.38,-1.25) G.

The second wire can be used to bring the field center back between the wires, see table 2. The field vectors on the 45° line rotate when the field moves left, so the second wire also can be used to rotate the vectors back to 45° and therewith optimize the quality of the quadrupole field as described below.

Current 1	Current 2	Height	Average $|\alpha|$ on y'
1.5 A	1.4 A	-0.681 mm	0.191
2.0 A	1.6 A	-0.001 mm	0.039
2.5 A	1.7 A	0.404 mm	0.057
3.0 A	1.7 A	0.695 mm	0.078
3.5 A	1.7 A	0.940 mm	0.083
4.0 A	1.6 A	1.131 mm	0.86
4.5 A	1.6 A	1.354 mm	0.096
5.0 A	1.5 A	1.516 mm	0.105

Table 2: Table of current 1 controls the height of the field and current 2 makes sure that the position of the field center is above the hole. The external field is (0,2.38,-1.25) G. The height value is the position of the field center on the z axis.
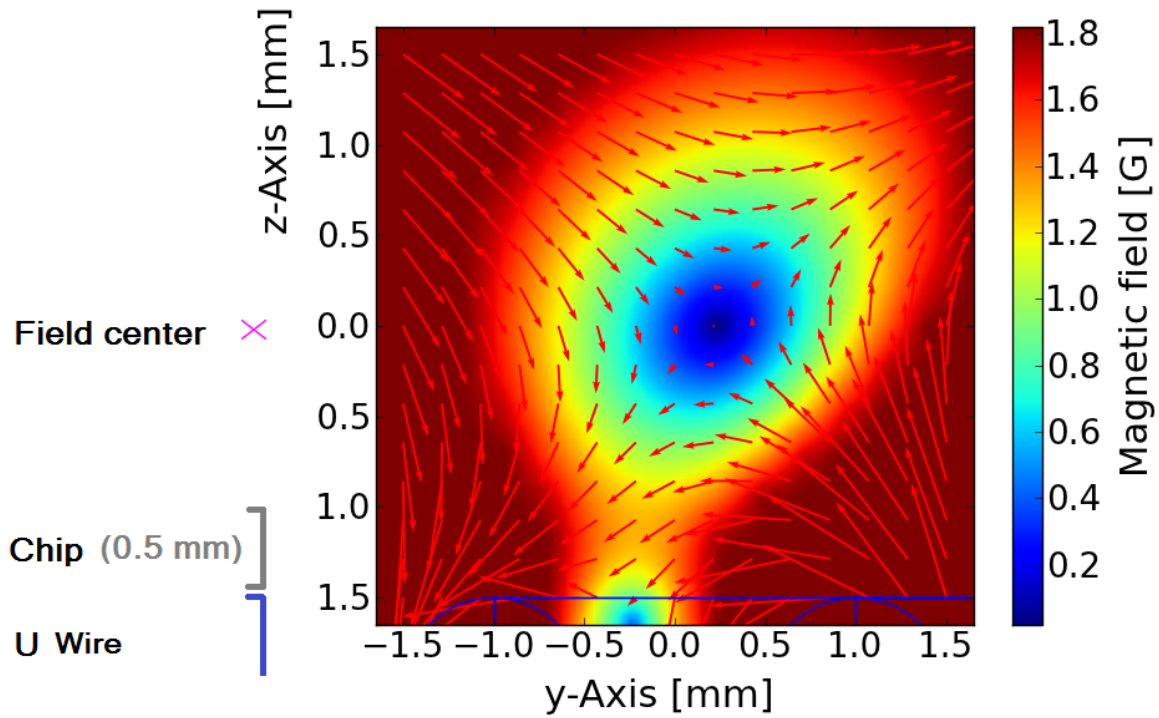
Figure 24: Field center above the double U wire, slightly shifted.

Finding the most effective quadrupole field is an iterative process because the control parameter influence each other. The parameter for the geometry and the current values need to to be optimized to realize an appropriate quadrupole field. The center should be fixed 1 mm above the surface of the chip. This means for a wire with a diameter of 1 mm and a chip plate with a thickness of 0.5 mm the center of the field needs to be 2 mm above the center of the wires in (along the z axis). In the entire manuscript this coordinate is defined as point (0,0,0).
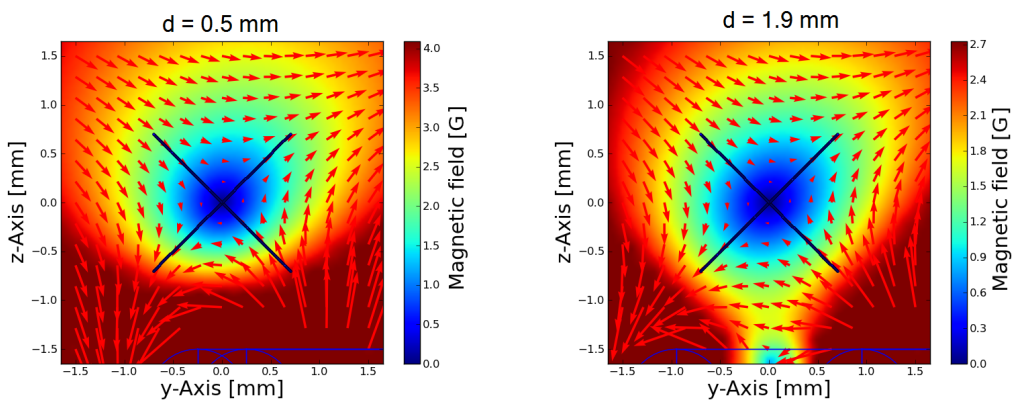
Figure 25: Two plots of the quadrupole field for lower quality values (left) and higher quality values (right)

30
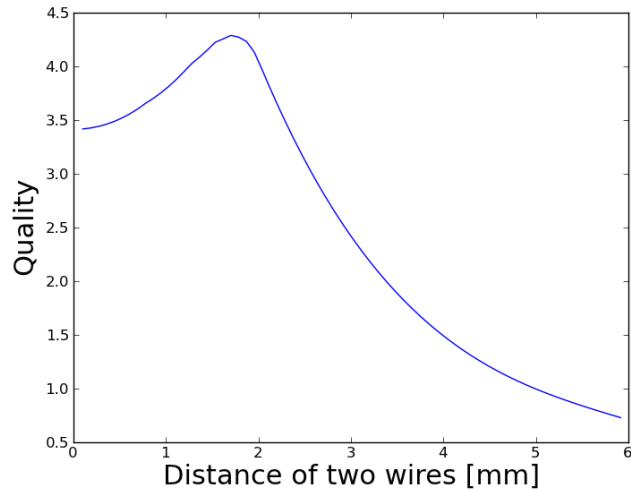
Figure 26: Plot of an optimisation run. The changed parameter was the distance d between the two wires and the quality is the inverse of the sum of the three average angular deviations. The magnetic field is calculated to have the zero field position in point (0,0,0).

As it can be seen in figure 25 the distance between the two U wires changes the shape of the quadrupole field. The field vectors should be as parallel to the laser rays (y' and z') as possible. In the (y,z) plane this is 45° along the axes in the figure. By running an optimisation code it was found that the best results are obtained around a distance of 1.9 mm between the two wires (center to center). The plot in figure 26 shows the results of the quality value calculation. For values above 5 mm the quadrupole field gets unusable. In general the range of usable distances is quite large, this offers the possibility of choosing the distance to have 1 mm space between the wires.

Change	Calculated minimum					Quality values			
Distance d	Current [A]		Magnetic Field [G]			Average $|\alpha|$ [°]		Max $|\alpha|$ [°]	
	1	2	x	y	z	y'	z'	y'	z'
1.8 mm	3.0	3.0	0.0	4.65	-2.21	0.123	0.110	10.8	14.8
1.9 mm	3.0	3.0	0.0	4.56	-2.21	0.118	0.113	9.7	14.6
2.0 mm	3.0	3.0	0.0	4.47	-2.21	0.115	0.122	9.3	14.5
2.2 mm	3.0	3.0	0.0	4.29	-2.21	0.116	0.143	8.8	14.2
2.4 mm	3.0	3.0	0.0	4.1	-2.21	0.116	0.169	7.5	13.6
2.6 mm	3.0	3.0	0.0	3.9	-2.2	0.123	0.204	8.6	16.8
2.8 mm	3.0	3.0	0.0	3.71	-2.2	0.187	0.252	12.9	24.6

Table 3: Example of optimization code results.

31

Table 3 shows a compendium of values to optimize the distance d. The currents in both wires are equal and the field is changed to control the field position. As it can be seen, the best value would be around 1.9 mm. However the experiment needs a hole of 1 mm. For a wire diameter of 1.1 mm the first possible value for distance d is 2.2 mm. At this value, the quality of the quadrupole field is pretty good.
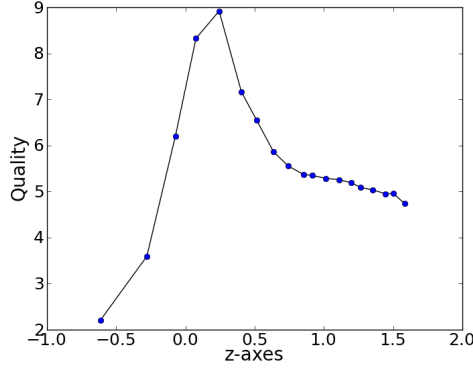
Figure 27: Plot of the quality values on y' and z' for different positions of the quadrupole field on the z-axis above the two wires.
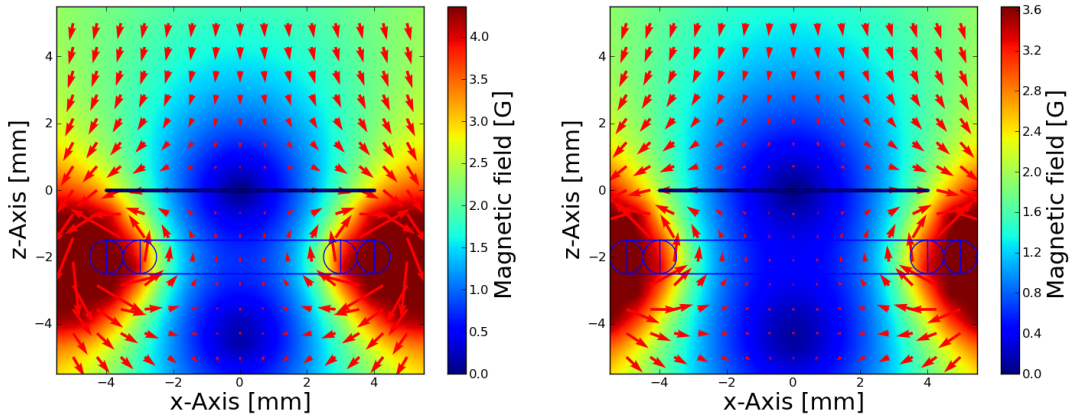
Figure 28: Quadrupole field in x direction for different widths of the U wire.

Optimizing the field in x direction is important to determine a good value for the width of the U wires to realize a good quadrupole field in (x,z) plane and (x,y) plane as well. Figure 28 shows two plots with different widths of the double U wire. It turned out, that the quality mostly depends on the external field in z direction. However this quality value is mostly a result of the wire construction itself and can not be controlled to a great extend. The width of the two U's have just a small influence, but it turned out that a good value for the width of the inner U wire is between 7 to 8 mm. The outer U has to be two times the wire diameter larger in this case.
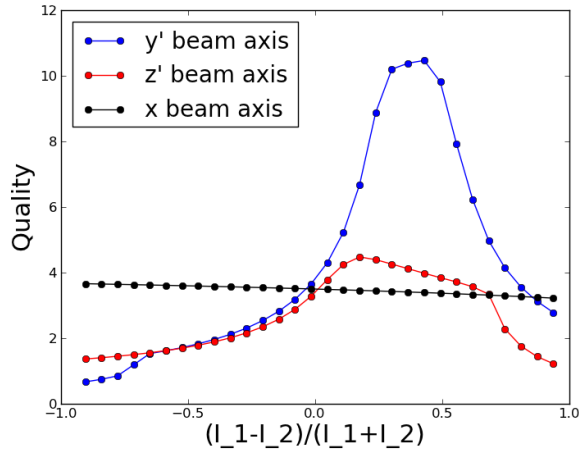
Figure 29: Quality values for different current ratios.

Figure 29 shows a plot where the current parameters in the wires are changed and the resulting quality values are plotted. The x axis quality is very constant for all current ratios. The quality values along the y' axis are better then on the z' axis. The calculation predicts that it is better to have a factor of about $\frac{4}{3}$ more current in wire 1 than in wire 2. Note that the quality value in the plot depicts one over the effective average angular value on the axes to get a better illustration of the quality values.
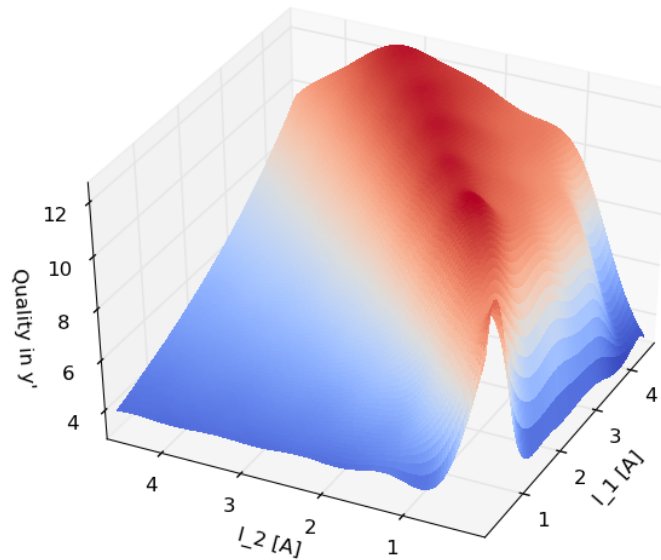
Figure 30: Quality along the y' axis in 3d view (right). It can be seen that the quality is better if the current in I_1 is a little bit larger.

Field amplitude and gradient

By making plots along the laser beam axes y', z' and x, the field characteristics can be analysed. Figure 31 to 33 are showing the resulting curves. The values are the projection on the laser beam axes. Typical values for MOT gradients are around 10 to 15 $\frac{G}{cm}$ [14, p=473]. This was modified with the variable parameters as well.

Resulting fields With the optimisations, useful configurations where found which provide the required fields. Below are the resulting plots of the field characteristics along the laser lines with the corresponding gradient curves.
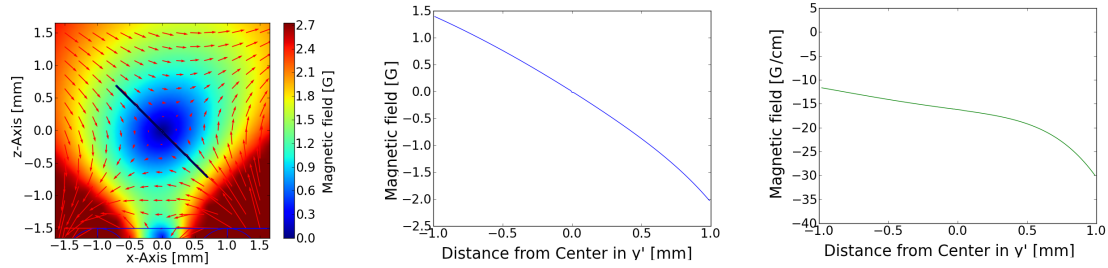
Figure 31: Field characteristics along y', line of points (left), intensity projection (middle) and gradient (right)
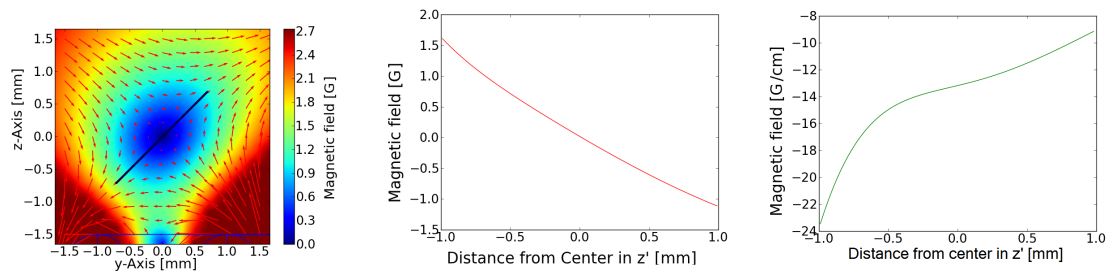
Figure 32: Field characteristics along z', line of points (left), intensity projection (middle) and gradient (right)
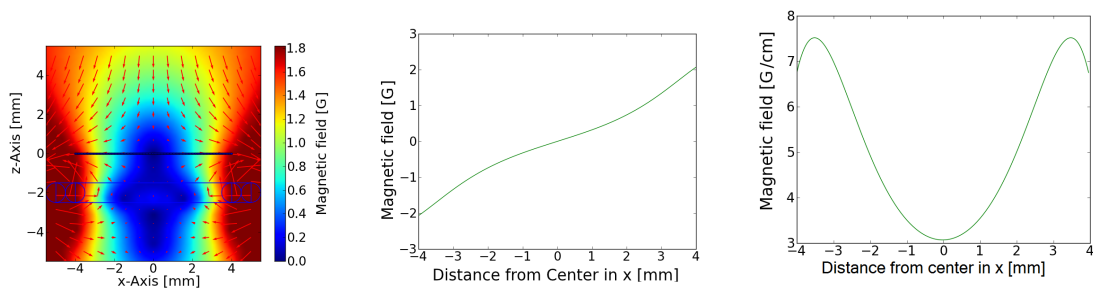
Figure 33: Field characteristics along x, line of points (left), intensity projection (middle) and gradient (right)

Final parameters

It could be demonstrated that the values obtained from the optimisation codes lead to a reasonable quadrupole field. The final geometry depends on the wire types used and is discussed later. The final values for the currents and the external field can also be optimized with the codes in the program. Some resulting example is given in table 4 and the corresponding quality values are listed in table 5.

Variable	Value
Current 1	3.3 A
Current 2	2.6 A
Field x	0 G
Field y	3.9 G
Field z	-2.25 G
Distance d	2.15 mm
Wire diameter	1.1 mm
U width	8 mm

Table 4: Example of good parameters for Version 1

Quality sheet			
	y'	z'	x
Average $|\alpha|$	0.097°	0.177°	0.31°
Max $|\alpha|$	6.4°	17.1°	25.8°
Average gradient	14.4 G/cm	15.1 G/cm	5.2 G/cm

Table 5: Resulting values of the quality calculation.

Version 1 turned out to be a promising possibility. The wire configuration can be easily implemented in the chip mounting and the quadrupole field is usable. The materials are comparative cheap and as an additional advantage the field quality and position can be controlled by two current carrying wires.

3.4.2 Version 2: Rectangular with hole

The second version seems like a very natural solution for the MOT. As known from literature [15], a rectangle formed U (Figure 34) provides a very useful quadrupole field. In this version the rectangle contains a hole in the middle of the U for optical access. The main part in this section will be to check the influence of the hole on the shape of the quadrupole field. To calculate if this version can be used for our project, a standard rectangle shaped U-MOT (without a hole) has been calculated at first and optimised for a perfect quadrupole field. This was done again mostly in Finitewiresolve 1.0.
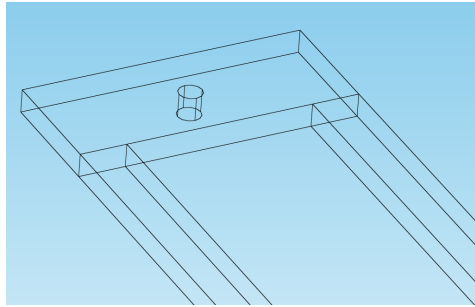
Figure 34: Version 2 design in Comsol Multiphysics.

The rectangle approximation in Finitewiresolve 1.0 is shown in figure 35. To find good values for geometry the optimisation codes have been updated. The density approximation was done by splitting the rectangle into 5 equal square parts[3] each with a slightly different current density (balanced with Comsol).
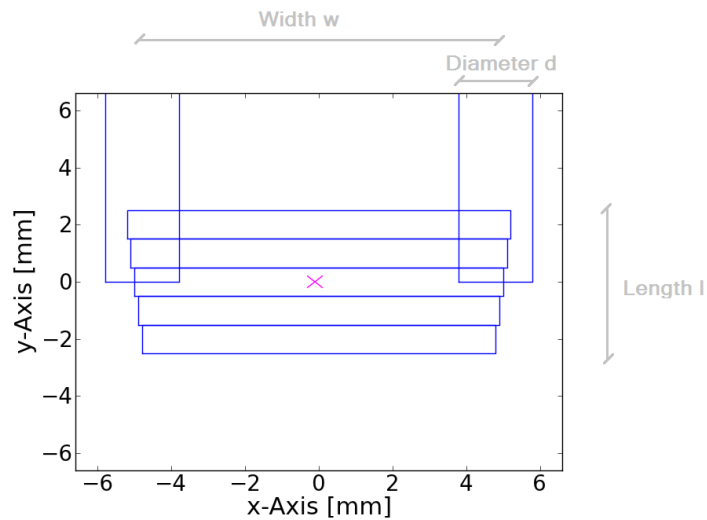
Figure 35: Version 2 design in Finitewiresolve without hole.

---

[3]It has been shown in section 3.2 that the solution of a square line can be well approximated by an infinite wire.

Optimisation

To find the optimum length l of the rectangle, the optimisation code in the Python program was updated. A main difference to the optimisation procedure in Version 1 was that fewer parameters are applicable. The program can only use one current value to control the position of the field. Therefore the program needs the external magnetic field to change the field position and bring the field center 1.5 mm above the configuration to operate with the optimisation codes.

Change	Calculated minimum		Quality values			
Length	Current [A]	Field [G]	Average $|\alpha|$		Max $|\alpha|$	
			y'	z'	y'	z'
3.0 mm	5.0	0, 4.0 , -1.68	0.095	0.137	14.4	15.3
3.5 mm	5.0	0, 3.81 , -1.68	0.083	0.123	12.2	14.4
4.0 mm	5.0	0, 3.62 , -1.67	0.075	0.112	10.7	13.8
4.5 mm	5.0	0, 3.44 , -1.67	0.071	0.103	9.7	13.3
5.0 mm	5.0	0, 3.26 , -1.67	0.074	0.095	9.1	12.9
5.5 mm	5.0	0, 3.1 , -1.67	0.084	0.09	8.7	12.7
6.0 mm	5.0	0, 2.95 , -1.67	0.102	0.095	9.7	13.6
6.5 mm	5.0	0, 2.81 , -1.67	0.115	0.092	10.1	13.9

Table 6: Example of an optimization run for the length l of the U-MOT rectangle.
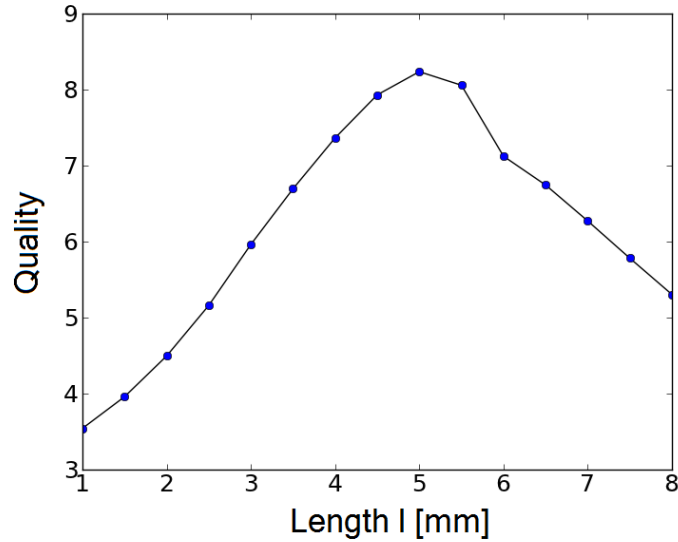
Figure 36: Version 2 quality value for different length l along the y' and z' axis.

Field amplitude and gradient

After optimising the quality values in the (y,z) plane, it was found, that the quality in x-direction is again not much controllable, the best configuration is shown in table 7. The plots for the field intensities along the laser beam axes are shown in figure 37 to figure 39 below.
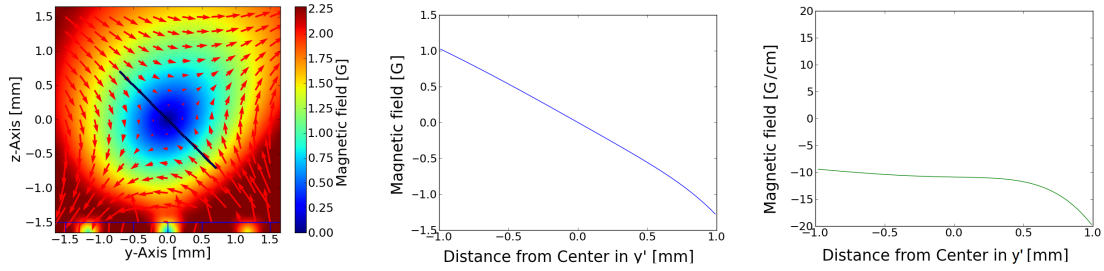
Figure 37: Field characteristics along y', line of points (left), intensity projection (middle) and gradient (right)
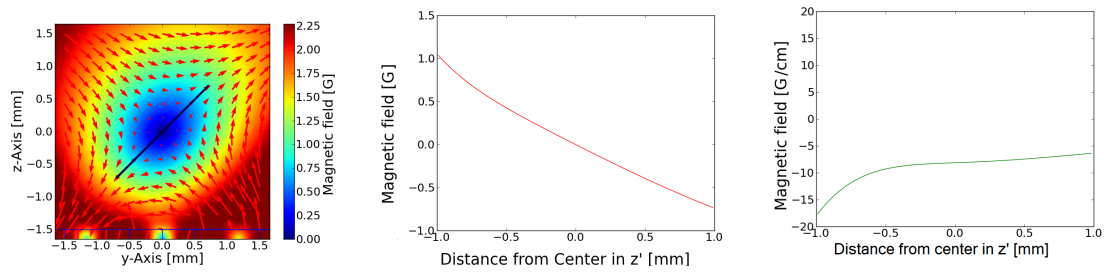
Figure 38: Field values for z', line of points (left), values (middle) and gradient (right)
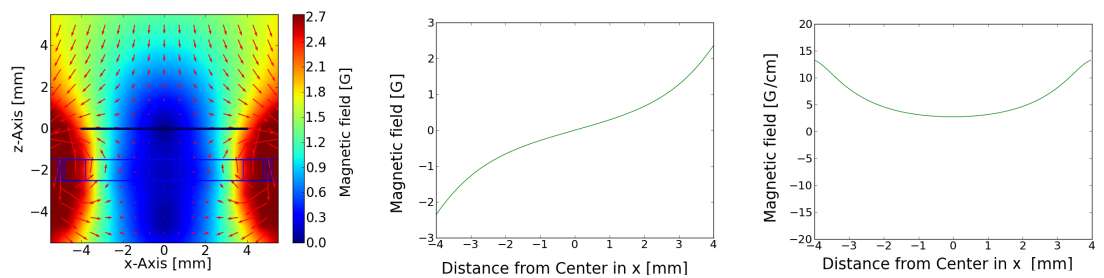
Figure 39: Field characteristics along x, line of points (left), intensity projection (middle) and gradient (right)

Variable	Value
Current	6 A
Field x	0 G
Field y	4.0 G
Field z	-1.88 G
Length l	5 mm
Width w	10 mm
Diameter d	2 mm

Table 7: Final values for version 2 without hole.

Quality sheet			
	y'	z'	x
Average $|\alpha|$	0.073°	0.102°	0.27°
Max $|\alpha|$	9.8°	13.7°	20.9°
Average Strength	10.4 G/cm	9.9 G/cm	6.2 G/cm

Table 8: Results of the quality calculations.

The quality values in table 8 are pretty close to version 1. The values along z' and x direction are slightly better. This comes from the lager width w and the rectangular shape.

Influence of the hole
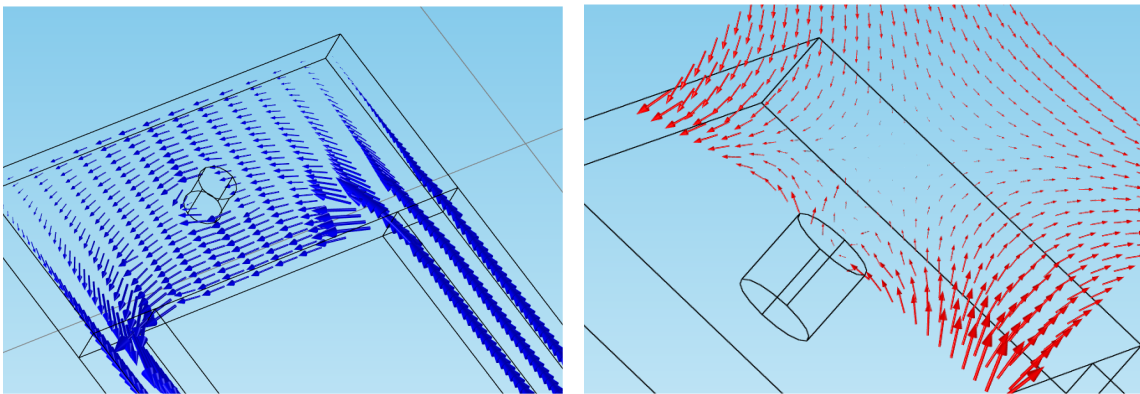
Figure 40: Solution of the geometry in Comsol. Current density (left) and field in (y,z) plane (right)

In the next step the influence of the hole has been considered. To measure the impact of the hole, the geometry was calculated in Comsol. In figure 40 current density and the field of the U-MOT is shown. To analyse the field, a closer look to the critical area was taken.
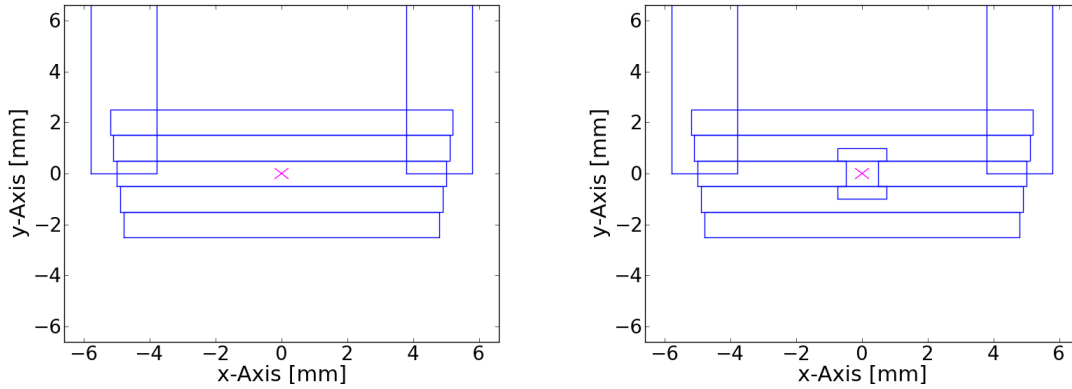
Figure 41: Geometric approximated current lines for the rectangle, without hole (left) and with hole (right).

The current density lines in Finitwiresolve 1.0 where updated to incorporate the hole, shown in figure 41. The current density from the middle line now splits into two parts around the hole. To get a useful current distribution, the solution was cross-checked with Comsol again.
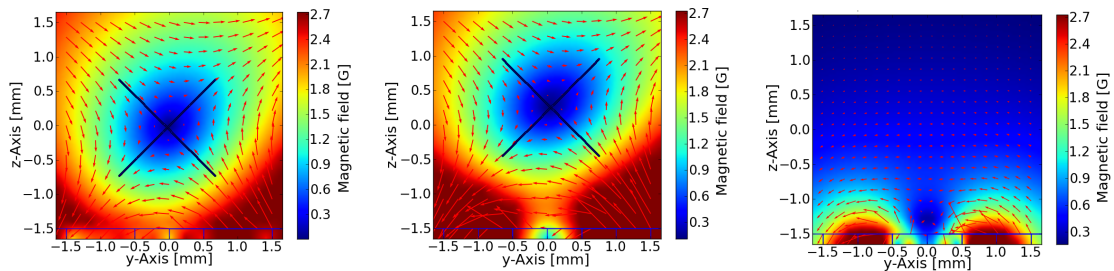
Figure 42: Impact of the hole: No hole (left), 1 mm hole (middle) and field difference (right). I=5 A and field=0/3.8/1.7 G.

In figure 42 the shift of the center caused by the hole is shown. The area where the field is affected is shown on the right side, where the difference of the two fields is plotted. In figure 43 the field with hole in (x,z) plane can be seen.
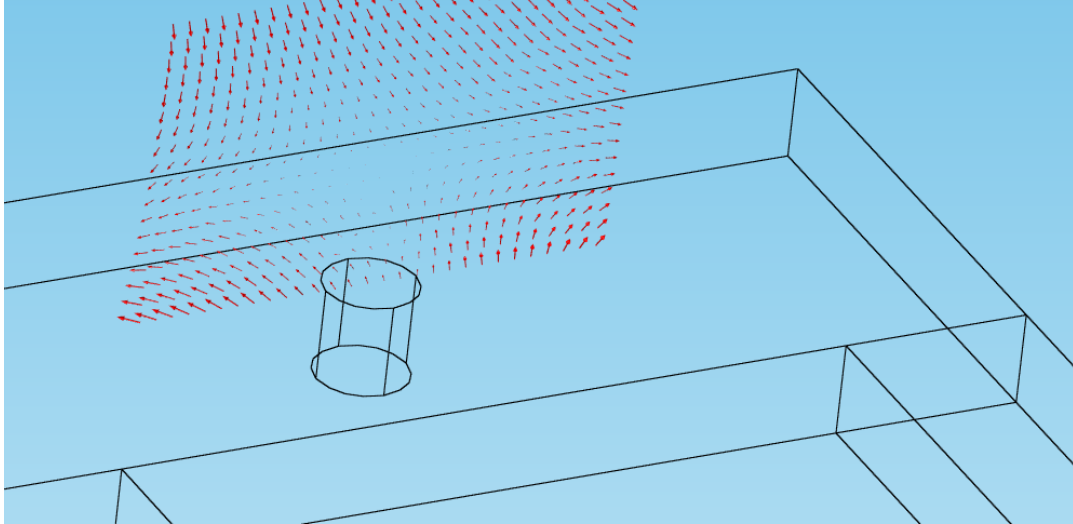
Figure 43: Magnetic field in (x,z) plane.

Final values

The geometric approximation in Finitewiresolve 1.0 is shown in figure 41. The adjusted MOT values are listed in table 9.

Variable	Value
Current	5.5 A
Field x	0 Gs
Field y	4.0 Gs
Field z	-1.8 Gs
Length l	5 mm
Width w	10 mm
Diameter d	2 mm
Hole	1 mm

Table 9: Final values for version 2 with hole.

In figure 44 the optimised quadrupole field with and without a hole in the U-wire structure is shown. It can be seen, that the influence of the hole is not degrading the field near the center. In the x direction the influence can almost be totally neglected. The quality values also do not suffer from the hole, because the 45° lines are pretty similar. The final "influence area" is shown in figure 45.
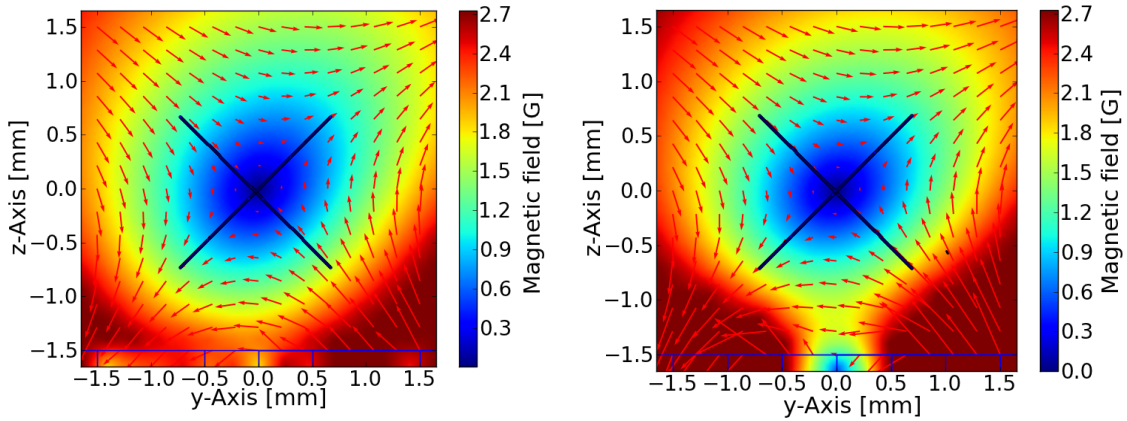
Figure 44: Resulting fields, without hole (left) and with hole (right).
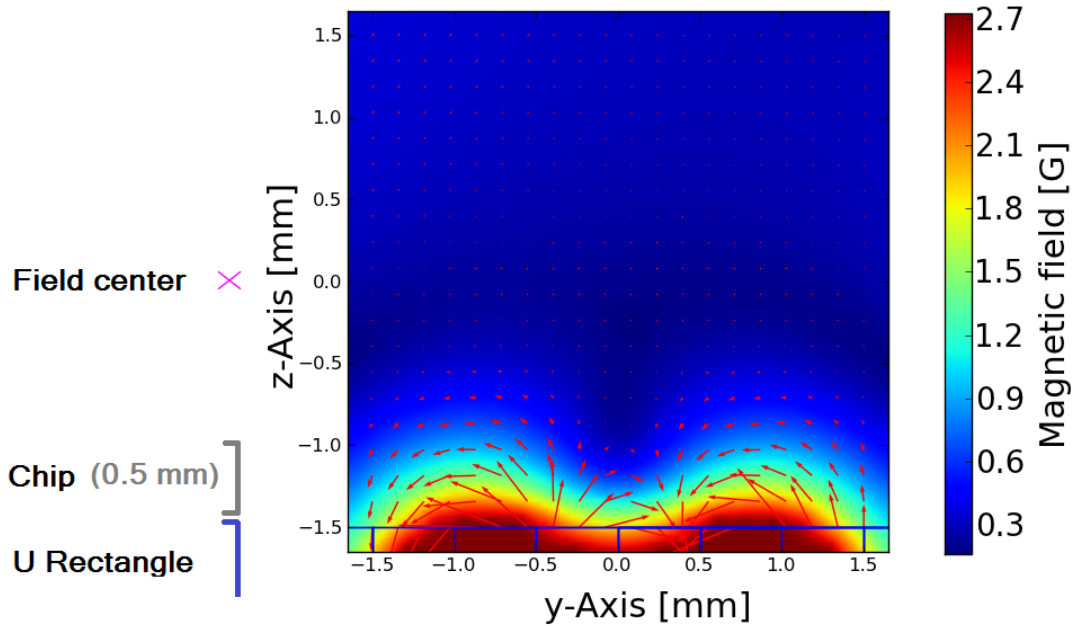
Figure 45: "Impact area" of the hole visualized by a subtraction of the fields from the U rectangle MOT with and without hole when the center of the field is in the same position.

Conclusion

The area affected by the presence of the hole is limited to the first 0.5 mm above the surface. This is where the chip is placed afterwards so there will never be atoms to catch. The calculation hence shows that the influence of the hole is too small to cause a significant deformation to the shape of the quadrupole field and therefore version 2 can be accepted as a good option.

3.4.3 Compare Versions

Both versions are able to provide quadrupole fields of sufficient quality, shown in figure 46. Version 2 has slightly better quality values and is probably able to trap more atoms because of the rectangular shape. Version 1 has the advantage of being very simple and easy to produce. Another advantage of version 1 is that the height of the quadrupole field can be controlled (and moved) by two current carrying wires. In version 2 there is just one current to change to position of the field, so the external magnetic field needs to be changed as well what made it a little bit more complicated[4].
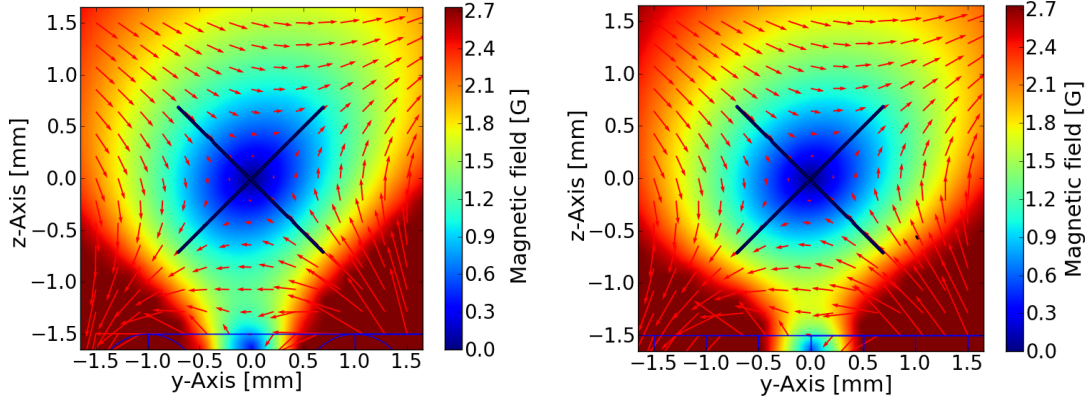
Figure 46: Quadrupole field in (y,z) plane of Version 1 (left) and Version 2 (right).

Production

Version 1 can be realized by milling two grooves into a plate and put two isolated wires in it. The problem is that the wires have a finite bending radius so the realisation can not be done with a perfect edge. The second version can be produced by milling a copper block to the rectangular shape and stick it on a ceramic block which isolates the copper structure from the mounting. This procedure is rather standard, but also elaborate and expensive compared to version 1.

Conclusion

For this diploma theses we decided to realize Version 1, because of the practical advantages and it fulfils all our demands. However version 2 was identified as good option as well, so the mounting (which is explained later) can be modified to version 2 or some other structure by only changing the chip plate.

---

[4]Moving the position of the field can be used to bring the atom cloud near to the single atom traps in the later experiments.

3.4.4 Bias Field

So far, the external magnetic field is created from a set of 3d Helmholtz coils, which are placed around the glass cell. The mounting should contain a wire geometry which is able to mimic this field as good as possible. The wires should not block the laser rays or the experimental setup and of course also fit into the glass cell. The feedthrough flange on the backside is specified for a maximum current of 55 A. Isolated copper wires who fulfill our demands (UHV compatible) are available up to a diameter of 1.8 mm so the cooling is very crucial, to enable the required currents.
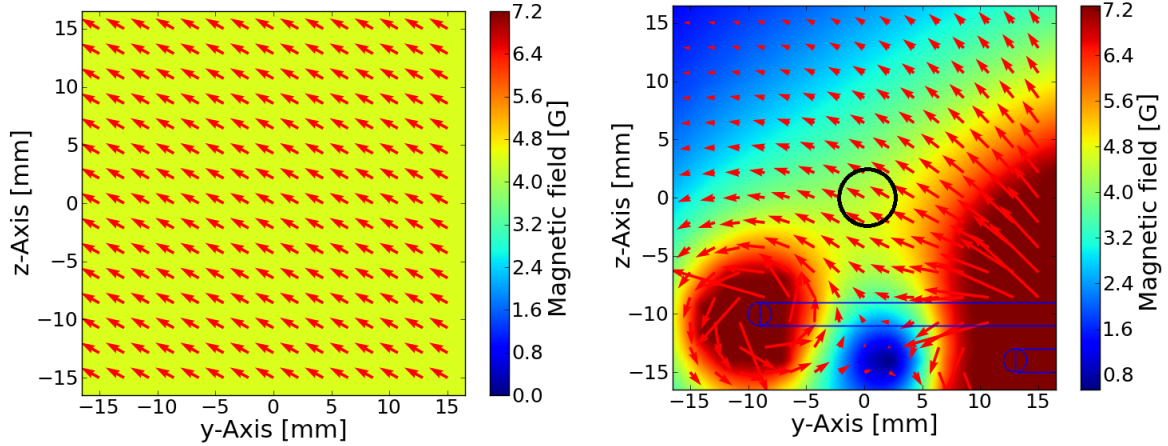
Figure 47: Required field (left) and provided field from two bias wires (right).

To find a good configuration, the created field needs to be reproduced as good as possible in the relevant area around the center of the field at point (0,0,0). Figure 47 shows on the left side the required field and on the right side the field that can be produced by two U wires (bias wires). The requested field in this plot is 4.42 G (Bx=0, By=-3.87 G and Bz=2.14 G) and the currents in the left wire is 15 A and 45 A in the right wire. They propagate in opposite direction as compared to the currents in the U-MOT wires on the chip.

Calculation of the field

Finitewiresolve 1.0 can be used to calculate the required currents in the bias wires. The functions work similar to the optimization codes as explained in section 3.2. At first it calculates the magnetic field in the required point (where the center of the quadrupole should be placed) by using the U-MOT wires with defined currents. Afterwards the program scans the currents in the two bias wires and compares the magnetic field in this point. If the generated field vector is equal a quadrupole field is resulting around this point accounted to the wire configuration. The result of the function is shown in figure 48.
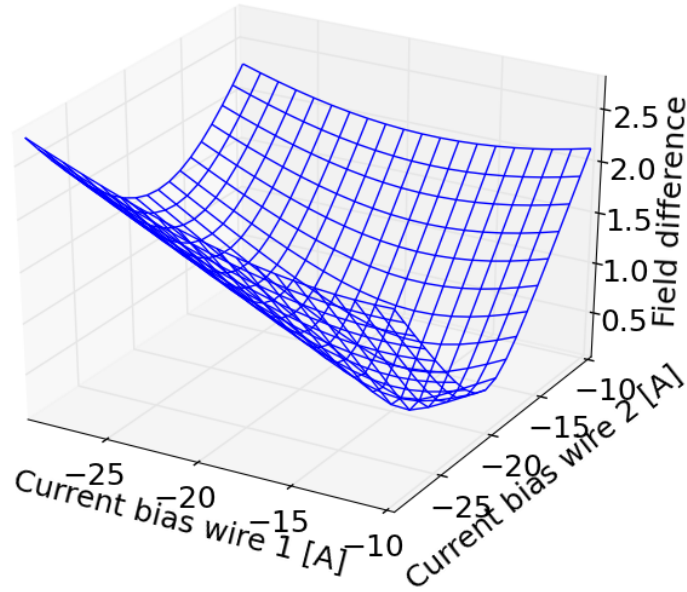
Figure 48: Plot to find the current settings in the bias wires to get the quadrupole field in point (0,0,0). U-MOT wires are constant.

In this example the currents of the bias wires need to be around -19.0 A and -14.0 A to locate the quadrupole field at the target point without an external field. The program can scan this area with smaller steps, interpolate them and find the current values with more accuracy. It can already be seen that there is only one set of currents that will produce the required field.
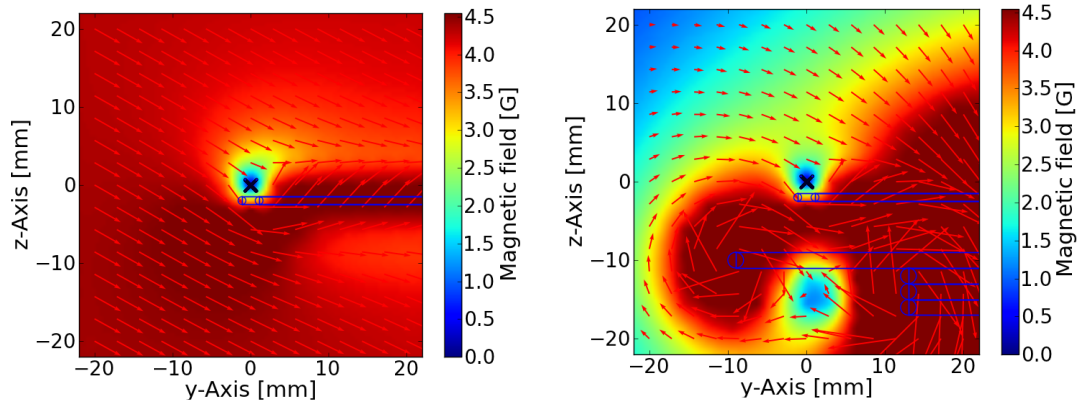
Figure 49: MOT field on a wide area: External field (left) and bias wire field (right).

In figure 49 the MOT is shown over a range of 40 mm. The deviation from the optimal field near the center can be calculated in Finitewiresolve 1.0 and should be as small as possible.
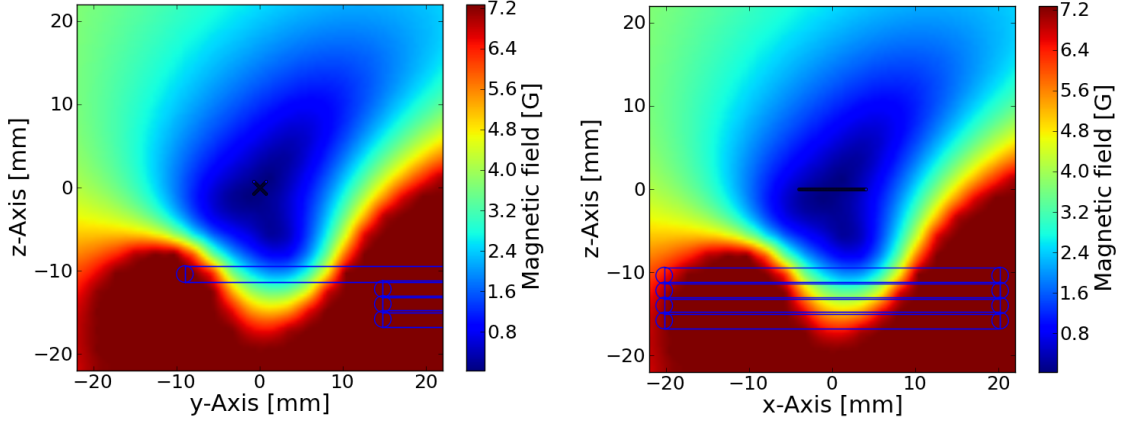
Figure 50: Difference plot substracting the external field from the bias wire field. The currents are: bias wire I_1=18.82 A and I_2=17.1 A. The magnetic field is (0., 4.22, -2.04) G.

To visualize the effect of the geometry it is possible to make a difference plots in Finitewiresolve 1.0. This means that both configurations are calculated and the results are subtracted from each other (see figure 50). Note that the MOT will need at least an area of $1\,\text{mm}^2$ in the (y,z) plane and 6 mm in the x direction, so in this area the field deviation needs to be as small as possible.
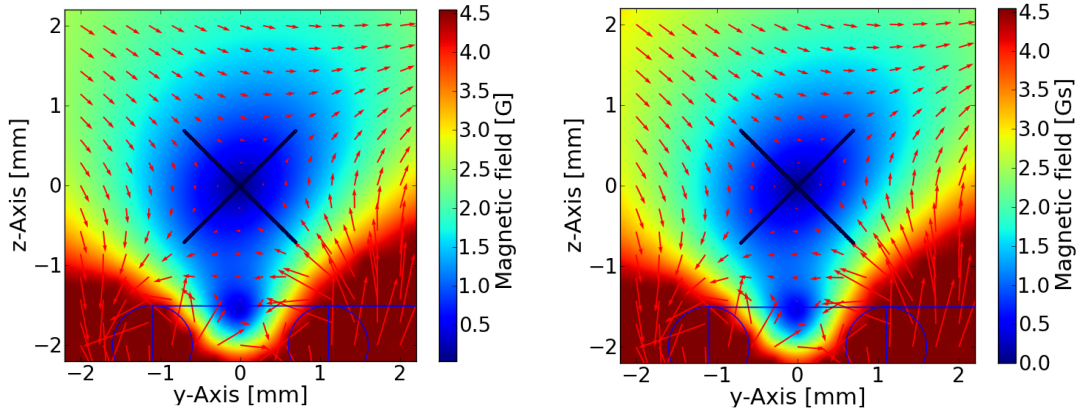
Figure 51: MOT field generated by: the external field (left) and the bias wires (right).

Figure 51 shows the quadrupole field from version 1 with an external field and generated from the bias wires. To see the impact of the bias wires compared to the external field, difference plots of the two fields are shown in figure 52 and figure 53. The deviation of the field along the laser beam axes is plotted on the right side. The currents in the U-MOT wires are I_1=3.6 A and I_2=2.8 A and in the bias wires the same values as in figure 50.
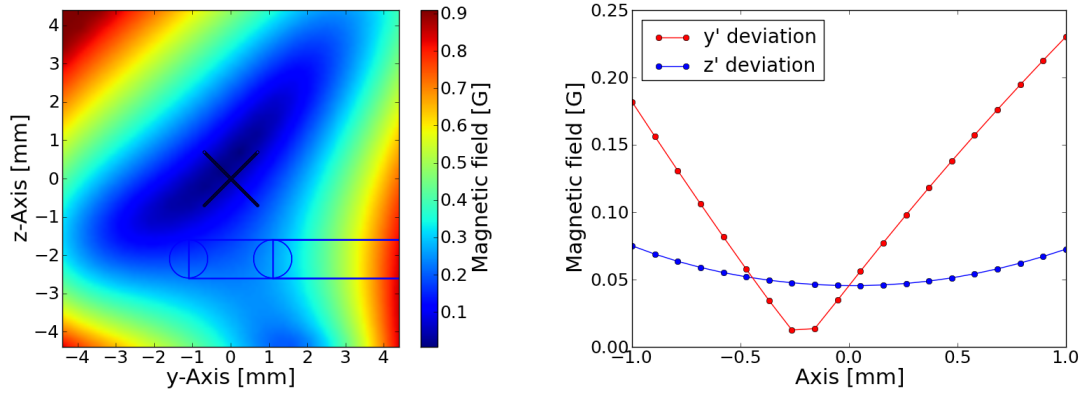
Figure 52: Difference plot of the quadrupole field in the (y,z) plane (left) and values on the y' and z' laser beam axis (right).
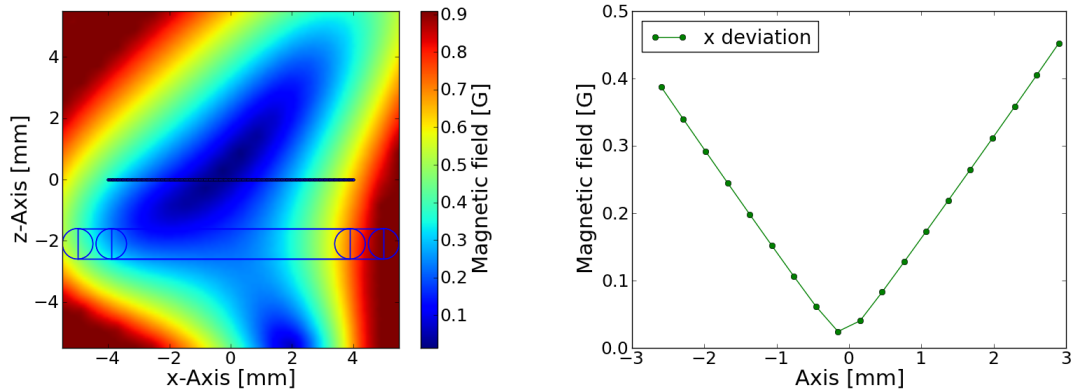
Figure 53: Difference plot of the quadrupole field in the (x,z) plane (left) and values on the x laser beam axis (right).

The deviation caused by the bias wires compared to an external field is $2.25\,\mathrm{G/cm}$ along the y', $0.25\,\mathrm{G/cm}$ along the z' and $1.66\,\mathrm{G/cm}$ along the x axes. Compared to the average gradient along this axis with the values from table 5 the largest influence is on the x axes where the field vectors get $32\,\%$ downscaled.

Bias wire geometry

Figure 54 shows the geometric arrangement found with Finitewiresolve 1.0. Bias wire 1 is winded 2 times, to alleviate the current and therewith reduce the heat production. The bias wires on the mounting are shown in figure 55 in Solidworks.

47
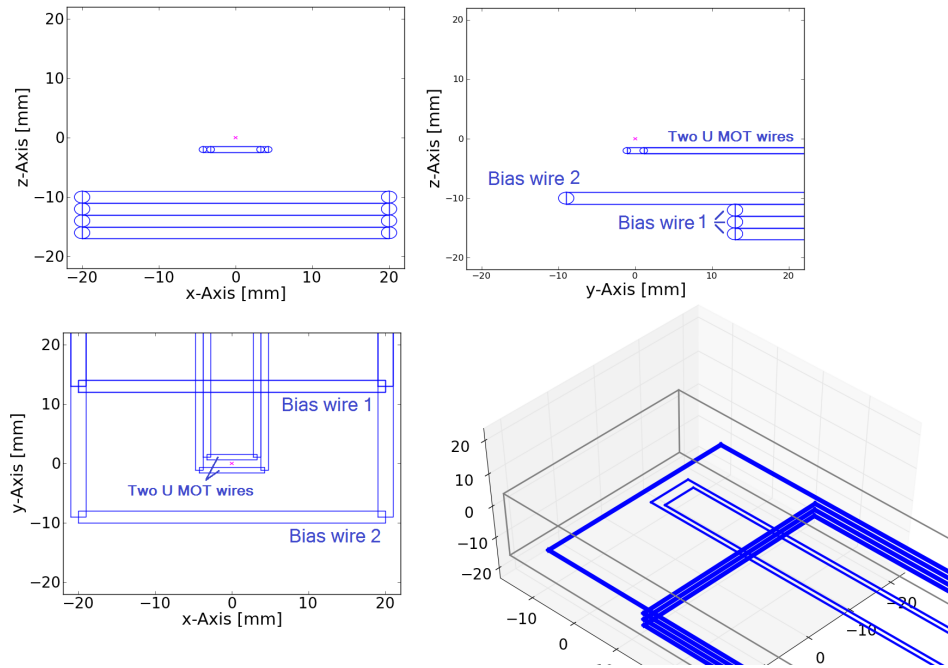
Figure 54: Profile plot of the geometric layout of the bias wires.
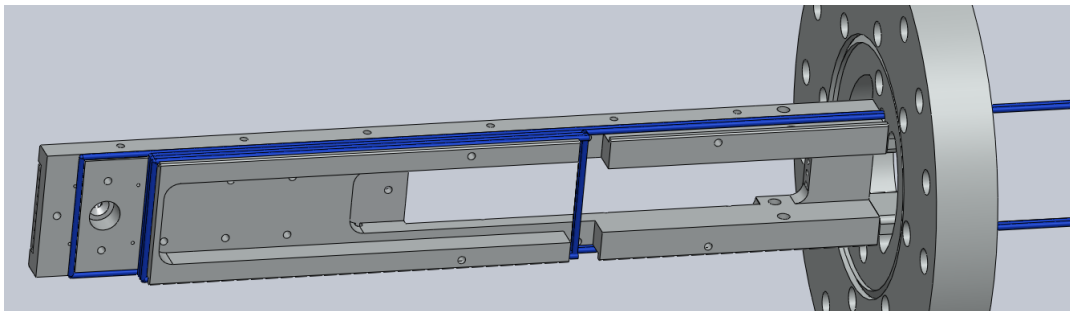
Figure 55: Mounting with the bias wires (blue).
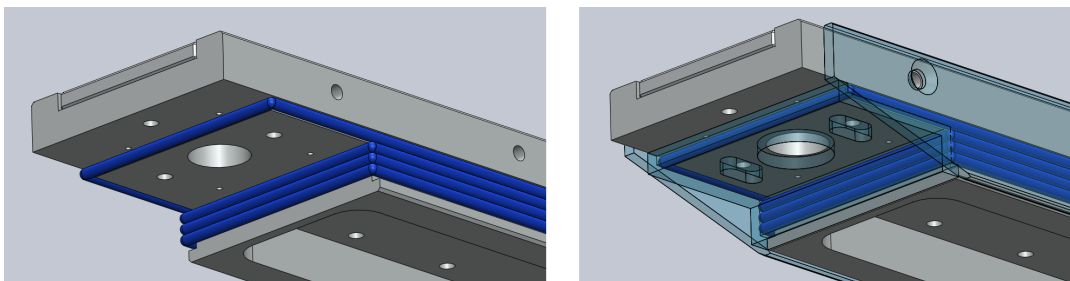
Figure 56: Wires on the head of the mounting (left) and with plates (right).

Heat production

In vacuum, the only way to dissipate heat of electric wires is by contact with other solids or to transfer the heat out of the chamber by the wire itself. Certainly, there is always a layer of isolation between the wire and the mounting. To reduce the heating as much as possible, the wires need to touch the mounting as much as possible, and the length of free standing wires in the vacuum need to be as short as possible. To create a force pushing the wires against the mounting wall, plates on the sides have been screwed on, shown in figure 56. The plates also fix the position of the wires.

Results

As the calculation has shown, the external field can be realized with a specially designed U wire geometry. The maximum deviation in the relevant area is 0.2 G in the (y,z) plane and 0.4 G on the x axis[5]. These influences reduce the quality of the field, which means that the optimization can never provide such a good quadrupole field as the external field. A special problem occurs along the x axis. The field strength on this axes is the smallest for the U-MOT in general, and with a bias field it gets even more weak. This will reduce the capturing rate a lot, as shown later in some calculation.
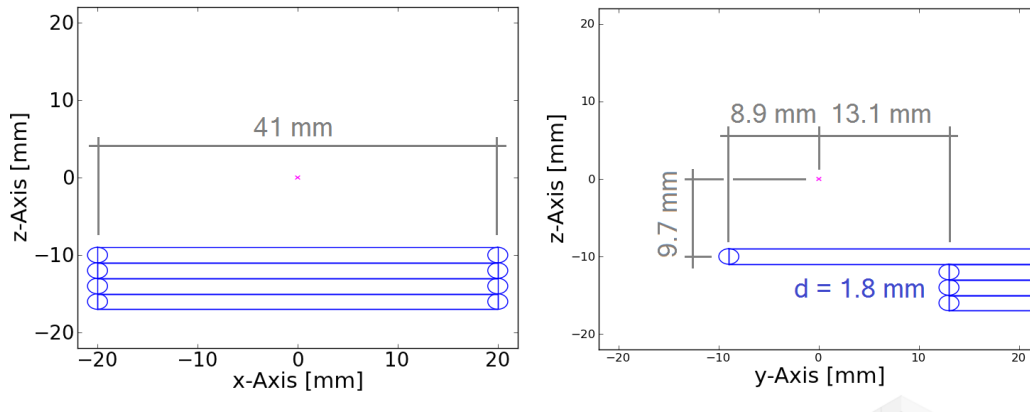
Figure 57: Dimensions of the wire configuration.

	Value
U-MOT wire 1	3.28 A
U-MOT wire 2	2.6 A
Bias wire 1	-14.8 A
Bias wire 2	-15.20 A

Table 10: Example values for a configuration that does not require an external field.

[5]The relevant area is $1\,\text{mm}^2$ in the (y,z) plane and 6 mm (3 mm left and right) in x direction.

3.4.5 Environmental Influences

Ambient magnetic fields in the room interfere with the quadrupole field and disturb the calculated shape. The earth magnetic field is usually around 0.7 G, but this is not the only influencing field. The ion pump has a large magnetic field as well and is approximately 100 cm away from the field center.
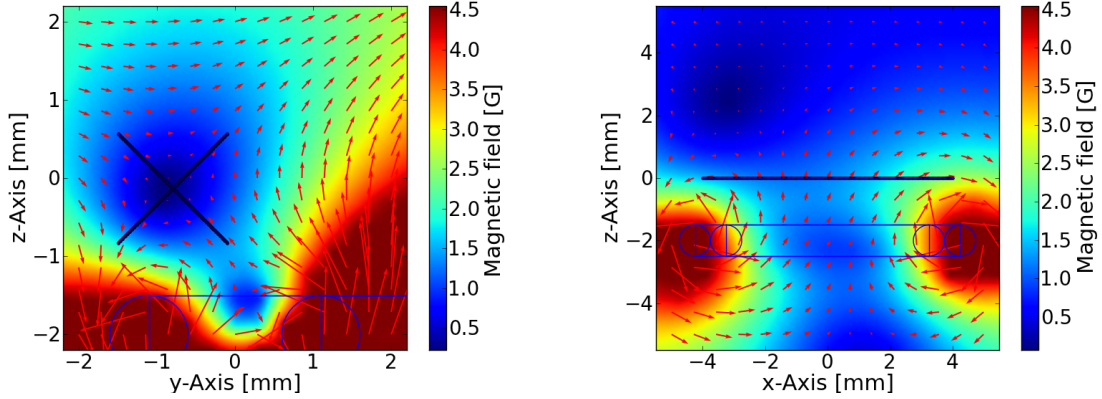

Figure 58: Example of the influence of an external field with B_x=0.4 G, B_y=0.0 G, B_z=1.1 G.

Figure 58 shows the shift of the center by an external field. The shift can either be balanced with 3d Helmholtz coils by just adding the opposite direction or with the bias field which is more complicated. The only option is to change the currents in the two bias wires, but this will only rotate the field in the (y,z) plane. The x direction cannot be compensated by changing wire currents. This means if there exists a field in x direction, the center of the MOT will shift away and the bias wires are not able to correct this influence.
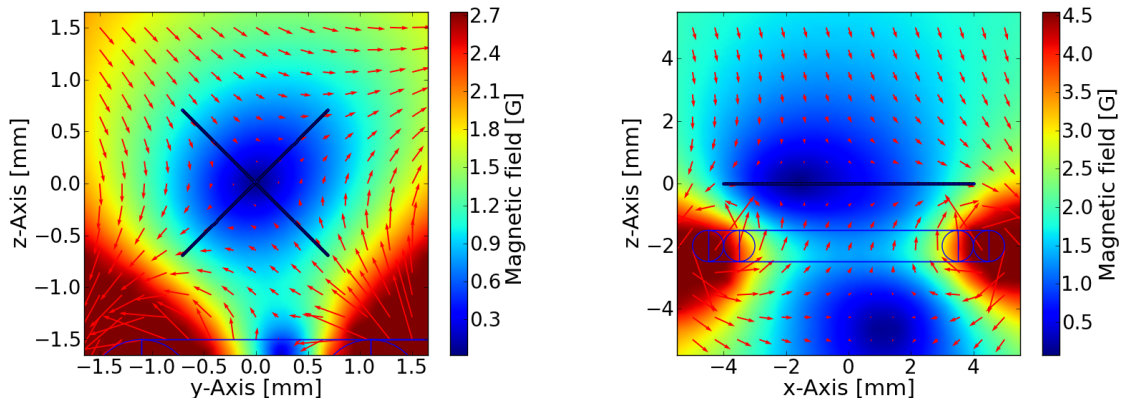
Figure 59: Quadrupole field with external influence corrected by the bias wires.

Figure 59 shows the MOT field in (y,z) plane and in the (x,z) plane when a magnetic field Bx=0.5 G, By=0 G and Bz=-1.1 G influences the field configuration. The currents in the bias wires adjust the quadrupole field center back to the point (0,0) in (y,z) plane, but the field is very distorted. The average angular deviation is increased up to 0.46 degree along the z' axis and to 0.68 degree along the x axis [6]. The plot also shows that the interfering field in x direction cannot be compensated by the bias wires and the quadrupole field center on the x axis gets shifted. This problem can just be solved with the 3d Helmholtz coils by adding a field in x direction.
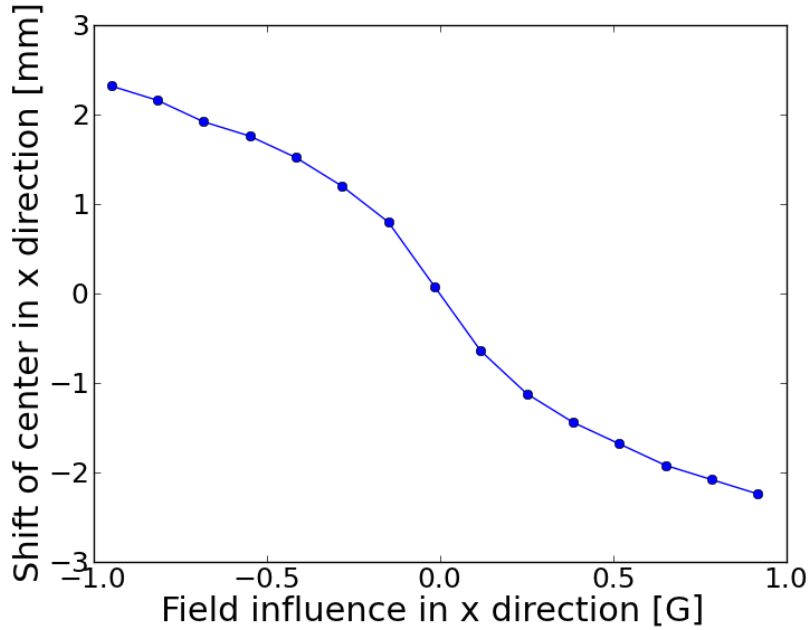
Figure 60: Shift of the MOT-field center depending on an external field in x direction.

The displacement of the center of the quadrupole field caused by an existing external field in x direction is shown in figure 60. The atom cloud is going to have a length of around 5 mm, this means a shift of the center by 1 mm and more is not acceptable.

Field in Reality

The external fields have to be compensated to better than 100 mG accuracy. The field in the room where the MOT is placed is mostly oriented in z direction (around 0.7 G). The bias wires should be able to compensate this with a bit of quality loss in the quadrupole field.

---

[6]The average deviation without an interfering external field is around 0.12 ° and 0.25 °.

3.4.6 Resulting Values

The final field characteristics were calculated in Finitewiresolve 1.0. The results of the quality management are compared below in table 11. The four examined scenarios are the U-MOT with Helmholtz coils, the U-MOT with the field from the bias wires and two different influences on the field in z direction where the bias wires are used to compensate the field.

Configurations				
	U-MOT	Bias U-MOT	Ext. Field +z	Ext. Field -z
Wire 1 [A]	3.6	3.6	3.6	3.6
Wire 2 [A]	2.8	2.8	2.8	2.8
Bias Wire 1 [A]	0	-14.6	-10	-19.2
Bias Wire 2 [A]	0	-19.6	-22.3	-16.71
Field x/y/z [G]	4.2/-2/0	0/0/0	0/0/0.7	0/0/-0.7
Quality values (y'/z'/x)				
Average $\|\alpha\|$ [°]	0.06/0.08/0.3	0.17/0.12/0.32	0.23/0.16/0.34	0.12/0.1/ 0.31
Max $\|\alpha\|$ [°]	6.7/15.3/26.3	13.2,10.8,30.6	17.3/15.1/31.2	10.1/14.0/ 30.4
Gradient [G/cm]	9.8/13.2/6.86	8.4/11.6/5.3	8.09/10/5.2	8.7/ 11.44/5.35
Capturing rate	17780 (100%)	14650 (82.4%)	13450 (75.6%)	14020 (78.8%)

Table 11: Resulting values for different configurations.

Capturing Rate

A subprogram was written in Finitewiresolve 1.0 to make an approximation of the capture rate for our MOT. Since this value depends on many parameter, like light intensity, which is not known exactly, the approximation is very coarse. The program uses the potential generated by the magnetic field to find the area where atoms are trapped and counts them in a Monte-Carlo like fashion. Figure 61 shows the atom cloud shape in the U-MOT configuration found by the program.
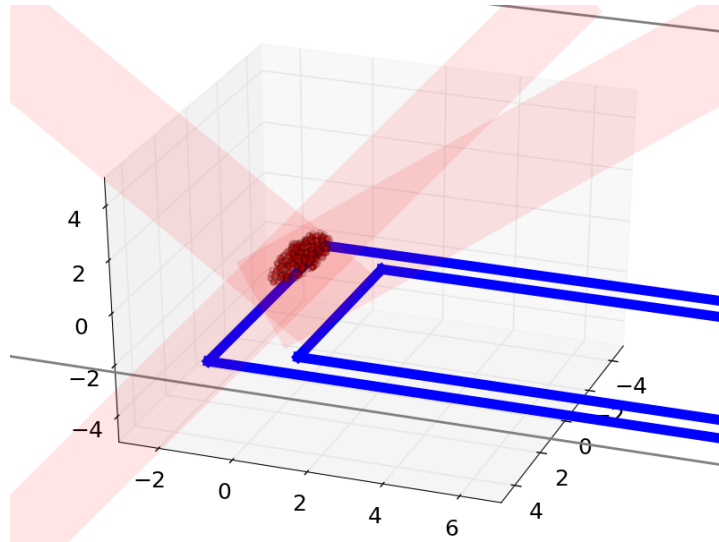
Figure 61: Atom cloud in U-MOT with laser beams. Monte-Carlo simulation of the loading in Python.

The typical capture rates for big U-MOT's go up to $3 \cdot 10^{-8}$ atoms [15]. Since our MOT is a lot smaller (just around $1 \, \mathrm{mm}^2$ in diameter) the atom number will of course be less. Note that the coarse approximation allows to compare different configurations. So the calculated capture rates can be used to create new optimisation codes beside the already existing quality values and also to have a reasonable value for the quality loss for the bias field.

3.5 Chip Mounting

In this section the layout of the mounting elements are shown and described. The assembly can be seen in figure 62. The basis of the construction is the mounting (orange) which is fixed on the same flange as the glass cell. The U-MOT wires are guided on the chip plate which is fixed on top of the mounting. Above the chip the imaging systems are mounted. All used materials must be out of a non-magnetic material like copper or stainless steel. For certain parts ceramic can be used as well. Aluminium is not an option, because its not UHV compatible. The screws should be made out of A4 material[7] to guarantee a minimal magnetisation.
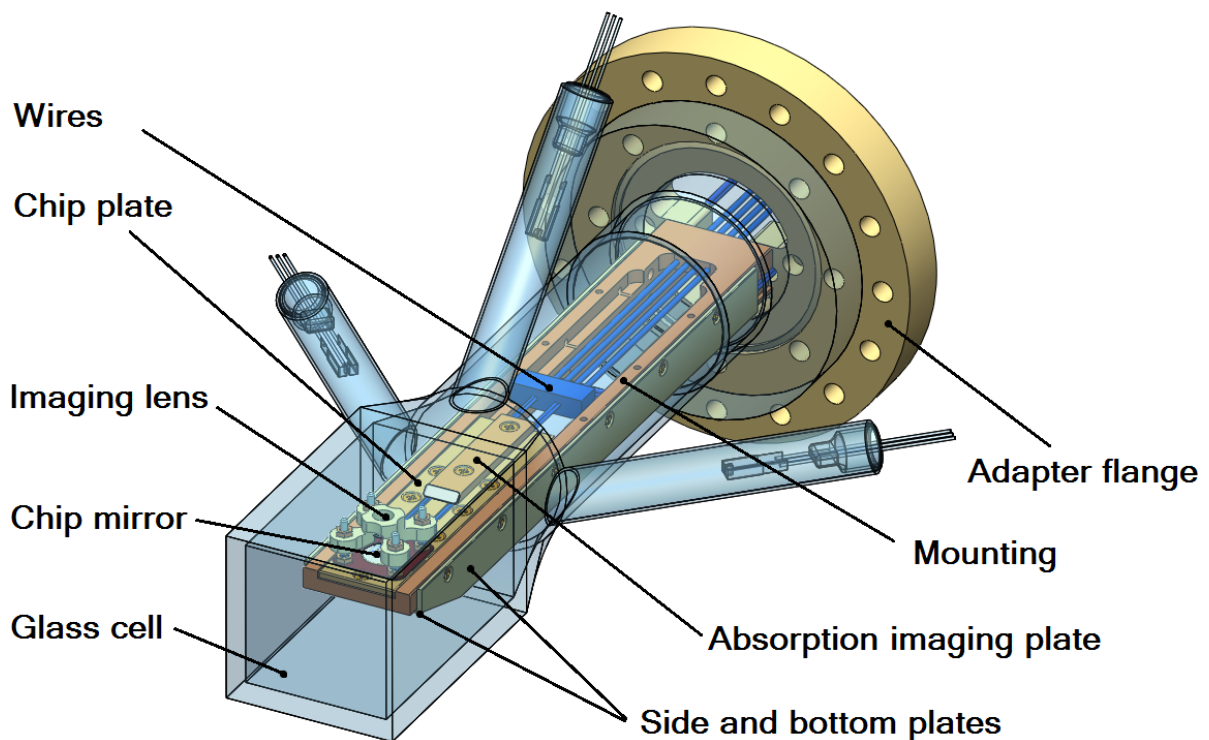
Figure 62: Assembly picture of the chip mounting.

---

[7]A4 material is an austenitic stainless steel with the alloy composition X5CrNiMo 17-12-2.

The Mounting

The basic element is the mounting, shown in figure 63. The chip is placed on the upper front side. The hole below the chip enables the bottom laser beam to pass. The grooves on the sides can guide the bias wires. The little cut in the groove is to be able to wind the second bias wire 2 times. The drills (which can be seen better in the technical drawings in section 7.3) are mainly to fix plates above the bias wire and to fix the chip. To economize the setup all drills are M3 sized, only four additional M4 drills on the back are required to fix the mounting on the flange. Some M3 drills on the upper side, are not used in the first construction, but they keep the option to fix additional cooling plates later in case the heat deposition is too high. The bridge in the back is needed to stabilize the construction during the manufacturing process. It contains four holes to guide the four U-MOT wires.

Front side

Back side
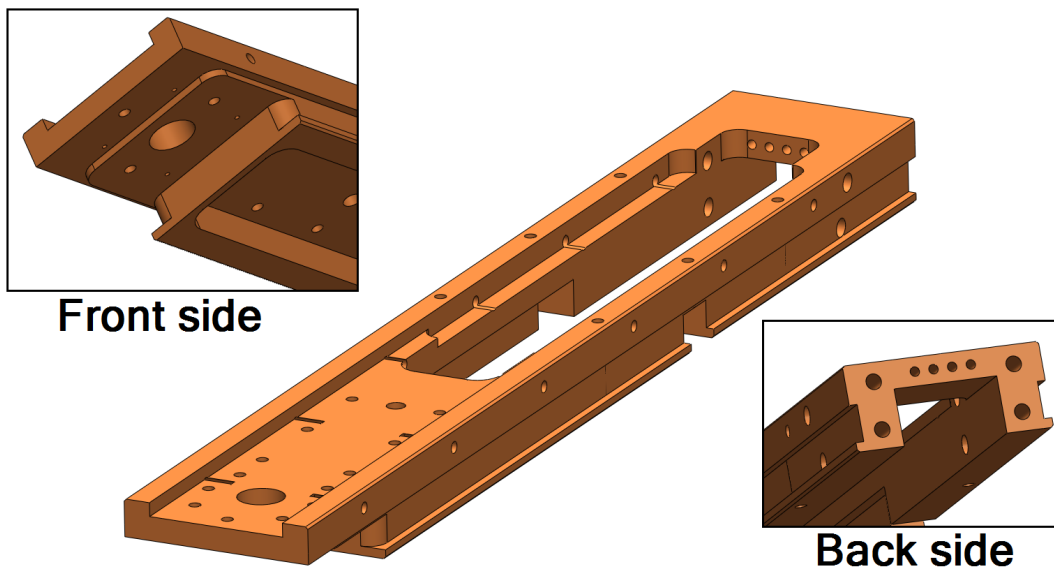
Figure 63: Picture of the mounting.

Note that the chip plate is fixed with 7 screws to the mounting. This amount of drills provides a good thermal contact and also offers the option to design a different chip plate in the future, which can be designed as two different parts and maybe have the possibility to adjust the chip in the xy-plane. The edges of the grooves for the bias wires need to have a radius of at least 4 mm to not have trouble with the Kapton isolation of the wires during the bending process.

The Chip Plate

The chip plate has grooves in which the U-MOT wires are guided. The width of the inner U-wire is 7.8 mm and the width of outer U-wire is 10 mm. The copper wires have a diameter of 1 mm, with Kapton isolation 1.1 mm.
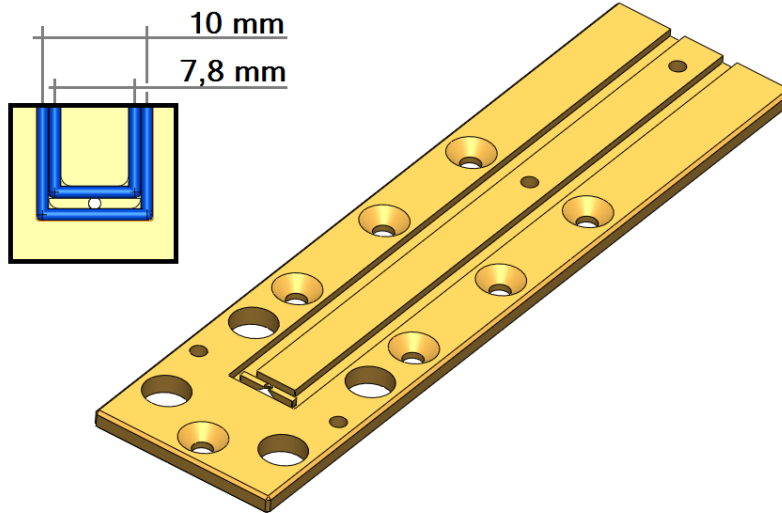
Figure 64: Picture of the chip plate.

In early experiments it was found that a good width for the groove is 0.1 mm wider than the wire diameter. In our case the single guiding grove is 1.2 mm and the groove where both wires are placed 2.4 mm. With this size the wires are self fixed, there is no need for an additional fixing plate or glue. Two M3 drills in the back side enable the mounting of a plate or an imaging system component. Note that the edges in the wire grooves, where a wire is bent, need to be at least 1 mm, otherwise the Kapton isolation gets damaged when the wires are pressed in.
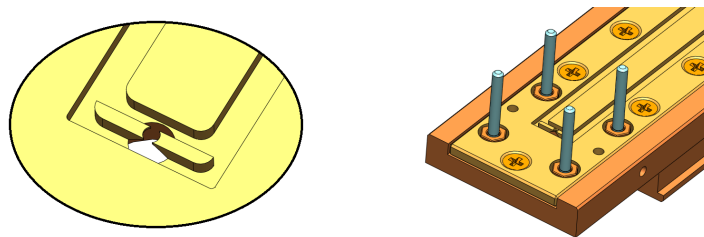
Figure 65: Chip plate zoom view of center (left) and mounted (right).

The hole in the middle shown in figure 65 in the zoom view is important for the laser beam from below. It should enable as much intensity as possible to pass through the center. The four large holes in the front are necessary to have space to fix the imaging rods with nuts as shown on the right side.

The Wires

The wires are placed on the mounting and on the chip plate as shown in figure 66. The two U-MOT wires (diameter=1 mm) on the chip plate are connected to four supply wires with a diameter of 2.5 mm to get a smaller resistance and thereby less heat production. Because there are no Kapton isolated wires of this size available, we choose to use blank wires and isolate them with Kapton heat shrink tubes.
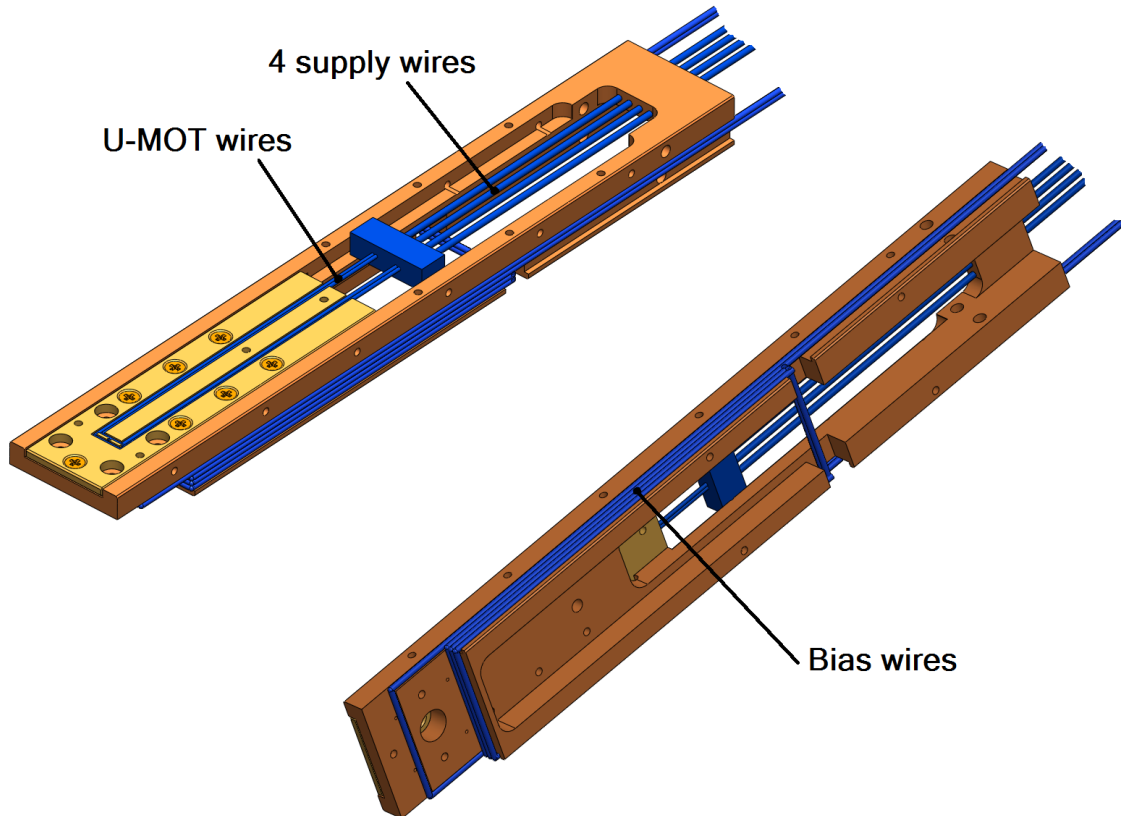
Figure 66: Picture of the wire layout.

The bias wires have a diameter of 1.7 mm and 1.8 mm with isolation. This was the largest size where Kapton isolation was offered[8]. The groove in the mounting offers 0.1 mm more space per wire to enable a good guiding of the wires.

---

[8]www.allectra.com

The Wire Plates
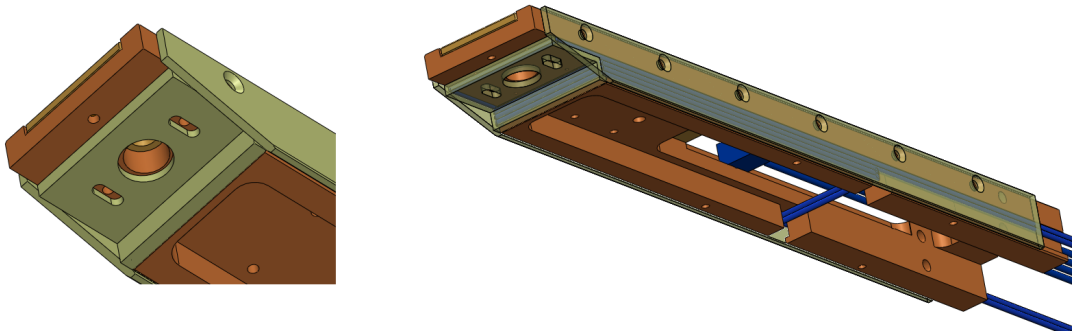
Figure 67: Picture of the plates without screws.

The plates are necessary to fix the bias wires into their position. The plates on the side are mounted with six screws each and the bottom plate with two screws. The two holes in the bottom plate are long-drawn-out to enable a little bit of moving space in x direction and press the wires to the mounting wall. The bottom plate also contains a hole for the laser beam from below.

Absorption Imaging Plate

To fix the U-MOT wires in the grooves a plate can be mounted on the chip as shown in figure 68. This plate can carry a mirror which is needed for the absorption imaging as explained in section 4.4.
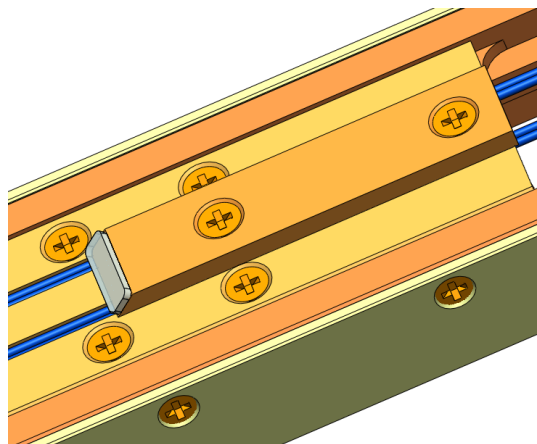
Figure 68: Mirror plate mounted on the chip.

The Imaging Lens
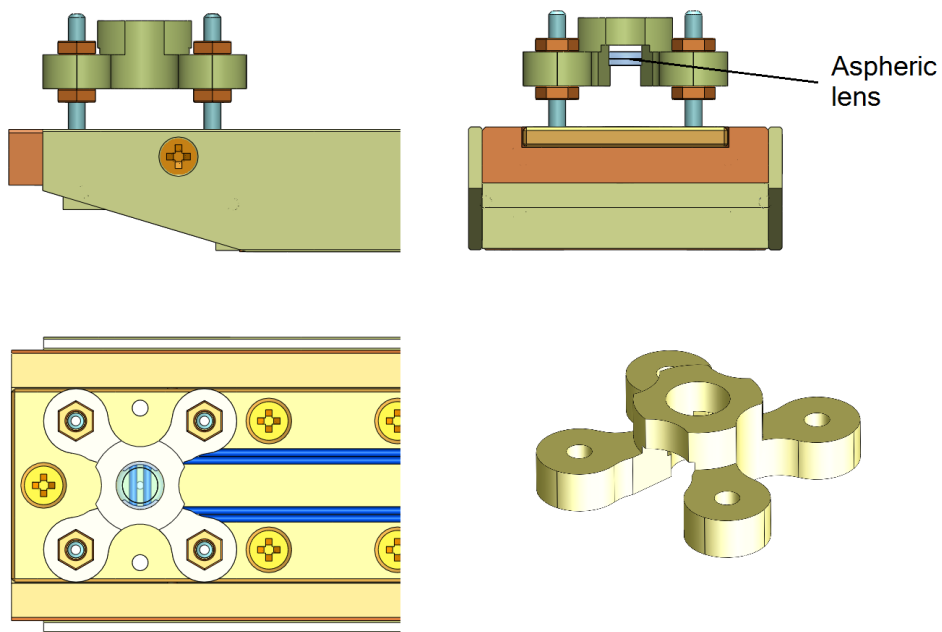
Figure 69: Lens mounting on the chip for the imaging system.

The imaging lens configuration was designed during a project work. An aspheric lens needs to be placed in the vacuum at a distance of around 8 mm from the chip surface to image the single atoms in the planned experiments. The design of the lens mount is shown in figure 69 and figure 70. The lens can be fixed with an UHV compatible glue. The center of the lens is exactly above the center of the hole in the chip plate.
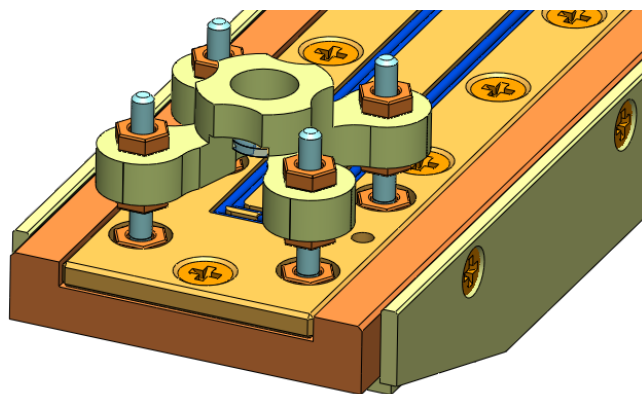
Figure 70: Lens mounting 3d.
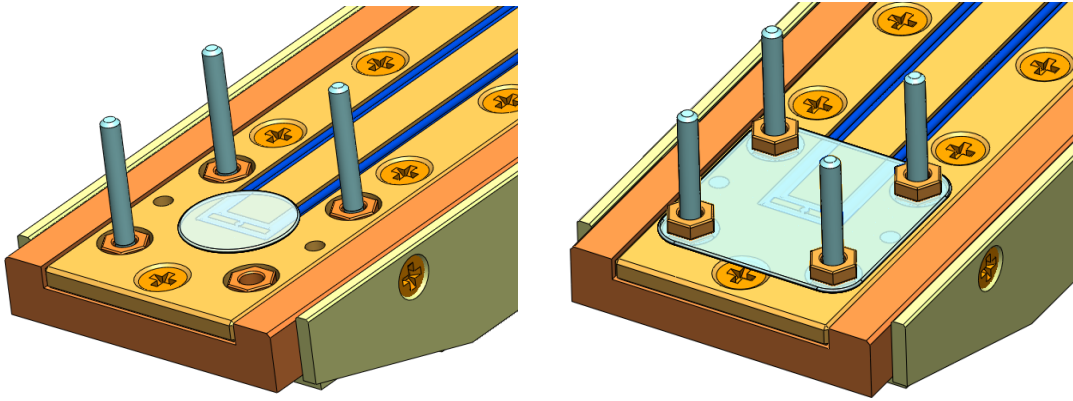
Figure 71: Mirror on the chip, fixed with glue (left) or with nuts (right).

The center of the MOT is placed 1.5 mm above the wires and 1 mm above the mirror surface. Therefore the mirror should have a thickness of 0.5 mm as shown in figure 72. The dimensions of the mirror must be large enough to enable the reflection of the MOT laser beams. This requires a diameter of at least 15 mm. In the planned experiments the mirror will be a crystal with small fabricated apertures of around 4 μm in the center as explained in section 2.6.
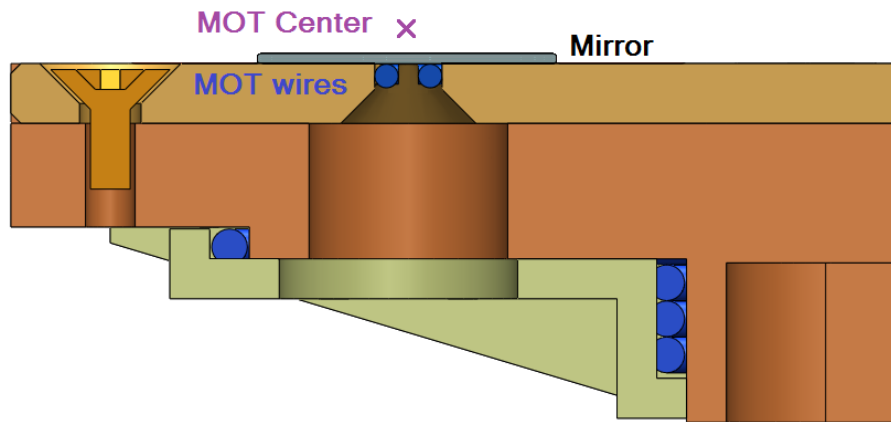
Figure 72: Cutaway view of the chip.

The mirror can be mounted with a special UHV compatible glue. In case the glue influences the experiment adversely the mirror can also be mounted with nuts to the imaging rods. This possibility has the advantage that the mirror is adjustable in the (x,y) plane. This can be very helpful for the imaging system to find the apertures on the mirror surface during the adjustment process.

The Adapter Flange

The mounting is fixed on the same flange as the glass cell and is mounted with four M4 screws. To provide a good vacuum quality, fast pumping the free space should be as large as possible and all wires should be able to pass through.
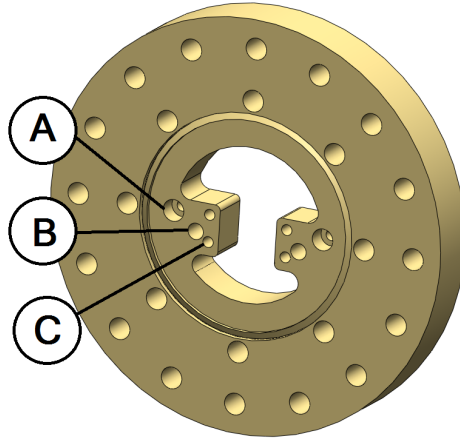
Figure 73: Picture of the adapter flange.

Figure 73 shows the final design. Everything has been milled out of a CF100 blind flange. The mounting is fixed with four M4 screws (C in the figure). The bias wires can pass through the two holes B. The U-MOT wires can pass in the free space in the middle of the flange. Two additional holes A are an option for the future in case the heating of the wires in free space is too high and an additional heating construction needs to be mounted.
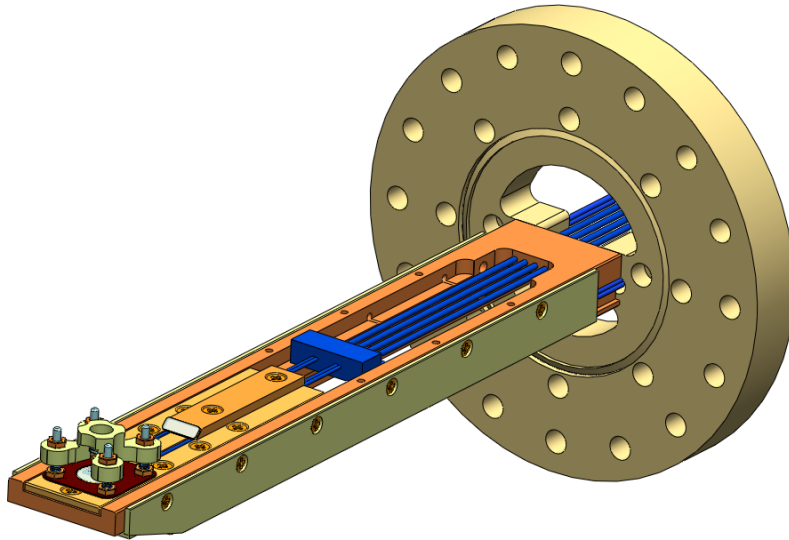
Figure 74: Adapter flange with the mounting assembly.

The Glass cell

The glass cell was made in the USA from the company Precision Glassblowing. The cylindrical part enables the mounting to have a good transition from metal to glass and the squared part made out of a special fused quartz to diffuse the laser beams from outside as less as possible. The three additional arms on the middle section were a special offer by the company. Two of them contain small sublimation pumps which can be operated from outside and the central one is the Rubidium source.
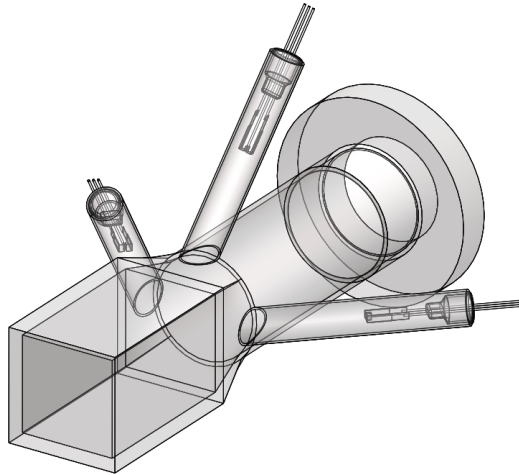
Figure 75: Glass cell from Precision Glassblowing.

The glass cell was ordered in March 2013 and since the company has troubles with the production, the MOT experiment was delayed.
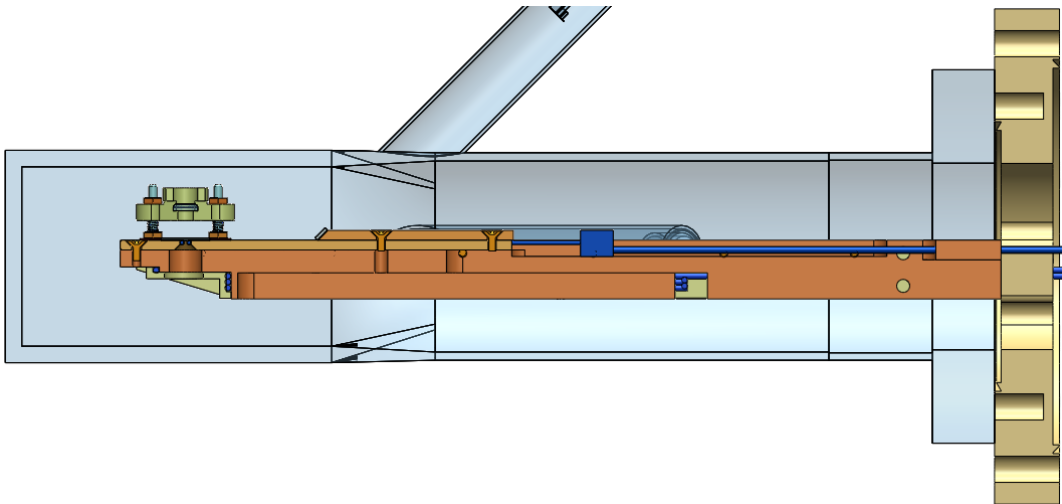
Figure 76: Cutaway view from the glass cell on the flange.

Head of the Mounting

For the planned experiments the imaging system needs to have two important adjustment possibilities. The first is to control the height of the lens with the cloverleaf formed lens mounting and the second is to find the position of the trapped atoms on the surface of the chip mirror with the imaging detector.
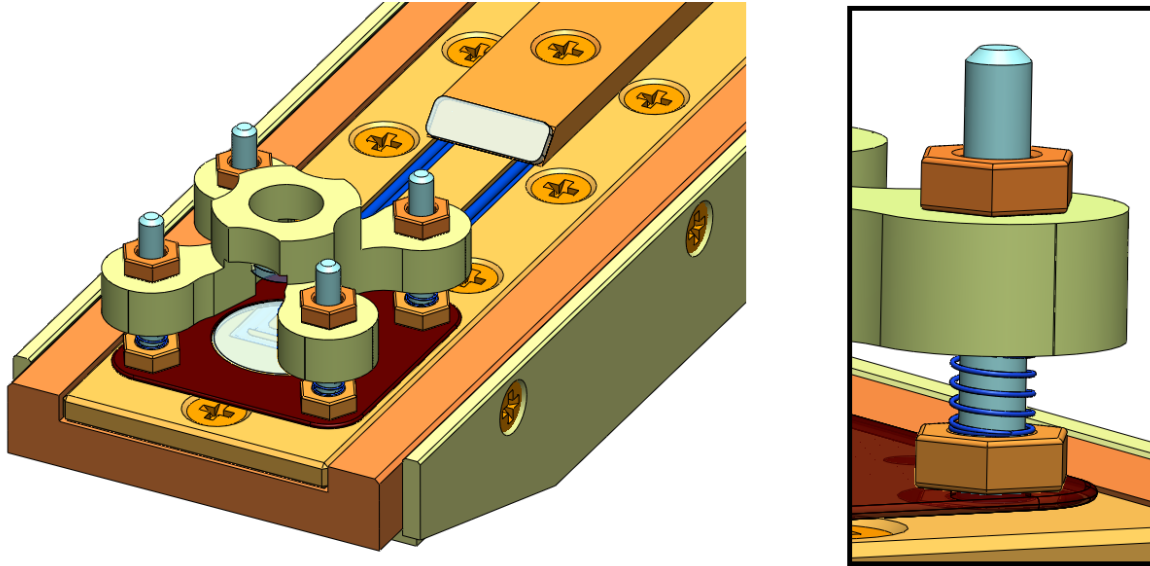
Figure 77: Suggestion for the head construction to enable a good adjustment.

To enable the adjustment in a comfortable way the head of the mounting can be designed as shown in 77. The height of the cloverleaf mount is fixed with springs and controlled with four screws above them. The position of the mirror is defined by a holding part (brown)[9]. This holding part is positioned by the screws of the imaging mounting and can only be moved a few hundred microns. This means that the possible location where the apertures can be found by the detector is defined by the holding part. The position can be adjusted and fixed with the nuts. The image area of the imaging detector will be around $120\,\mu\mathrm{m}^2$. A single aperture has a diameter of $4\,\mu\mathrm{m}$ and a distance from $6\,\mu\mathrm{m}$ to its there neighbours. A matrix of 8x8 apertures leads to a field of around $74\,\mu\mathrm{m}^2$. An additional advantage of this design is that no glue is required.

Sketches of the Laser Beams

The following shows pictures of the laser beams made in Solidworks.

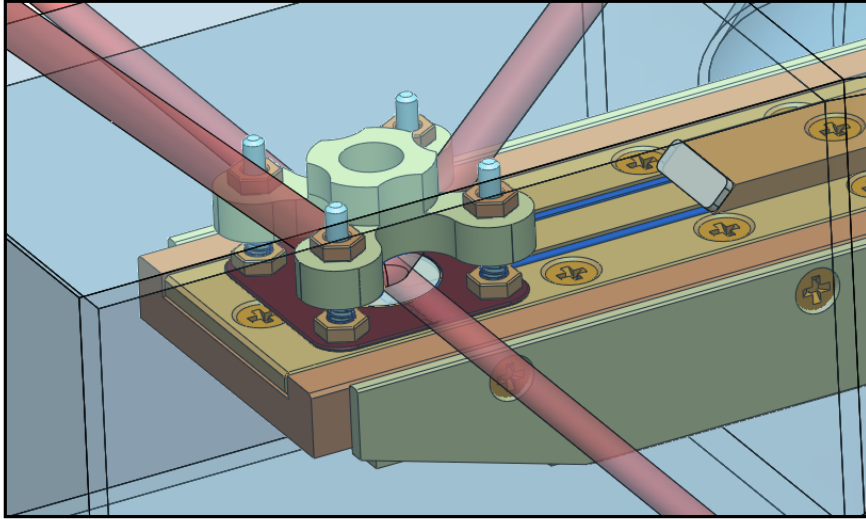[9]The mirror is very sensitive and cannot be drilled.

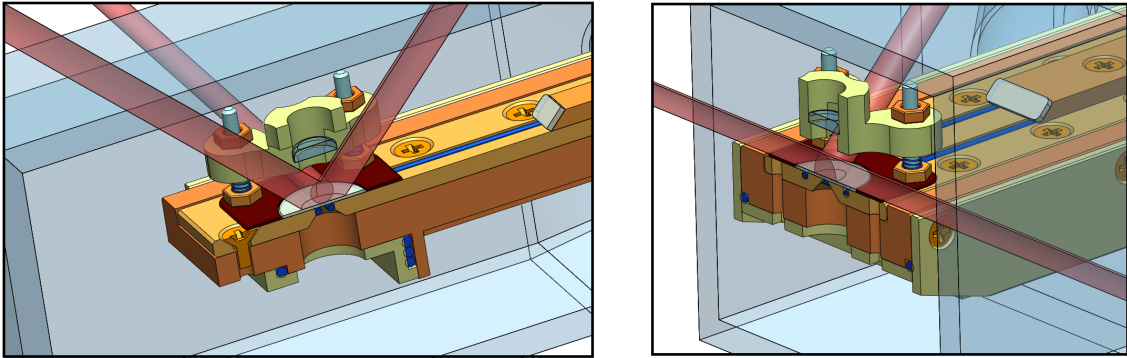Figure 78: MOT beams from outside the glass cell.

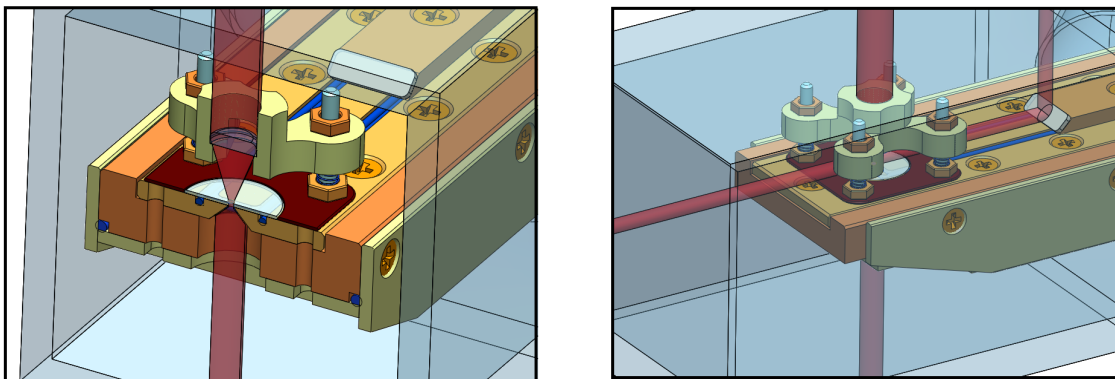Figure 79: MOT beams from two cutaway views.

Figure 80: Beam of the aperture trap (left) and with additional beam of the absorption imaging system (right).

4 Construction and Technical Layout

In this section the experimental setup is described which is needed to run the MOT. This includes the laser system components, the imaging systems, the vacuum chamber and the coils for the external fields. Images and descriptions of the current progress are given as well.

4.1 Laser Beam Components

The following shows the diverse steps, which are needed to realize laser beams for a MOT. Figure 81 shows the necessary components which lead to four equal intensities and frequency stable laser beams. In this section all parts are explained separately.
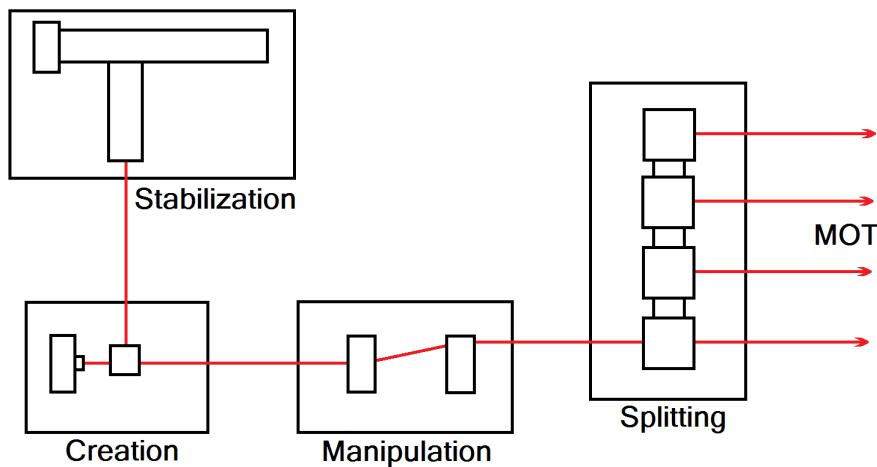
Figure 81: Sketch of the steps to prepare laser beams for the MOT.

In most laser experiments, the whole laser setup is placed on a big table and the laser beam is guided by mirrors directly to the required spot. If a laser system is divided into several parts (at different places) the beam needs to be guided in a single mode fiber. These fibers only support the first order of the gaussian beam waist. Therefore the performance of the first coupling process is not very high. But the beam waist afterwards is well shaped and the further coupling process in return, is much more efficient (70 to 80 %).

Concept   Our required beam power is small in comparison to other experiments, so it is acceptable to have small losses in different coupling processes. This presents the opportunity to divide the laser beam system into several parts and build them up individually in cage systems. For the MOT experiment different project works where performed so it was reasonable to design all laser system components independently and link them together afterwards with mono mode fibers.
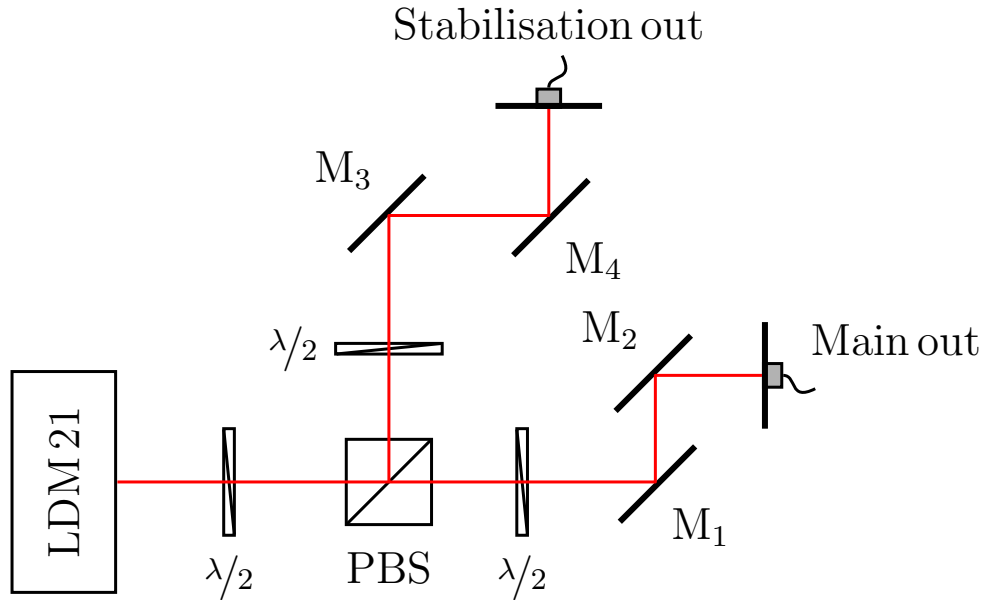
Figure 82: Layout of a laser beam splitting.

The laser beam source is a diode from Toptica (Type DFB). The beam frequency can be controlled by temperature and current. The first assignment is to divide the beam into one main beam and a secondary beam. The main beam is for the atom trap and the second beam is for the stabilization. This means the second beam is used to lock the frequency of the main beam to a hyperfine peak. The intensity can be around a few hundred μW. The splitting ratio proportion is controlled by the angle of the first $\lambda/2$ waveplate as shown in figure 82. The beam splitter cube (PBS) divides the beam according to its polarization. The other two $\lambda/2$ plates and the mirrors are necessary to couple the beams into the fibers. The couple elements consists of a fiber mount and a lens with high NA[10] which is fixed on a z-translation stage to control the position of the beam waist.

---

[10]NA means numerical aperture.
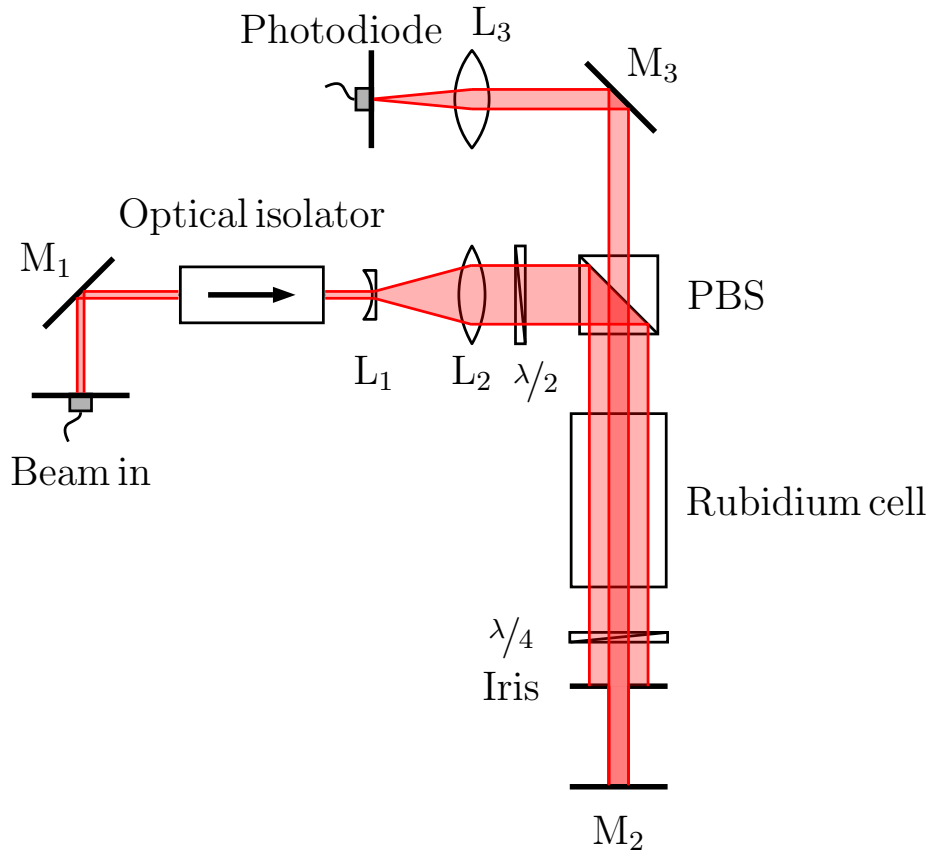
Figure 83: Layout of a Doppler-free saturation spectroscopy.

To stabilize the beam frequency to a hyperfine peak, Doppler-free saturation spectroscopy is used as explained in section 2.4. Figure 83 shows a layout of a realisation. After the incoming beam, an optical isolator is needed to avoid standing waves and feedback in the system. The lenses L_1 and L_2 increase the beam diameter. This can be realised with two lenses where the first has a negative and the second has a positive focal length. A larger beam waist is able to excite more atoms in the cell. The beam splitter cube directs the beam through the Rubidium cell. The $\lambda/2$ plate has to be adjusted to maximize this reflected beam. The iris cuts the size of the beam, so the reflected beam has a smaller diameter which leads to a better signal. The $\lambda/4$ plate makes sure that the reflected beam passes the beam splitter cube straight and the lens L_3 focuses the beam on the photodiode where the signal is measured. For the saturation a few electrical components are required to control the laser and process the signal from the photodiode. In our case a computer program is doing this automatically. More information on the detailed components can be found in [16].

Laser Beam Manipulation

An acusto-optic modulation (AOM) is necessary to shift the frequency of the laser beam to the driven transition frequency of the the atoms. Depending on the demands, aa adequate setup has to be chosen. The transitions for our MOT are shown in section 2.5. An AOM separates the first order brag reflected beam which is frequency shifted. To do so, a small diameter (of around $400\,\mu m$) beam is required, this is why two telescope lenses are needed, L_1 and L_2 in figure 84. L_1 has a large focal length and L_2 a small focal length, in our case the lenses are a LA1422-B (f=40 mm) and a C230TME-B (f=4.51 mm). The distance of the beam waist is very sensible to the exact distance of the two lenses, so a μm-translation stage for one lens can be very helpful for finding the best position. To cut of the zero order beam an iris element can be used, named PH in the figures.
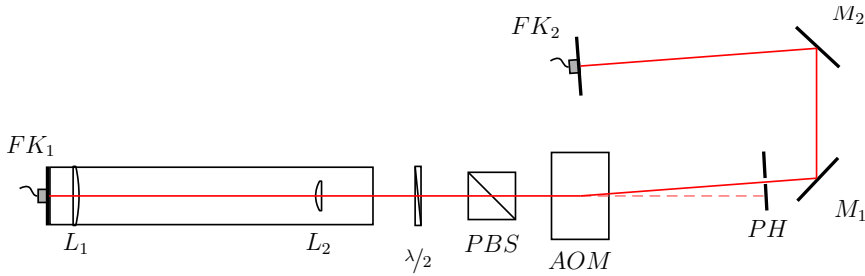
Figure 84: Layout of a single pass AOM setup, where the beam only passes the AOM element one time.
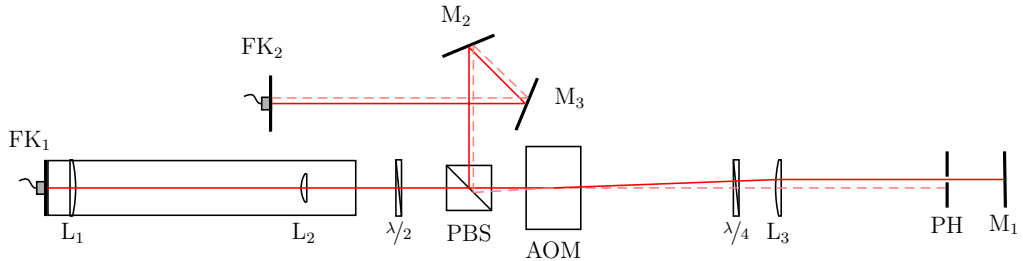
Figure 85: Layout of a double pass AOM setup with cat's eye.

In figure 84 and figure 85 two possible realizations are shown. The frequency shift of the laser beam is due to the bragg reflection similar to the driven frequency of the AOM. For the repumping laser the required frequency shift is of the order of 80 MHz, this is why a single pass AOM is appropriate in this case. For the cooling laser the frequency shift is around 160 MHz, so in this case a double pass AOM is needed, because the beam needs to pass the AOM element two times. The achievable efficiencies are around $85\,\%$ with the single pass setup and around $75\,\%$ with the double pass cat's eye setup [8] [17]. There is also a third type possible for the double pass AOM where the cat's eye is replaced

by an aspheric mirror, but it turned out, that the handling is very sensitive and the efficiency is worse.

Laser Beam Combination

Repump beam in

M$_2$

M$_1$

Main beam out

M$_4$

$\lambda/2$

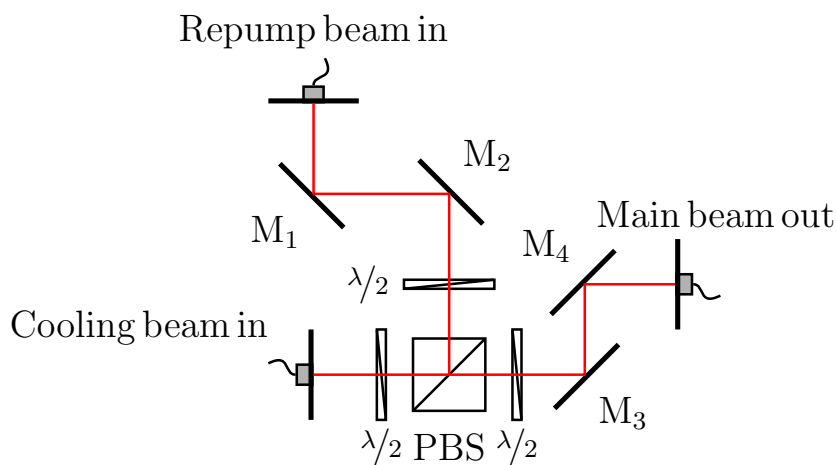Cooling beam in

M$_3$

$\lambda/2$ PBS $\lambda/2$

Figure 86: Layout of a beam connection setup.

Excited atoms in the MOT can fall into an unfavorable "dark" state which makes a repump laser beam necessary as explained in section 2.5. This means the laser beam creation, the stabilization and the AOM setup is needed two times. One laser beam needs to be stabilized to trap the atoms and the second beam need to pump atoms from the dark state back to a useful state, see figure 9. In an experiment the repumping laser beam can be oriented straight into the atom cloud from some random angle, but since this laser beam also influences the movement of the atoms by a small amount, a better solution is to couple the beam into the same fiber as the cooling beam to trap the atoms. In figure 86 an example of a realisation is shown. The $\lambda/2$ plates are needed to control the polarization and the mirrors to control the direction of all beams. M_1 and M_2 are necessary to bring the two input beams together after the polarization spitting cube and M_3 and M_4 couple the overlaid beam into the main fiber.
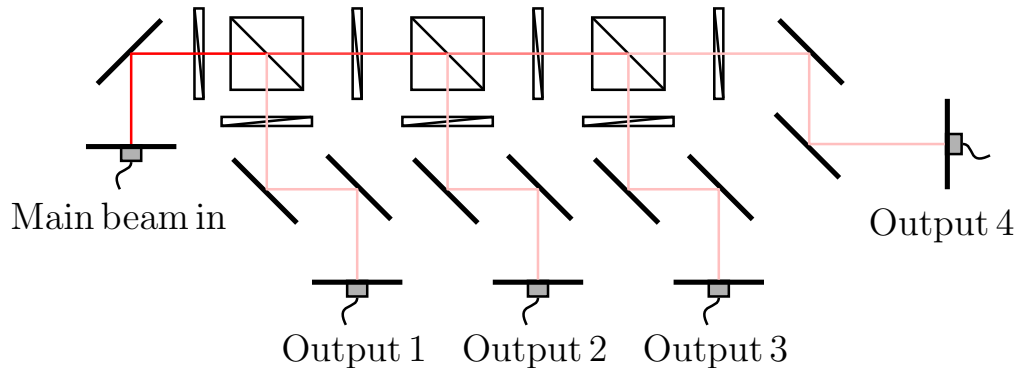
Laser Beam Splitting

Figure 87: Layout of a laser beam splitting.

The prepared beam is now divided into four beams with equal intensities. An example is shown in figure 87. At this point the laser beam should have a remaining intensity of at least 20 mW. The $\lambda/2$ plates needs to be adjusted to provide the same intensity in every output fiber. In our case this can be done by a comprehensive prepared module from Schäfter & Kirchhoff.
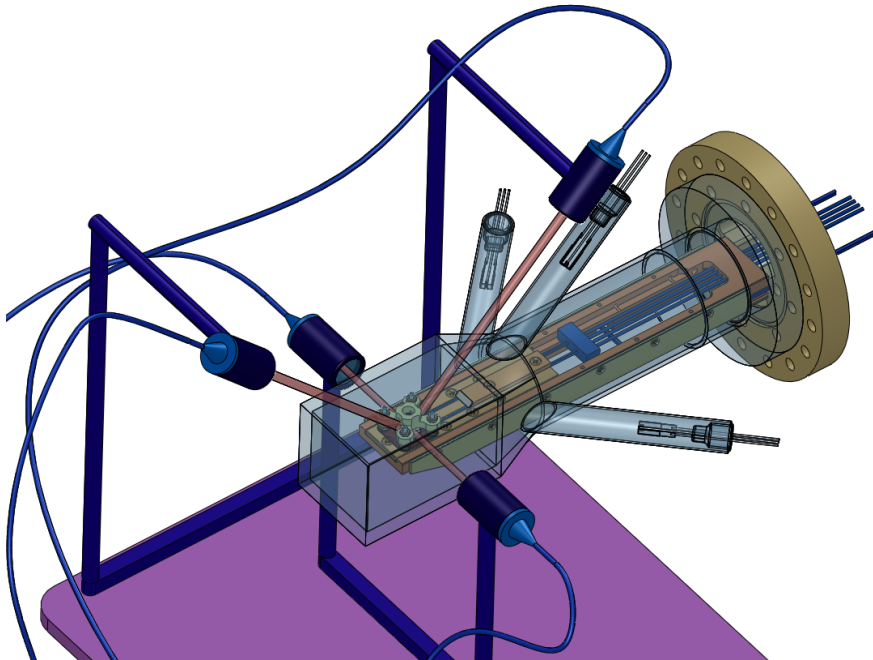
Laser Beam Alignment

Figure 88: Expander alignment to direct the beams to the MOT center.

The four laser beam fibers are linked with a beam expander and aligned to the center of the MOT as shown in figure 88. The expanders are mounted on rods where they do not block the Helmholtz coils (not shown in the figure). An expander consists of a lens which is positioned to provide a collimated beam and a $\lambda/4$ waveplate which adjust the polarisation of the beam. The beam diameter depends on the NA of the lens.

4.2 Laser Beam Construction

The aim is to make the setup as compact as possible. The required space of the components was minimized during a couple of project works. The system is shown in figure 89.
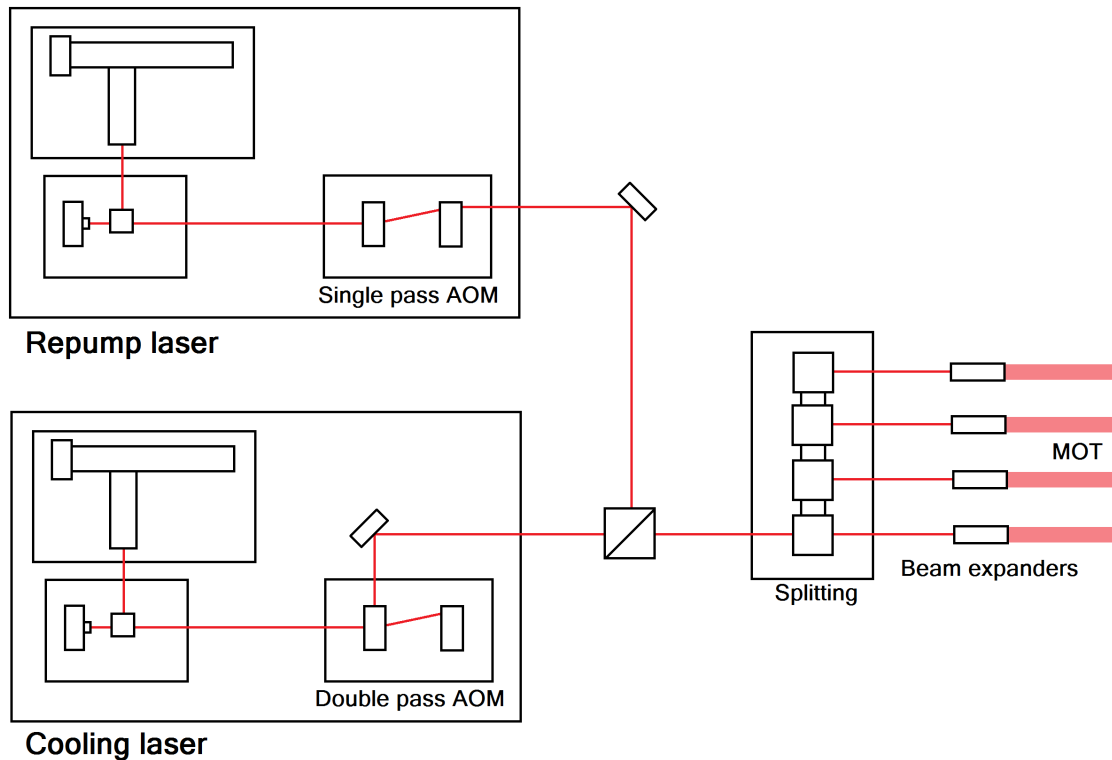
Figure 89: Assembly of the laser beam system.

The diode laser and the frequency stabilization where built up together in a cage system as shown in figure 90. The setup fits into a 30x30 mm box.
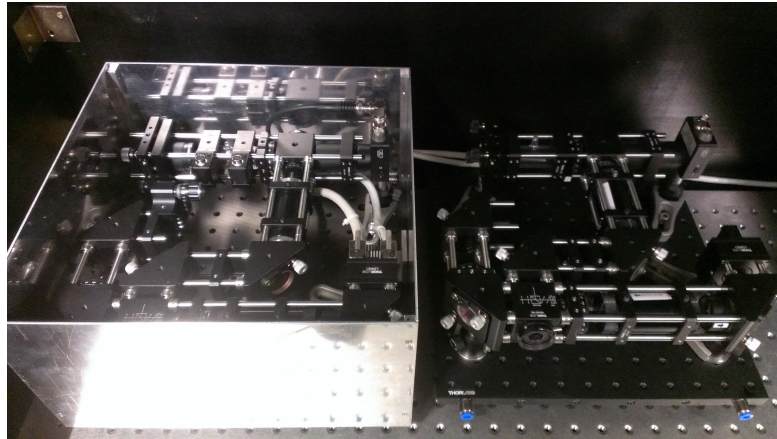
Figure 90: Layout of the beam creation combined with the stabilization. The cooling beam in an Aluminium box (left) and the unfinished setup for the repump beam (right).
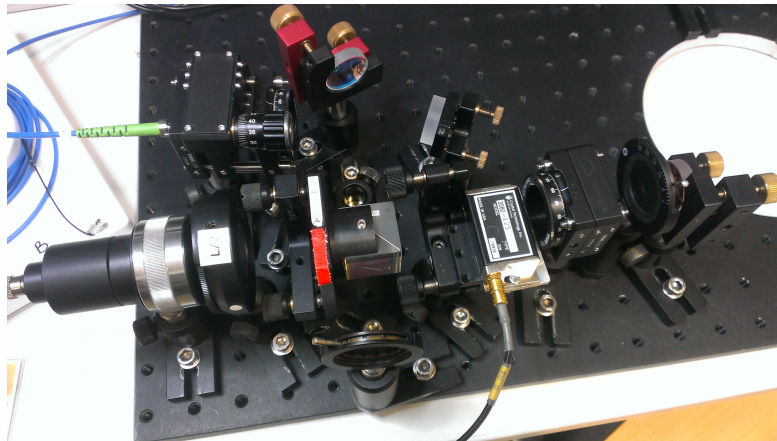

Figure 91: AOM double pass layout.

Setups in figure 90 and figure 91 where developed during project works [?] [17].

Efficiency

The efficiency needs to be as high as possible. There are losses in every step and the performance needs to fulfill the target power. The diode laser offers a power of around 65 mW. In the end there should be four similar laser beams each with at least $3.58\,\text{mW/cm}^2$ (saturation intensity of ^{87}Rb). Lets consider a laser beam radius of 5 mm, then the requirement is 11.24 mW in total. This means the overall losses of all system components should not be higher than 80%.

Component	Acceptable intensity
Diode laser	65 mW (100 %)
Stabilisation	1 mW (1.5 %)
First coupling	40 mW (61.5 %)
AOM double pass	20 mW (30.7 %)
Splitting	15 mW (23.1 %)
Beam expander	12 mW (18.5 %) each beam 3 mW

Table 12: Example of a possible scenario for the efficiency of the laser system to run the MOT. The values are at the fiber output of each component. Not included here is the beam combination.

If the required efficiency can not be achieved, an optical amplifier can be used to increase the intensity.

4.3 Mounting Manufacturing

All mounting parts where milled out of copper blocks in the workshop of the Atominstitut. In the following, images of the manufacturing are shown.

Before

After
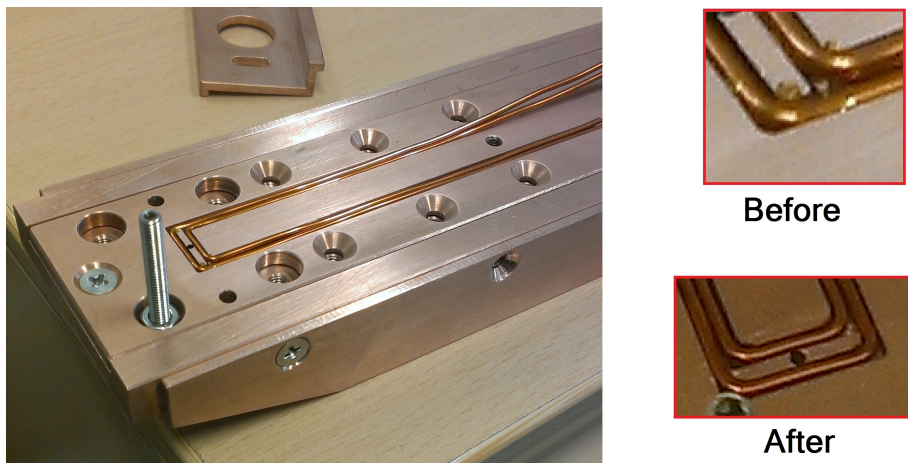
Figure 92: The mounting during the manufacturing process.

In figure 92 the mounting is shown with a zoom to the wires. The grooves are small enough so that the wires are self holding, but it can be seen that the capton isolation of the wires was damaged at the edges of the grooves. This is why they where rounded with a diameter of 1 mm in an improved version.
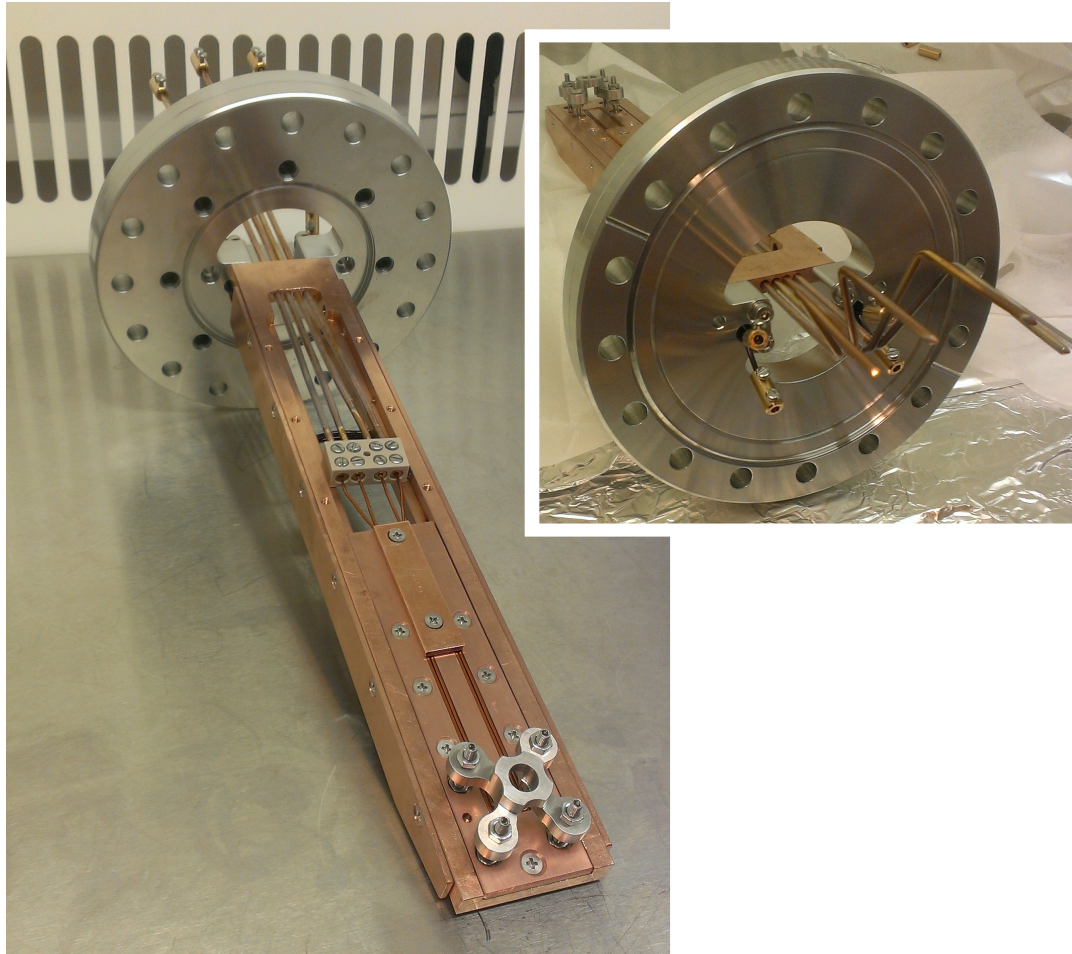
Figure 93: Mounting on the flange.

The end of the wires where equipped with copper based connectors to link them with the wires of the feedthrough flange in the vaccum chamber.
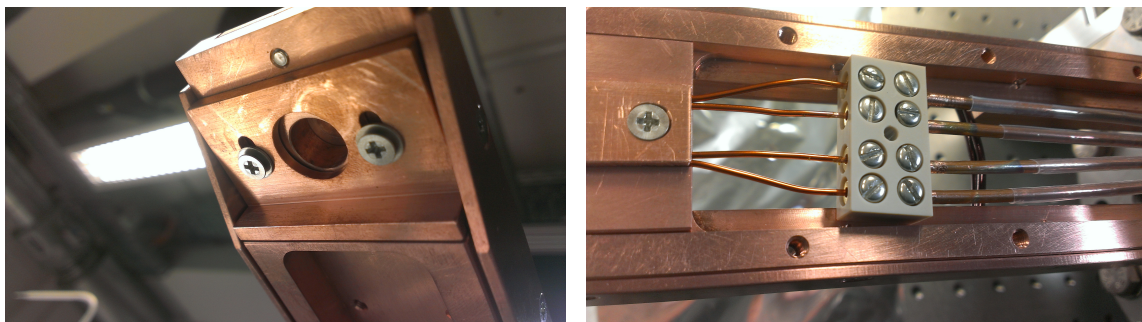

Figure 94: Bottom view (left) and view of the U-MOT wire connection (right) of the mounting.
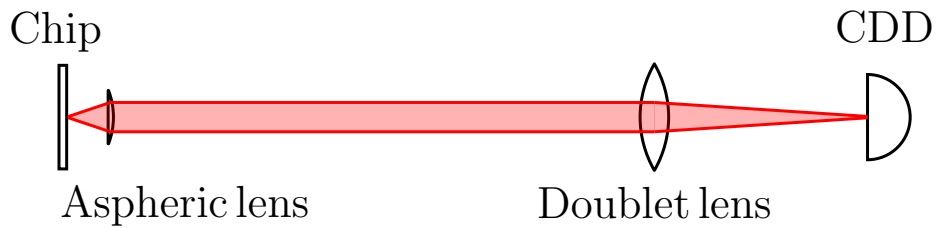
4.4 Imaging Systems

Lens Combination

Figure 95: Layout of the lens combination.

The imaging system is inspired by an experiment working with single atoms from the Laboratoire Charles Fabry de l'Institut d'Optique - France [18] and our demands where calculated in a project work [19]. The result was that the resolution of a small NA lens A397TM-B a few millimeters above the chip in the vacuum chamber in combination with an AC254-200-B lens further away outside is appropriate to image the chip surface. A picture taken of this lens combination and a CCD detector (DMK21BF) of the chip surface is shown in figure 10 on the right side. The final lens mount for the aspheric lens was designed during this diploma thesis. Figure 96 shows the cloverleaf-shaped part. The complex shape is needed to allow all laser beams to pass to the MOT center.
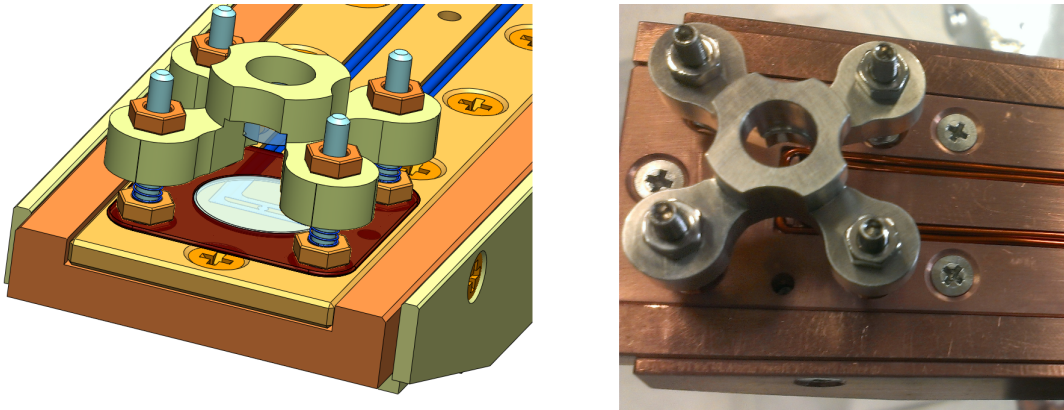

Figure 96: Clover leave-shaped mount in Solidworks (left) and in reality (right).

The clover leaf-shaped mount is fixed with four M3 rods above the chip surface. To make the adjustment more comfortable, springs can be used to force the mount up to the nuts on the top and thereby stabilize the position.
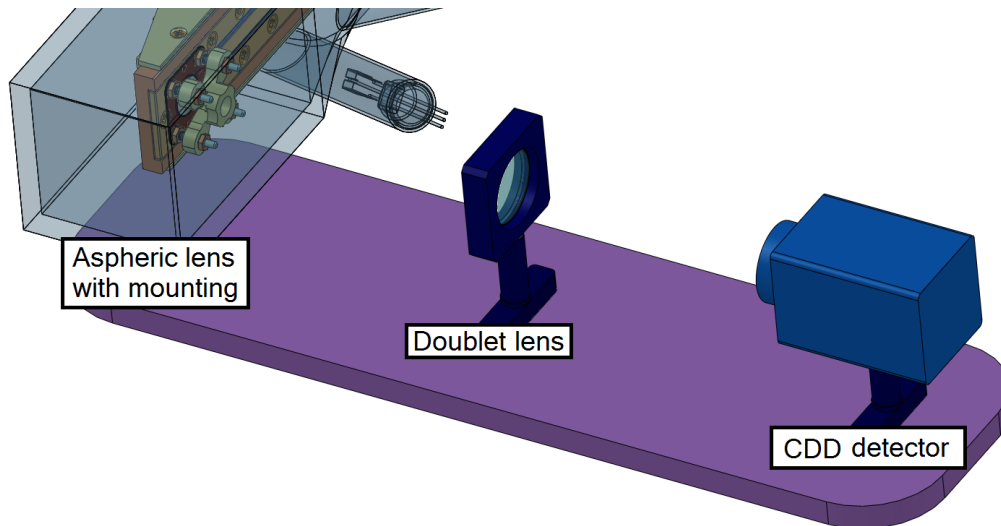
Figure 97: Sketch of the imaging system

The imaging system outside the chamber is shown in figure 97. The lens and the camera need to be aligned to the same axis as the aspheric lens above the chip surface. The distance from the doublet lens to the aspheric lens can be changed from 50 to 200 mm and the distance to the CCD detector needs to be in the area of the focal length of the doublet lens. Note that the Helmholtz coils which are placed around the glass cell are not shown here.
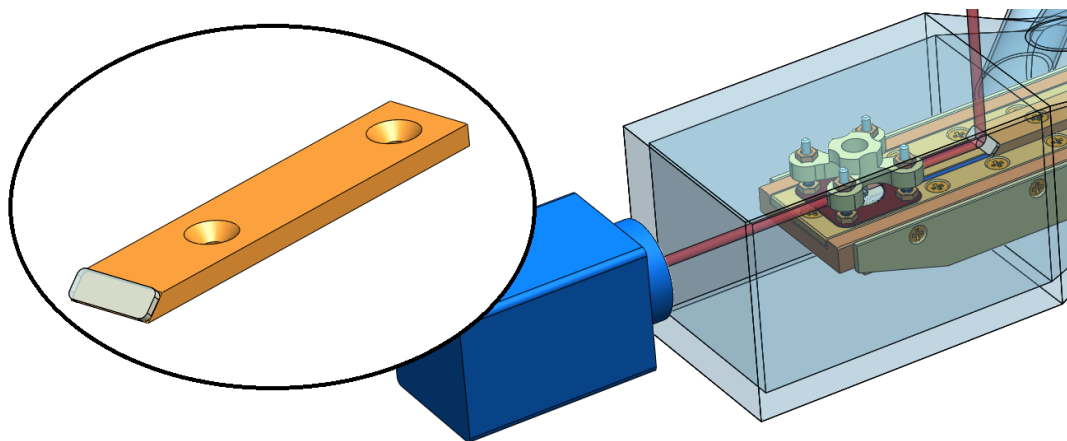
Absorbtion Imaging

Figure 98: Solidworks drawing of the mirror mounting in the vacuum chamber.

To get a proof of the presence of single trapped atoms, it is important to have a reference systems. This is why a second imaging system can be implemented with a different working principle. In this case a mirror is needed with a 45° angle mounted on the chip

as shown in figure 98. The mirror directs a laser beam through the center of the MOT with the frequency of the atomic transition. A detector can make a reference image of the beam with no atoms and afterwards an image with the loaded trap. If atoms are in the trap they will absorb a bit of the laser intensity so the image will look different. The mirror mount in this case also fixes the U-MOT wires into the chip groove.
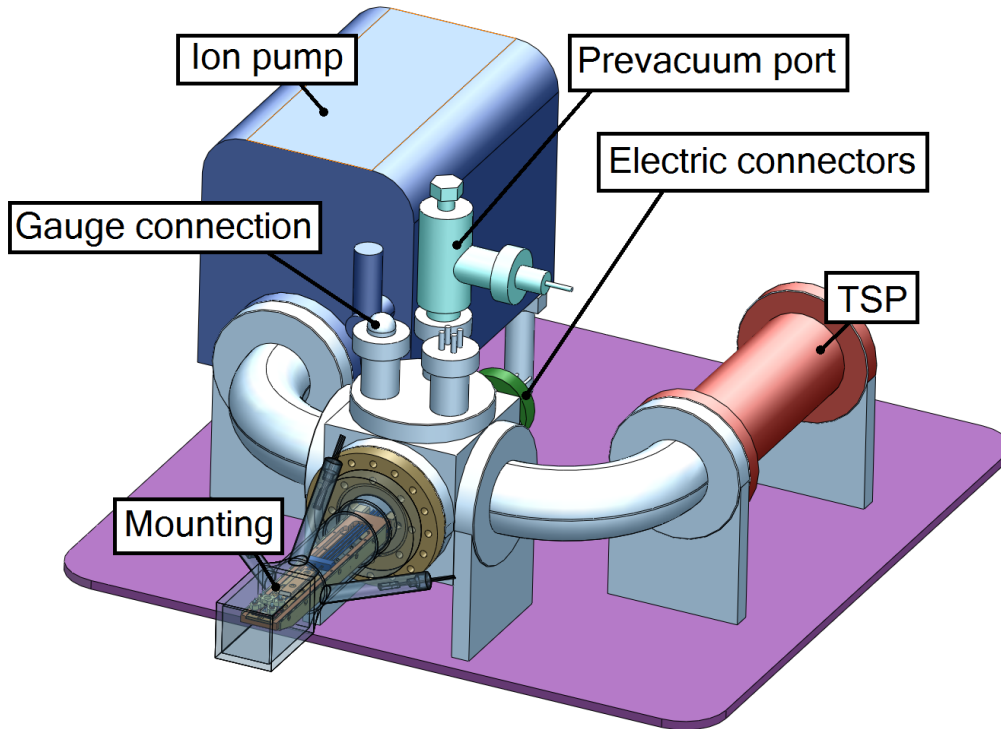
4.5 Vacuum System

Figure 99: Sketch of the vacuum chamber.

The vacuum chamber design was adapted from an older project and modified. The prevacuum port connects the chamber with a prevacuum pump (Pfeiffer) and a turbomolecular pump (Pfeiffer ID No. 0000024108 + TC 110 controller). An additional gauge for the prevacuum was also implemented between the pumps (Pfeiffer PKR251 full range gauge). The center of the chamber is the quadratic cube to which everything is linked. The ion pump (VacIon Plus 150, Agilent Technology) is shown on the left with a controller from Varian (Model 9290290) and the Titanium-Sublimations pump (TSP) with a controller from Varian (Model 9290023) is placed on the right side. In the front is the mounting with the glass cell and in the back is the feedthrough flange from Vacuum Praha where the wires from the current supply can be connected to the wires from the mounting. The vacuum is measured with a multi-gauge from Varian (Part No. L8350301) with a range down to 10^{-12} mbar.
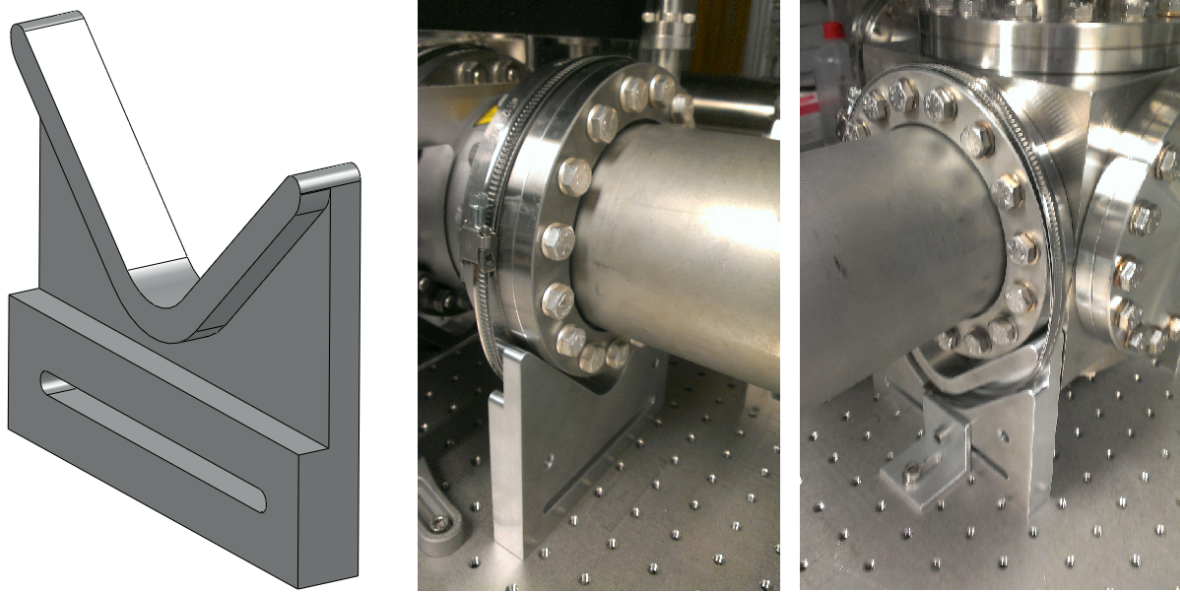
Figure 100: Vacuum mounting part in Solidworks and used in reality.

The whole chamber is placed on an Alu-plate (720x720x12 mm) with holes in the required positions. The plate has already been produced but is not implemented at the moment. The vacuum holding parts are used to stabilize the chamber construction. They can be mounted with L-section parts as shown in figure 100 on the right side. With this construction the chamber positioning has a margin of a few cm in x- and y-direction on the plate.

Heating Tubes

The heating tubes are from Horst (Typ HBS). The controller units are from Horst as well and are self regulated in combination with the temperature probes (NiCr-Ni, Typ K). Six additional sensors on relevant positions where used to control the process (Fluke 80FK-1, Bread Probe).

First Bake Out

The chamber has an inside volume of approximately 30 liters. To test the functionality of the vacuum components the chamber was operated the first time from 22.03.2013 to 31.07.2013. The setup without heating tubes is shown in figure 101 and the procedure is summarized in table 13.
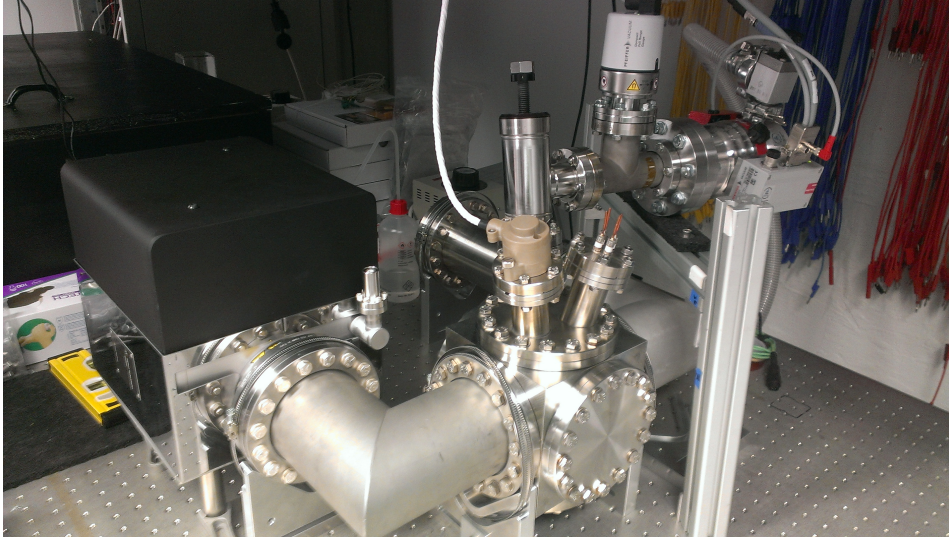
Figure 101: Vacuum chamber without heating tubes at the first bake out.

Date	Time	Process	Temperature	Pressure
22.03.2013	17:00	Prevacuum	-	$2 \cdot 10^{-7}$mbar
25.03.2013	11:00	Bake out	70°C	$3 \cdot 10^{-8}$mbar
25.03.2013	16:00	Bake out	100°C	$2 \cdot 10^{-7}$mbar
25.03.2013	19:00	Bake out	140°C	$1 \cdot 10^{-6}$mbar
26.03.2013	13:00	Bake out	160°C	$3 \cdot 10^{-7}$mbar
26.03.2013	16:00	Bake out	170°C	$4 \cdot 10^{-7}$mbar
26.03.2013	17:00	TSP shot; Ion pump test	170°C	$2 \cdot 10^{-7}$mbar
28.03.2013	10:00	Close chamber; start Ion pump	170°C	$6 \cdot 10^{-8}$mbar
02.04.2013	11:00	Cool down	170°C	$2 \cdot 10^{-8}$mbar
02.04.2013	21:00	Cool down	70°C	$1 \cdot 10^{-9}$mbar
03.04.2013	11:00	TSP shots every 2 hours	-	$1 \cdot 10^{-10}$mbar
05.04.2013	11:00	Ion pump only	-	$< 10^{-11}$mbar

Table 13: Procedure of the first bake out (second bake out proceeded pretty similar).

At the 05.04.2013 the pressure was around 10^{-12} mbar (end of range of the gauge) was reached. The formula for an ideal gas is:

$$P \cdot V = N \cdot k_B \cdot T \qquad (3)$$

where P is the pressure (10^{-10} Pa), V the volume ($0.03 \, \text{m}^3$), T the temperature ($295 \, \text{K}$), k_B the Boltzman constant and N the number of particles. The result for N is below 10^9. This equals 1.6×10^{-14} g Carbon or $3.3 \times 10^7 \frac{particles}{cm^3}$ in the chamber.

Second Bake Out

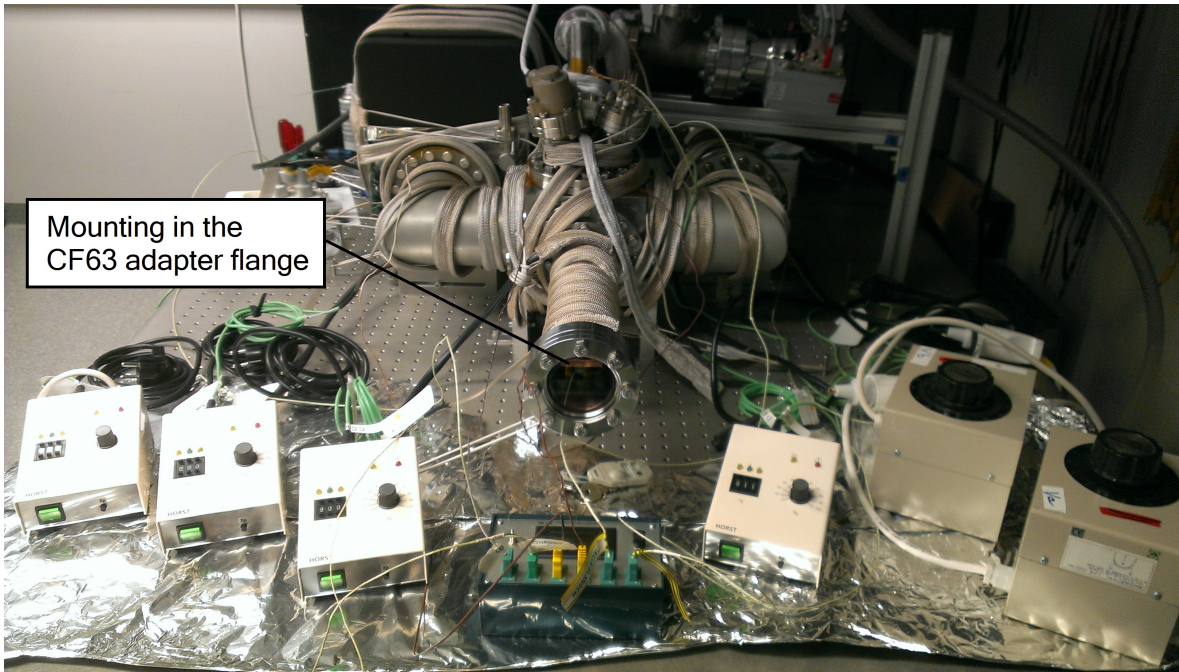

Mounting in the
CF63 adapter flange

Figure 102: Vacuum chamber with heating tubes and their control units at the second
bake out.

The second test run started at 1.08.2013. This time the mounting elements where
implemented and covered by a CF 63 flange adapter with a length of 30 cm from Hositrad,
as shown in figure 102. With this additional chamber part, the volume to pump increased
by about $0.0014\,\mathrm{m}^3$. The new size and also the new material parts has not influenced
the pumping process significant.

Third Bake Out

The third run was planned as the final run for the MOT when the glass cell arrives.
However the company which was commissioned with the production had problems by
the manufacturing. The delay went up to month and the cell could not be delivered
during this diploma thesis. This is the reason why this thesis completed without a
vacuum test with the glass cell.

Current Connection

In figure 103 the chamber is shown opened. The flange with the mounting is fixed on
the left side of the cube and on the opposite side is the flange with the feedthrough
contacts. The wires are connected with Power Inline Connectors from Allectra as shown
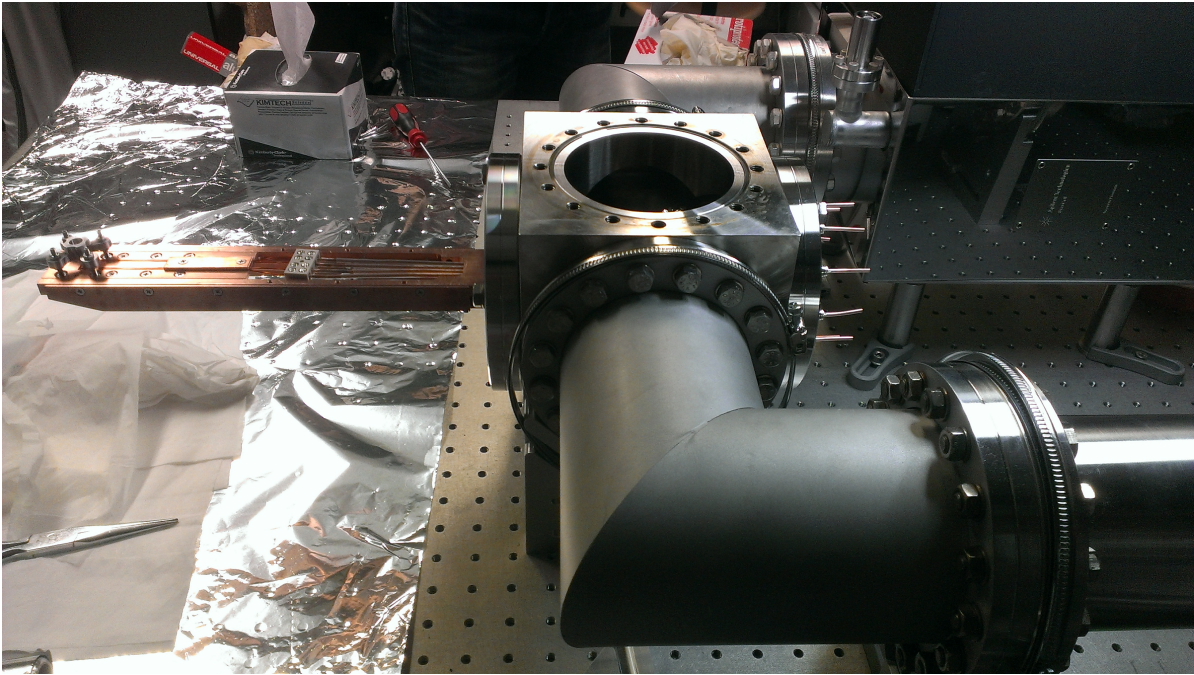in figure 104.

Figure 103: Open vacuum chamber with the mounting on the cube.

The feedthrough flange was mounted at first. Afterwards the flange with the mounting wires was carefully brought closer and fixed on the cube as well. The last part of this connection process was a little bit tricky. All eight wires had to be connected at the same time by not having much space to operate in the chamber. To do so the wires should be cut just in the right size. A z-shaped wire offers more margin but also increases the length of the free wire in the chamber. Note also that the wires are not isolated at some places, so it needs to be checked that there is no electrical short.
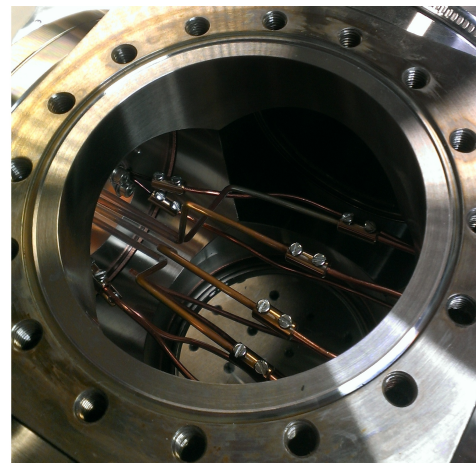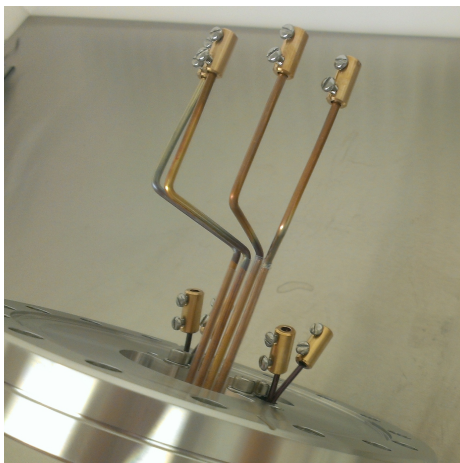
Figure 104: Connection of the mounting wires with the wires from the feedthrough flange inside the vacuum chamber.
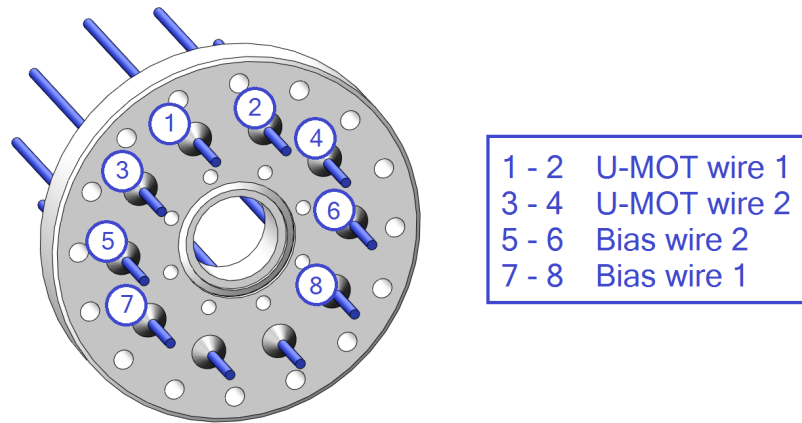
Figure 105: Current connections on the feedthrough flange.

4.6 Helmholtz Coil

The layout of the coils was designed in a project work [20]. The coils have each 60 windings with a wire diameter of 1 mm. With a current of around 2 A, one Helmholtz pair coil is able to provide the required field of 10 G.
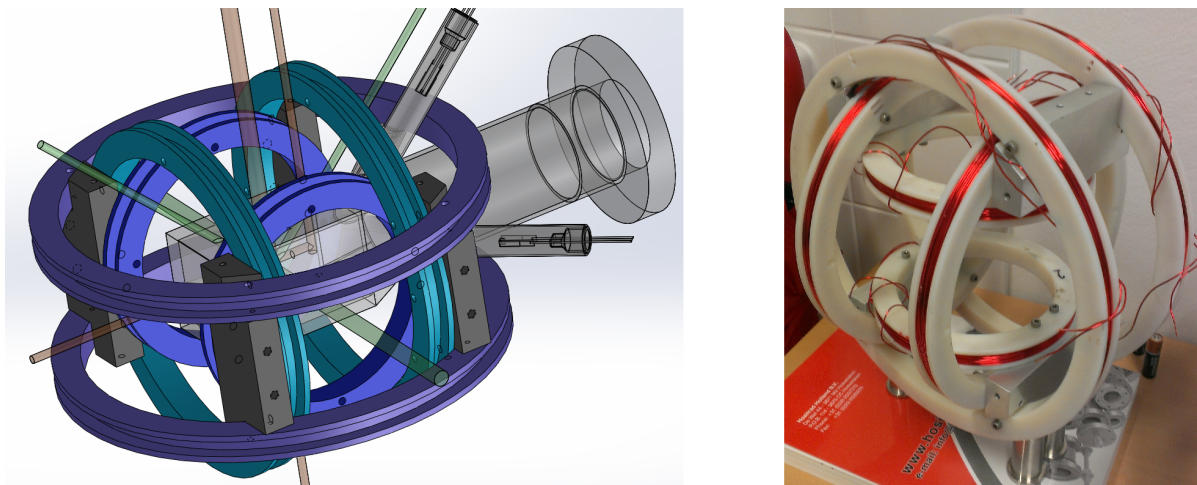

Figure 106: Picture of the 3d Helmholtz coil.

5 Discussion and Outlook

Conclusion

This diploma thesis was started in February 2013 and was finished in October 2013. During this time the structure of a new chip MOT experiment was calculated and optimized in a python code based on the Biot–Savart law. Two different versions where analysed and compared to each other. Also a wire configuration to generate a bias field has been found to enable the MOT to operate without an external magnetic field. The mounting system has been designed to enable the chip structure in the vacuum chamber and to fulfil all requirements to enable the later experiments. The elements were manufactured at the workshop at the Atominstitut. Other missing parts, required to run the MOT where ordered from different companies. All components which are included in the MOT where explained and discussed as well.

Current Status

The most precious part of the MOT was the glass cell, made by Precision Glassblowing in America. The cell is very unique and specially designed for our experiment. It was ordered in March 2013 with an expected delivery time of two month. However the small company has troubles with the production and was not able to supply the cell during this diploma thesis which means it was not possible to run the MOT. The mounting parts where manufactured and are currently fixed in the vacuum chamber only without a mirror or a reflective chip surface. The aspheric lens in the clover mount is not fixed with glue at the moment. The current supplies for the chip wires have arrived, but where not tested. The components for the vacuum chamber are in operation and able to provide a pressure of 10^{-12} mbar within ten days. The Helmholtz coils with the required power supplies have been tested and are ready to be implemented.

Manufacturing Outlook of the Mounting

The mounting part construction was chosen to keep as many options for the future as possible. The MOT wire structure is placed on the chip plate, which can be redesigned easily to offer for example an adjustably chip surface. It can also be made of ceramic and therewith be used to carry different copper structures. The imaging system which is mounted on the rods above the chip surface can be modified with springs to enable a better adjustment. The absorption image mirror is not implemented at the moment.

Manufacturing Outlook of the Vacuum Chamber

The vacuum chamber is currently placed on a large table at the Atominstitut in room Zb 02 54. The components should be rebuilt on a 720x720x12 mm Aluminium plate (which is already manufactured) before the next bake out. The plate offers the possibility to mount Aluminium profiles on the edges and thereby build a box around the system

to make it more compact. Depending on the further process of the experiment it is also planned to bring the chamber into different room in the basement of the Atominstitut.

Manufacturing Outlook of the Laser Beam Components

All necessary laser system elements are individually available at the institute but not finally assembled at the moment. Only the beam expanders and in case an optical power amplifier are currently not ordered. The cooling laser system in the box is ready but not adjusted, the repump laser has to be finished during a project work which has not yet completed. The elements for the AOM single pass are prepared and the AOM double pass is already working with an efficiency of around $45\,\%$ (including the coupling process). The laser beam splitting box is not tested but should be ready to operate. The different laser beam components should be optimized in efficiency and built up in compact boxes in future project works.

6 References

References

[1] J. Denschlag, D. Cassettari and J. Schmiedmayer, "Guiding Neutral Atoms with a Wire", *Phys. Rev. Lett. 82*, 1998

[2] J. Dalibard and C. Cohen-Tannoudji, "Laser cooling below the Doppler limit by polarization gradients: simple theoretical models", *JOSA B, Vol. 6* 1989

[3] S. Chu, "The manipulation of neutral particles", *Rev. Mod. Phys. 70*, 1998

[4] W. Phillips, "Laser cooling and trapping of neutral atoms", *Rev. Mod. Phys. 70*, 1998.

[5] C. N. Cohen-Tannoudji, "Manipulating atoms with photons", *Rev. Mod. Phys. 70*, 1998

[6] A. Haase, D. Cassettari, Björn Hessmo and Jörg Schmiedmayer, "Trapping neutral atoms with a wire", *Phys. Rev. A 64*, 2001

[7] J. Reichel, W. Hänsel, and T. W. Hänsch, "Atomic Micromanipulation with Magnetic Surface Traps", *Phys. Rev. Lett. 83*, 1999

[8] E.A. Donley, T.P.. Heavner, F. Levi, M.O. Tataw and S.R. Jefferts, "Double-pass acousto-optic modulator system", *Rev. Sci. Instrum. 76*, 2005

[9] Daniel A. Steck, "Rubidium 87 D Line Data", 2001

[10] M. Saffman, T. G. Walker and K. Molmer, "Quantum information with Rydberg atoms", *Rev. Mod. Phys. 82*, 2010

[11] M. Fuechsle, M. Miwa, J. A. Mahapatra, S. Ryu, H. Lee, S. Warschkow, O. Hollenberg, L. Klimeck, G. Simmons and M. Simmons, "A single-atom transistor", *Nature Nanotechnology 7*, 2012

[12] T. D. Ladd, F. Jelezko, R. Laflamme, Y. Nakamura, C. Monroe and J. L. O'Brien, "Quantum computers", *Nature 464*, 2010

[13] W. Demtröder, "Demtröder 2 - Elektrizität und Optik", 2009

[14] D.E. Pritchard and W. Ketterle, "Proceedings of the International School of Physics 'Enrico Fermi'", Course CXVIII - edited by E. Arimondo, W.D. Phillips and F. Strumia, 1992

[15] S. Wildermuth, P. Krüger, C. Becker, M. Brajdic, S. Haupt, A. Kasper, R. Folman and J. Schmiedmayer, "Optimized magneto-optical trap for experiments with ultracold atoms near surfaces", *Phys. Rev. A 69* , 2004

[16] S. Back and M. Maiwägter, "Doppler-free saturation spectroscopy", *Project work at the Atominstitut*, 2013

[17] F.S. Strobl, "Double Pass AOM for a Chip MOT", *Project work at the Atominstitut*, 2013

[18] Y. R. P. Sortais, H. Marion, C. Tuchendler, A. M. Lance, M. Lamare, P. Fournet, C. Armellin, R. Mercier, G. Messin, A. Browaeys, and P. Grangier, "Diffraction-limited optics for single-atom manipulation", *Phys. Rev. A 75*, 2007

[19] O. Gugenberger, "Imaging system for optical aperture traps", *Project work at the Atominstitut*, 2013

[20] L. Ginner, "3d Magnetspule", *Project work at the Atominstitut*, 2013

7 Appendix

7.1 List of involved Companies

In table 14, a list of all contracted companies is given. Also the self made components at the atomic institute within the scope of this thesis are listed.

Company	Components
Precision Glassblowing	Custom glass cell
Thorlabs	Optic equipment
Pfeiffer Vacuum	Vacuum components
Allectra	Kapton isolated wires
	Power line connectors
Hositrad	CF 63 flange adapter
Vacuum Praha	Feedthrough flange
Alu-Verkauf.de	Alu plate
Schäfter & Kirchhoff	Laser beam splitting box
Agilent Technology	Ion pump
Horst	Heating tubes
Varian	Vacuum gauge
Epotec	Glue
ZMNS	Chip mirror
RS Bochum	A4 crews and nuts
Custom made	Adapter flange
	Mounting
	Chip plate
	Side plates
	Imaging lens mount
	Vacuum holder
	Ion pump holder
	Vacuum chamber plate
	Helmholtz coil

Table 14: List of involved companies.

7.2 Used Programs

Program	Description
Comsol Multiphysics 4.3	Finite element analysis program
Solidworks 2010	3D-CAD-Program
IPython	Python console
Enthought	Python distribution
Notepad++	Editor for Python
PdfLatex	Latex compiler
BibTex 0.34	Latex library
TexStudio 2.5.1	Editor for Latex code
PS Tricks	Optical drawings for Latex
IC Capture 2.2	Image acquisition program
Mendeley 1.8.3	Program for managing research papers
Gimp 2	Editor for pictures
Snipping Tool Plus 3.4.1	Easy creating desktop shot

Table 15: List of used programs

7.3 Technical Drawings

In the following are technical drawings of all produced parts during this thesis. The 3d CAD files of all parts can be found in the folder on the server of the Atominstitut where this thesis is stored.
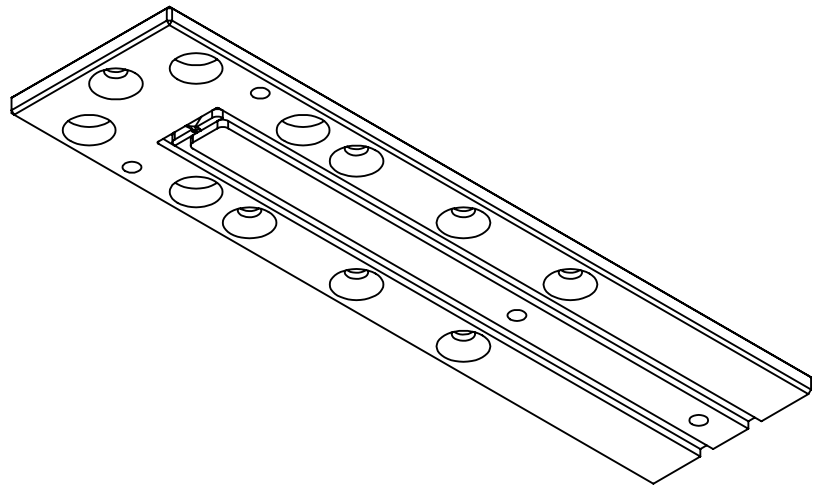
Lens mount

Flange

ϕ82,55

ϕ77,20

20

15

ϕ4

ϕ6

9

9

C

C

M8 Gewinde (8x)

ϕ8

46,050

29

19,9

15

ϕ4

C-C (1 : 1)

90

Mounting

Chip plate

Ø3.1

15
20

B

Ø7

24

Ø2.5

Ø3.1

45° Phase

5
10
10
20
10

20

20

M3

20

6

M3

3

30

10

11,4

10

R1

R1

Ø1.2

6,600

1,2
1
1,2

1,2 mm deep groove

B (2 : 1)

45°

C (2 : 1)

C

1,2

120

92

Side plate left

250

40 40 40 40 40 30

1,3

45° 2

4

6

30

18

⌀3,2

Side plate right is mirror inverted

Bottom plate

26

5

21

24

⌀12

11,5

R1,5

9,5

42

2

2

3,5

3,5

93
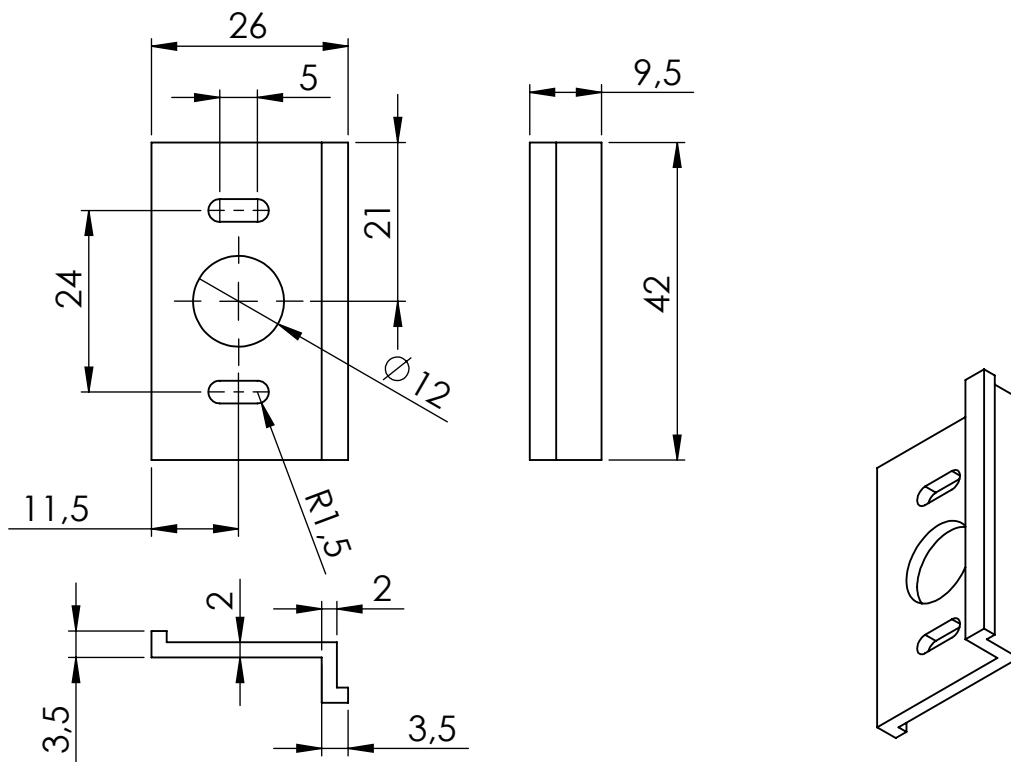
Vacuum chamber holding part

R4

R30

R20

10

40

7

45°

20

110

150

10

20

Ion pump mount

A

A

50 mm | 50 mm | 62 mm | 50 mm | 5 mm

262 mm

10 mm

10 mm

20

111 mm

111 mm

Ø 4.5

M4

Ø 8

A-A (1 : 2)

Ø 8

18 mm
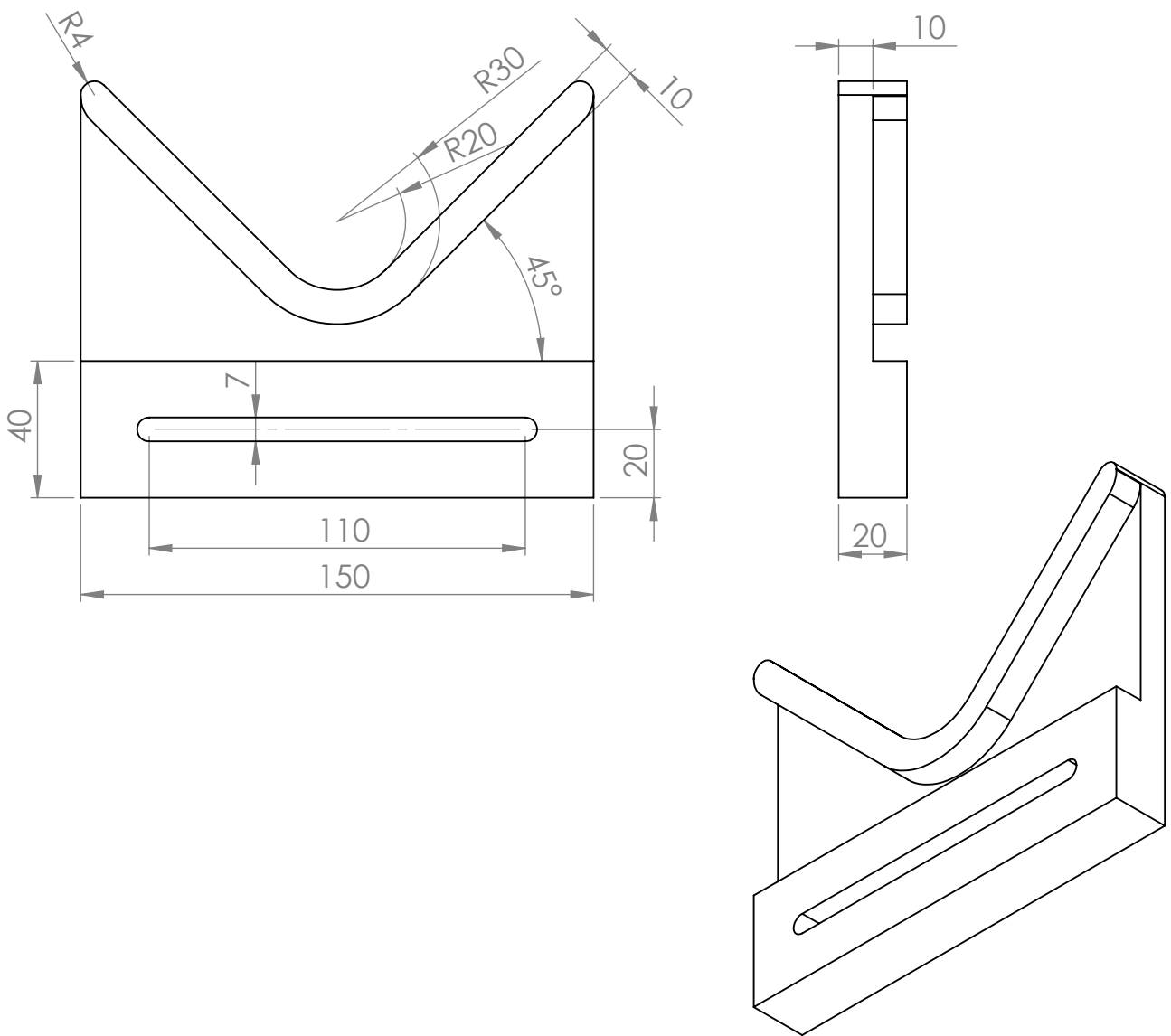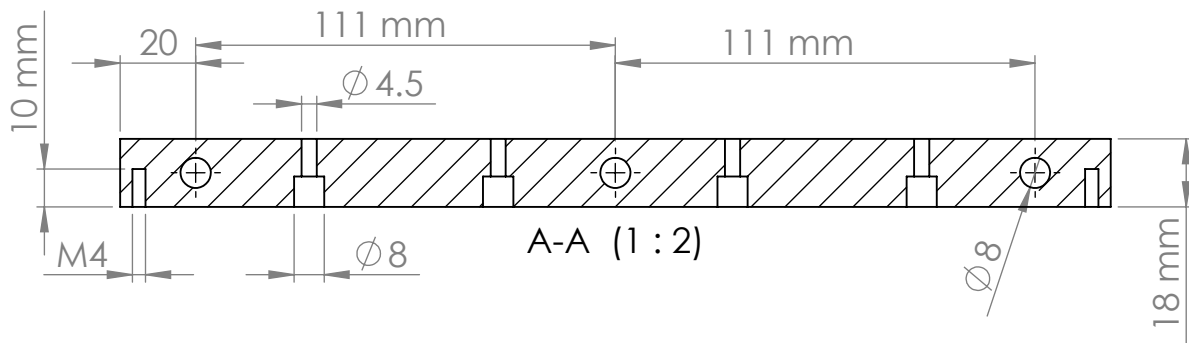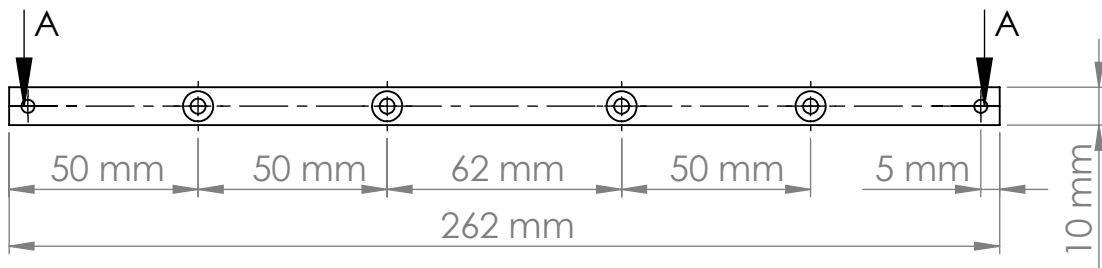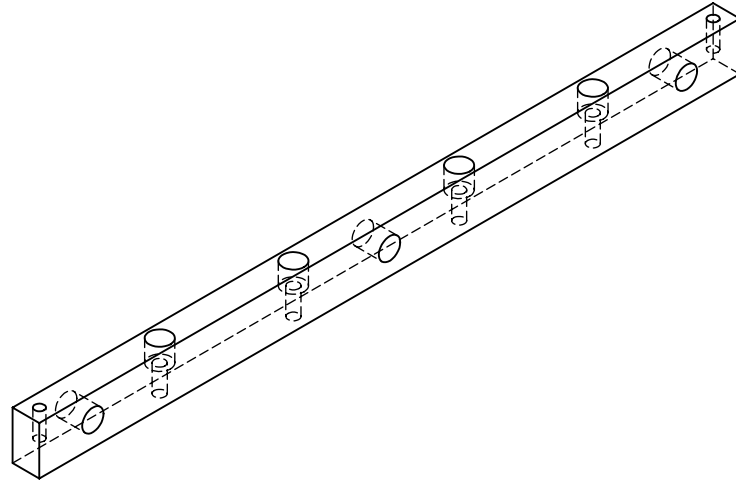
Vacuum chamber base plate